POLITECNICO DI MILANO

Scuola di Ingegneria Industriale e dell'Informazione

Corso di Laurea Magistrale in Ingegneria Spaziale

Optimal location and gains of sensors and actuators for feedback vibroacoustic control of plates

Relatore:
Prof. Lorenzo Dozio

Tesi di laurea di:
Silvio Patruno
Matr. 771437

Anno accademico 2013/2014

"Scientists discover the world that exists;
engineers create the world that never was."
Theodore von Kármán

Acknowledgments

My first and dutiful thanks go to Prof. Lorenzo Dozio, for guiding me in the writing of this thesis, masterfully, with great willingness and confidence; and for having instilled in me a passion for the control of structures through his teachings and advice.

My thanks also go to all the teachers met during these years of study at Politecnico di Milano. This thesis is the result of all their precious teachings and passion that they managed to send me. I owe them a message that I managed to catch in recent years: *Engineering is not a way to do, but a way of thinking and seeing things.*

I would also like to remind all my fellow travelers. Years have been challenging, full of sacrifice and hard times. A big "thank you" goes out to all my friends and colleagues with whom I shared and overcome these moments. I would like to mention the unforgettable members of *Laputa Team*, a group of fantastic people, old and new college mates, and a distant but close companion of life, Federico Secondi.

Finally, a special thanks goes to my *little scricc*, my family and my old friends, for the patience, the support, and the encouragement during this whole period of studies.

Contents

List of Figures

List of Tables

Abstract

The dynamic response of the structures in the elastic range is very important in the majority of engineering applications, particularly in Space and Aeronautics field, where a wrong control of vibrations can produce unreliable safety conditions and sometimes catastrophic. In addition to uncontrolled movement, another effect of the vibrations of the structures is given by the radiated acoustic power that is perceived by the human ear in form of pressure waves. This phenomenon, for some types of applications, it may be undesirable or unpleasant.
For this reason it is very important the optimum design of the structure and a control system that is able to reduce its vibrations to an acceptable level of safety and comfort .
Some types of structures, for their shape and boundary conditions, have limitations in being able to design an appropriate monitoring system, often leading to suboptimal results .
The work of this thesis, starting with some recent methods for finding optimal solutions of placement for sensors and actuators on two-dimensional membranes (Xu et al. - "Optimum Location and Gains of Sensors and Actuators for Feedback Control "; Abdullah - "Optimal Location and Gains of Feedback Controllers at Discrete Locations"), wishes to extend the search for optimal solutions in plates with variable characteristics, dimensions and arbitrary boundary conditions. The work will also explore the optimal solutions for the minimization of the acoustic radiation power produced.
The result obtained was a complete algorithm for the analysis of a generic model of plate, to control both the vibratory and acoustic behavior, with good results from the convergence point of view.

Sommario

La risposta dinamica delle strutture in campo elastico è molto importante nella stragrande maggioranza delle applicazioni ingegneristiche, in particolar modo in campo Spaziale e Aeronautico, dove un errato controllo delle vibrazioni può produrre condizioni di sicurezza non affidabile e a volte catastrofiche. Oltre al movimento incontrollato, un altro effetto delle vibrazioni delle strutture è dato dalla potenza acustica irradiata che viene percepita dall'orecchio umano sottoforma di onde di pressione. Anche questo fenomeno, per alcuni tipi di applicazioni, può risultare indesiderato o sgradevole.
Per questo motivo è molto importante il progetto ottimale della struttura e un sistema di controllo che sia in grado di ridurre le sue vibrazioni a un livello di sicurezza e comfort accettabili.
Alcuni tipi di strutture, per come sono fatte, hanno delle limitazioni nel poter progettare un sistema di controllo adeguato, portando spesso a risultati non ottimali.
Il lavoro di questa tesi, partendo da alcuni recenti metodi per la ricerca di soluzioni ottime di posizioni per sensori e attuatori su membrane bidimensionali (Xu et al. - "Optimum Location and Gains of Sensors and Actuators for Feedback Control "; Abdullah - "Optimal Location and Gains of Feedback Controllers at Discrete Locations"), intende estendere la ricerca di soluzioni ottimali a pannelli dalle caratteristiche, dimensioni e condizioni al contorno arbitrarie. Questo lavoro intende inoltre esplorare soluzioni ottime anche nel campo di una minimizzazione della radiazione acustica prodotta.
Il risultato ottenuto è quello di un algoritmo completo per l'analisi di un modello generico di piastra, per un controllo sia vibratorio che acustico, con buoni risultati dal punto di vista della convergenza.

Chapter 1

Introduction

In general, elasic structures, and in particular space structures, such as a space station and the large solar arrays of a solar power station satellite have the characteristics of a flexible structure by the demands for light weight and large size. Hence, in large space structures that are characterized by their inherent natures -infinite dimension, distributed parameter, low damping, and densely populated modes- and stringent performance requirements in space, there are many vibration modes within the frequency band of disturbances and control bandwidth. Once they are disturbed, these modes are likely to remain excited for a long time because of their low natural frequency and small damping, which might hamper their missions in space. Therefore, to comply with the request of vibration suppression, the concept of actively controlled large flexible structures with sensors and actuators located on the structure has to be introduced.
Generally, a large number of sensors and actuators are required for the active vibration control of flexible structures. Thus, the problem of choosing the appropriate number and locations of actuators and sensors is important, since an arbitrary decision is expected to degrade the system performance and directly limit the range of practical applications. In choosing the appropriate number and locations of sensors and actuators, our aim will be to excite the structure with minimum control effort for vibration suppression and also minimize the sensor signal power for the measurement of a given excitation of the structure. For instance, a poor system in which actuators are placed on or near the nodes (or node line) of vibration mode requires an excessively large control force at best, or uncontrollable at worst. Consequently, the optimal placement of actuators and sensors to maximize the degrees of controllability and observability can improve the control and estimation performance of a closed-loop system.

The design of an optimal feedback control systems for flexible structures, includes two sets of design parameters, the gains of the control matrix and the positions of sensors and actuators. There are well-established methods for determining optimal gains; however, methods for optimal placement are relatively new. Previously, for the minimization of a certain functional, the location of the sensors and actuators was only supposed, and then the optimization of feedback gains was done separately. Schultz and Heimbold developed a method of concurrent design of both placement and gains. The method is optimal in that it maximizes energy dissipation due to control action. The solution to the optimization problem was obtained by a gradient-based nonlinear programming technique.
The original method from Xu et al. [9] consisted of calculating the gradients of the performance function not only with respect to the feedback gains but also with respect to sensor and actuator placement. Only the dimensions of the example structure limited the placement of the collocated sensors and actuators. In most gradient-based optimal control problems, each of the design variables are permitted to take any real value. But is not always possible to place control sensors and actuators at arbitrary positions. In many cases, there is a discrete and finite set of possible locations within the structure where the sensors and actuators can be placed. In solving problems of this nature, it is necessary to use integer-programming techniques, that is the work developed by Abdullah [1]. For problems where all or some of the design variables must be from a discrete set, the most feasible way to find a solution is using integer-programming methods. Abdullah used an integer-programming method to find optimal placement of controllers and actuators at discrete locations.
Relatively very little work has been done in the area of nonlinear and mixed integer (problems with both integer and continuous design variables) programming. In many cases, linear integer programming techniques have been used to solve some nonlinear problems. It is known that these nonlinear integer-programming methods are not as robust as their continuous counterparts.
A new method was proposed by Abdullah [1], for well-defined functions. It has been shown that a constrained nonlinear problem can be converted into an unconstrained problem using a transformation of variables. This technique is very easy to program. In the proposed method, the use of transformations was generalized where a change of the dependent variables was used to transform the constrained integer problem to an unconstrained continuous one. Because the performance function is well defined, it was demonstrated that this change of variables is an effective means of finding integer optimal

values.

However, since the purpose of this thesis is to provide a model of the structure much more complex of the previous works, including loads and generic boundary conditions, as well as a refined model of the acoustic radiated power, sensors and actuators are permitted to take any positions on the structure, belonging in a real domain. So the problem is focused on a nonlinear real-programming technique.

The method used for the numerical optimization is the very robust DavidionFletcherPowell (DFP) algorithm. Knowing analitically the expression of the gradient for the cost functional for a feedback optimal control approach, the only difficulty lies in understanding the dependence of the position variables from such a gradient.

Once the complete state space model for the system will be defined, including the structural state and the "acoustic state", finding an optimal solution becomes quite straightforward although it requires some computation time.

1.1 Problem understanding

The considered vibrating structure is a rectangular Kirchoff plate.

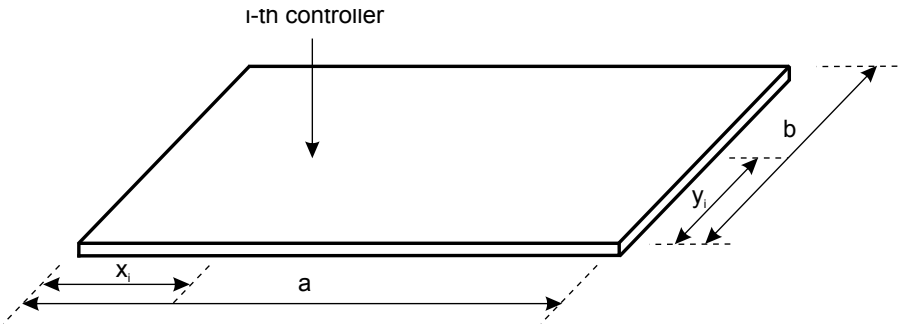

Figure 1.1: Rectangular Kirchoff plate.

Once the structural and acoustic modelization will be performed, the augmented state space system will be the starting point for the optimization process.
For the control, a feedback control strategy will be considered, with a certain number of sensor and actuators.

$$\begin{cases} \dot{\mathbf{x}} = \mathbf{A}\mathbf{x} + \mathbf{B}\mathbf{u} \\ \mathbf{y} = \mathbf{C}\mathbf{x} \\ \mathbf{u} = -\mathbf{G}\mathbf{y} \end{cases} \tag{1.1}$$

After the performance index has been modeled as

$$J = \frac{1}{2} \int_0^\infty \left(\mathbf{x}^\mathbf{T} \mathbf{Q} \mathbf{x} + \mathbf{u}^\mathbf{T} \mathbf{R} \mathbf{u} \right) \, dt \tag{1.2}$$

Consider the optimization problem

$$\min J(\mathbf{x}_s, \mathbf{x}_a, \mathbf{G}) \rightarrow \mathbf{x}_s^*, \mathbf{x}_a^*, \mathbf{G}^* \tag{1.3}$$

where J is the cost functional defined in Eq.(1.2), $\mathbf{x}_s$ and $\mathbf{x}_a$ are the placement of sensors and actuators respectively, and $\mathbf{G}$ is the feedback gain matrix, whereas $\mathbf{x}_s^*$, $\mathbf{x}_a^*$ and $\mathbf{G}^*$ are the optimum values that minimize J. The variables $\mathbf{x}_s$ and $\mathbf{x}_a$ in a continuous case are subject to constraints

$$\mathbf{x}_s \in \mathbf{X}_s, \qquad \mathbf{x}_a \in \mathbf{X}_a \tag{1.4}$$

where $\mathbf{X}_s$ and $\mathbf{X}_a$ are subsets of the real domain limited by the dimensions of the structure.

As can be noted, it is a multivariable optimization problem, whose size and computation time depend on the number of actuators and sensors adopted in the procedure.

Chapter 2

State of the Art

MANY numerical research has been done since the 80's on combined methods for the reduction of vibration and acoustic radiation caused by structures of automobiles, airplanes and buildings in general.
There are active and passive methods on which one can base the control of a structure. Passive approaches are based on the design of material properties or shapes of the structure so as to minimize vibrations and radiated noise. Exploiting damping layers in the structure is a good example of passive noise control. Recent advances in computing resources and numerical optimization procedures have made optimization feasible for complex structures using active techniques.
Smart materials or structures have emerged as promising active techniques to reduce the kinetic energy and the radiated sound. In longer available structures, piezoelectricceramics are widely used as active devices on the structures. Much research has been done experimentally, analytically and for piezoelectricactive, adaptive, or intelligent structures. However, the design of smart structures for minimal sound radiation is a multidisciplinary and challenging problem, which involves a complex model of the structure with active devices made of piezoelectric materials, understanding of structural acoustics, and large numbers of parameters that affect the active system performance.

2.1 Optimal locations on a membrane - K. Xu, P. Warnitchai, T. Igusa - 1993

The purpose of the study was to present a new and efficient method for optimal design of placement and gains of actuators and sensors in output

feedback control systems. This work extends the method developed by Levine and Athans by solving for optimal placement. It is efficient and can handle a large number of optimization variables. Multiple local minima for the performance function were found for the optimal placement problem, and a randomly generated initial values for the optimization variables were used to obtain a set of solutions.

2.1.1 Formulation of the problem

Consider the response of a general elastic structure subjected to an applied force $F(\mathbf{x}, t)$

$$\left[m_0 \frac{\mathrm{d}^2}{\mathrm{dt}^2} + c_0 \frac{\mathrm{d}}{\mathrm{dt}} + \lambda L\right] w(\mathbf{x}, t) = F(\mathbf{x}, t) \tag{2.1}$$

The considered structure was a rectangular membrane with dimensions $a = 1.00$ and $b = 1.03$, as shown in Fig. 2.1. The open-loop modal damping rations are 0.005 for all modes; a total of 11 modes are considered in the numerical analysis. For the derivation of the dynamic and control equations refer to [9].

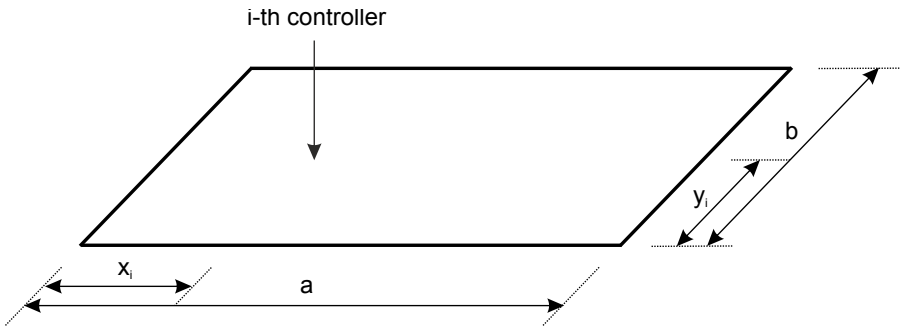

Figure 2.1: Rectangular membrane.

An optimal design procedure is developed for the actuator placement, $\mathbf{x}_{aj}$, sensor placement, $\mathbf{x}_{sp}$, and feedback gains $\mathbf{F}$. First, a performance function is chosen which includes both the structural response and the control effort. The standard performance function is considered

$$J = \frac{1}{2} \int_0^\infty \left(\mathbf{x}^\mathbf{T} \mathbf{Q} \mathbf{x} + \mathbf{u}^\mathbf{T} \mathbf{R} \mathbf{u}\right) \, dt \tag{2.2}$$

with the following weighting matrices:

$$\mathbf{Q} = \begin{bmatrix} \mathbf{\Lambda} & 0 \\ 0 & \mathbf{I} \end{bmatrix}, \quad \mathbf{R} = R \begin{bmatrix} \mathbf{I} & 0 \\ 0 & \mathbf{I} \end{bmatrix}. \tag{2.3}$$

For the control strategy a de-centralized control is assumed, with collocated sensor and actuators.

2.1.2 Results

Three numerical studies where presented: optimal placement and gains for 1 and 11 actuators, and optimal gains for 100 actuators. Single-loop feedback control gains where used, making the gain matrix diagonal. A separate study had shown that performance function differs by less than 1% when diagonal or full gain matrices are used.

Optimal placement and gains for a single actuator/sensor . The simplest optimal design problem is for a single actuator and collocated sensor. There are only three optimization variables: the velocity gain, x and y coordinates of the controller. The control penalty is $R = 10$. If the coordinates of the controller are fixed, there is only a single value for the velocity gain which minimizes the performance function. However, with the three optimization variables, there are many local minima. To obtain as many different local minima as possible, many simulation are executed with random initial values.

Six distinct solutions were obtained. The placement of the actuators, and the corresponding values for the performance function J, and gains f_{opt}, are shown in Fig.2.2. The difference between the smallest and largest performance values is only 5%, but the difference between the smallest and the largest gains is 34%. Thus, for this problem, the multiple local minima yeld, nearly equivalent performance values.

The six placement results are superimposed in Fig.2.3; they are plotted only in the upper-right portion of the structure. The nodal lines of the open-loop mode shapes are also indicated by dashed lines. The figure shows that the placement of the actuators lie away from the nodal lines, as expected from controllability theory. In each of these regions, local minima exist; however, they are considerably higher than the remaining six local minima.

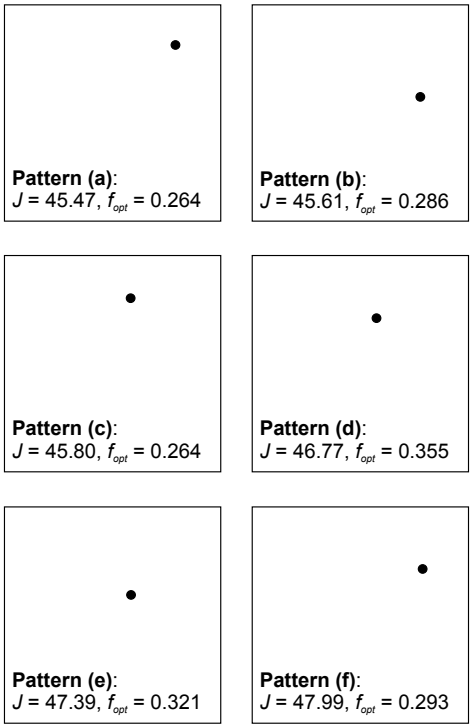

Figure 2.2: Placements for the single controller case.

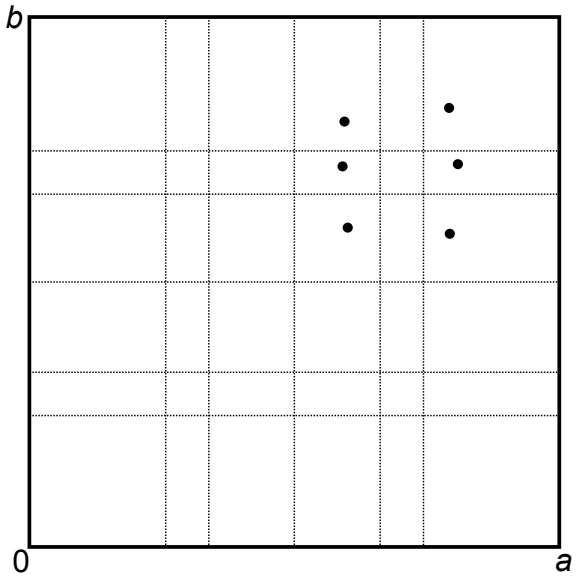

Figure 2.3: Superimposed placements for the single controller case - nodal lines for the open loop modes.

Optimal placement and gains for 11 actuator/sensors. In this case, the number of actuators is equal to the number of modes in the structural model. There are 33 optimization variables: three for each controller. As in the previous case, the control penalty is $R = 10$.

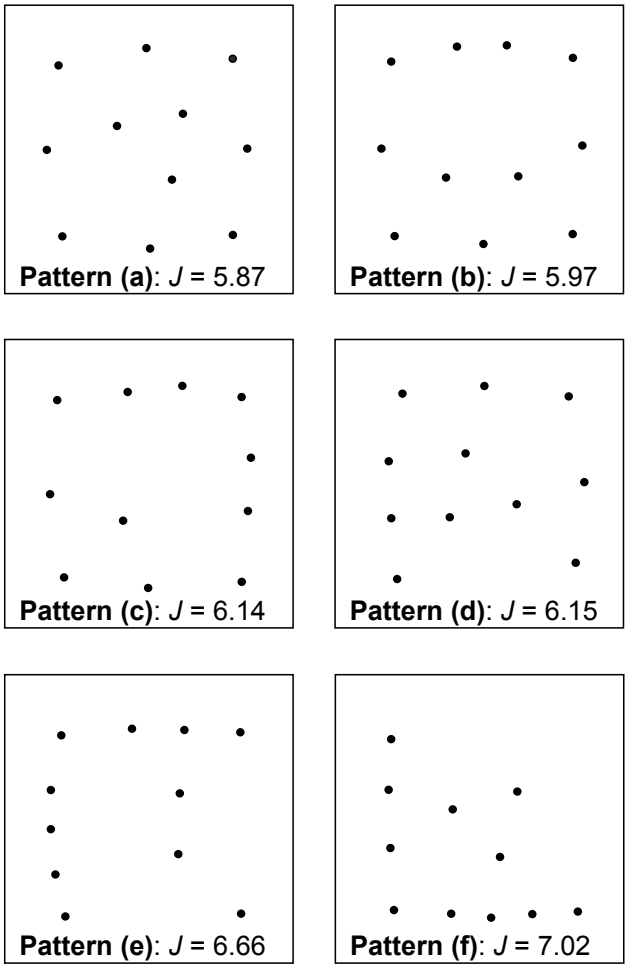

Figure 2.4: Placements for 11 controllers case.

Six distinct solutions were obtained. The placement of the actuators, and the corresponding values for the performance function J, are shown in Fig.2.4. Solution (a) yields the smallest values, $J = 5.87$, which, as expected, is considerably lower than the value for a single controller. Solution (f) yields the largest value, $J = 7.82$, which differs from solution (a) by 20%. Fig.2.4 shows that solution (a) has the most evenly distributed placement pattern. Some of the other solutions have placements which are concentrated on one side of the structure. For all cases, the gains of the single-loop actuators are close 0.2.

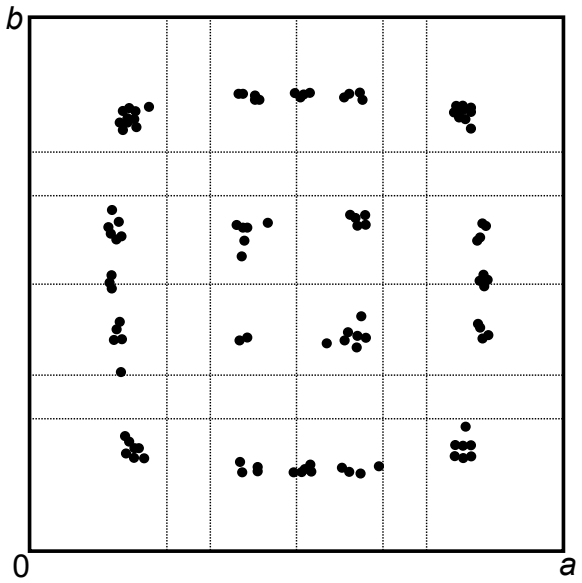

Figure 2.5: Superimposed placements for the 11 controllers case - nodal lines for the open loop modes.

The placement results are superimposed in Fig. 2.5, and, as in Fig. 2.3, the nodal lines of the open-loop mode shapes are indicated by dashed lines. The actuator placements are clustered in certain nearly symmetric locations about the membrane. Some of the actuator locations lie on nodal lines; these actuators are still effective since several of the open-loop modes do not have nodal lines at these locations.

Optimal gains for 100 actuator/sensors. The placement of controllers is shown in Fig.2.6. Since the actuators are uniformly placed throughout the structure, optimal placement is not considered. The control penalty is $R = 100$, which yields control with relatively low authority. This optimization problem is a simple study of distributed control, which have wide potential applications. The problem is also a demostration of how easy the nonlinear programming algorithm can handle 100 variables.

2.2 Optimal discrete locations on a membrane - M. Abdullah - 1998

It is not always possible to place control sensors and actuators at arbitrary positions. It is possible that for many structures the optimal locations for sensors and actuators to minimize vibrations are not feasible. Simply round-

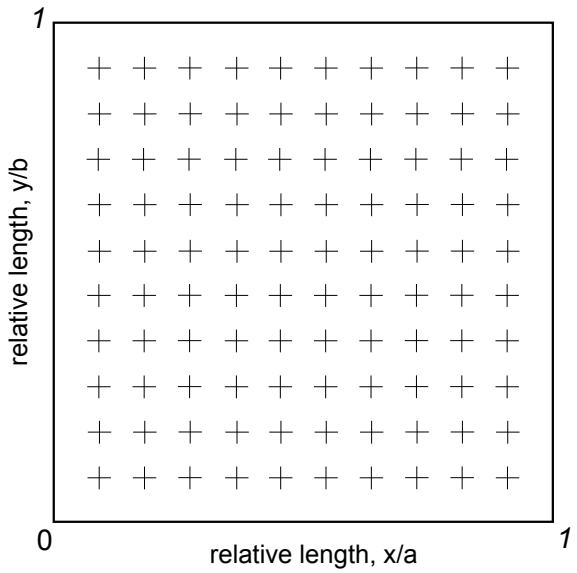

Figure 2.6: Placements of 100 controllers.

ing solutions can give very umpredictable results. It is possible to round the location of an actuator to a position where a mode would be uncontrollable. In this case, the desired and actual control effects can differ drastically.
A new method where proposed. For well-defined functions, it has been shown that a constrained nonlinear problem can be converted into an unconstrained problem using a transformation of variables. This technique is very easy to program. In the proposed method, the use of transformations is generalized where a change of the dependent variables will be used to transform the constrained integer problem to an unconstrained continuous one. Because the performance function is well defined, it is demonstrated that this change of variables is an effective means of finding integer optimal values.

2.2.1 Discrete location programming technique

The problem is now (or can be represented as) a mixed integer problem, where a partial set of variables (actuators and sensor placements) are integers and the remaining variables (gain assignments) are non-integers. It is useful to find a transformation to make all of the variables non-integers so that the problem becomes a non-integer problem. Taking into account the Eq.(1.3), this objective would be accomplished if a function $\mathbf{x} = h(\mathbf{y})$ could be found so that

$$\min J(h(\mathbf{y_s}), h(\mathbf{y_a}), \mathbf{F}) \rightarrow \mathbf{y_s}^*, \mathbf{y_a}^*, \mathbf{F}^* \tag{2.4}$$

subject ton constraints

$$\mathbf{y_s} \in \mathbf{X_s}, \qquad \mathbf{y_a} \in \mathbf{X_a} \tag{2.5}$$

where $\mathbf{y}$ is a continuous variable that produces an integer value for $\mathbf{x}$, and $\mathbf{X_s}$ and $\mathbf{X_a}$, still are the subsets of the domain of the structure.
The function h should be a round-off step function, which would round any number to the closest integer. However, this step function is discontinuous and, therefore, its derivative is undefined at each step. This renders gradient-based nonlinear programming methods unusable because the gradients of $J[h(\mathbf{y}), \mathbf{F}]$ would also be discontinuous. Thus, it is important to use a function that looks like a step function and is yet continuous.
It can be shown that the sine function raised to an even power, as the even power becomes large, begins to look like a periodic impulse function. If this function is multiplied by a constant to make the area under each impulse equal to one, the following integral becomes an approzimation for the step function:

$$x_i = h(y_i) = A_{2N} \int_0^{y_i} [\sin(\pi u)]^{2N} \, du \tag{2.6}$$

where

$$A_{2N} = \frac{2^{2N}(N!)^2}{(2N)!} \tag{2.7}$$

and N is an integer for the approximation of the step function. The constant values for A_{2N} were found analytically. As N increases, the approximation to the step function improves, getting quite accurate for reasonable values of N. But as N gets large, it becomes increasingly difficult for nonlinear-programming methods to find noninteger values, because: First,

the gradients at integer values are much smaller that those at noninteger values; Second, the noninteger values begin to occupy a smaller range. This can also be seen in Fig.2.7.

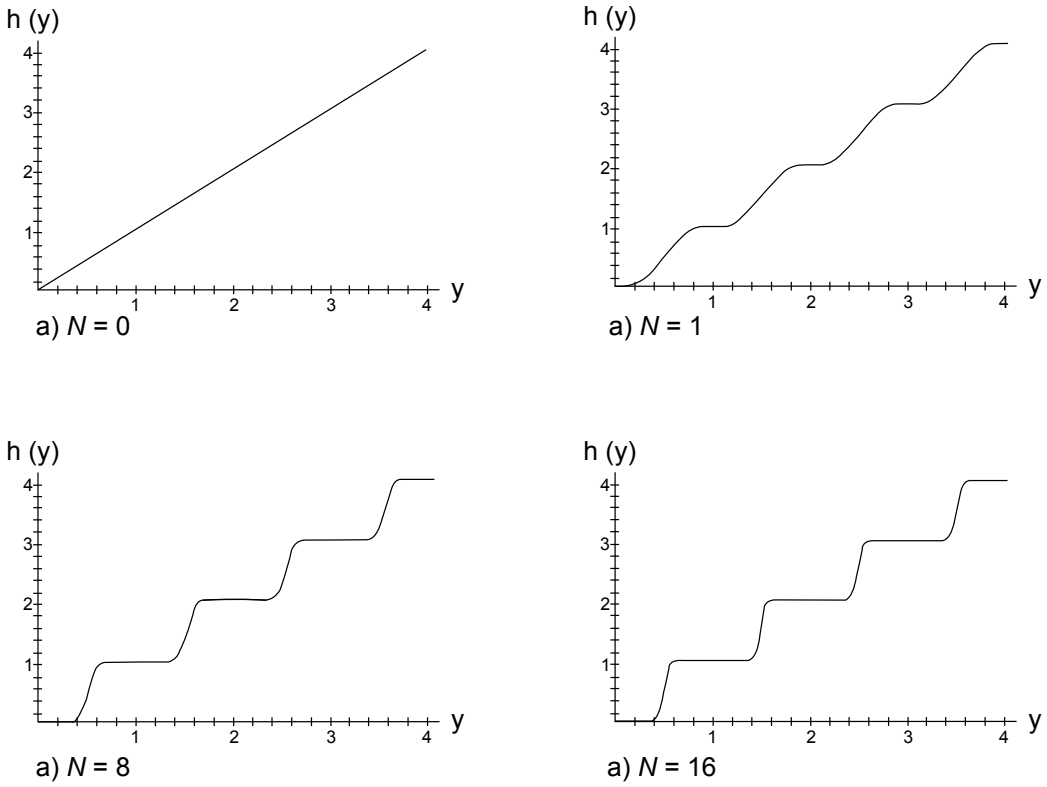

Figure 2.7: Transformation of variables.

2.2.2 Results

The example structure was a rectangular membrane with the same dimensions of the previous one, as shown in Fig.2.1. The derivation of the quations of motion and the control strategy are similar. For more details refer to [1].

During the study, several numerical examples of an elastic membrane were completed. Three arrangements were considered: the placement of 1 actuator with 1 mode, the placement of 1 actuator with 11 modes, and the placement of 11 actuators using 11 modes. The discrete location one-actuator example was done for five equally spaced divisions on both the x and y axes. This produces 36 discrete locations, 16 on the interior and 20 on the boundary. The discrete location 11-actuator example was done for 11 equally spaced

divisions on both the x and y axes. This produces 144 discrete location, 100 on the interior and 44 on the boundary. Each case was performed with and without the integer-programming technique to compare with the results of Xu et al.. Because the complexity of the cost function, also in this case, it is possible for the control algorithm to settle on many possible local minima. The minima that yielded the lowest value of the cost function were deemed the optimal solutions. The percentage of occurence of the optimal solutions is also found for each of the examples. This is defined as the percentage of optimal solutions found from the 20 initial points. All of the continuous examples converged in much less than the allowed 100 iterations for 100% convergence.

Single actuator/sensor for one mode. The simple optimal design problem is a single actuator and collocated sensor with one mode. There are only three optimization variables: the velocity gain and the x and y coordinates of the controller. The control penalty is $R = 10$, which yields control with relatively high authority. With only one mode, there is only one local minima, which is at the center of the membrane. It is expected that the best solution will be the one nearest the local minima. For the plot of the cost function J with respect to the placement coordinates, shown in Fig.2.8, the gain of the controller was held constant. Fig.2.8 shows that the minumum values of J is at the crossing of grid lines nearest to the minimum, as shown in Fig.2.9, as expected. Because this membrane is symmetric about the center, this solution represents all four solutions surrounding the center.

Table 2.1: One actuator/sensor, one-mode case

Design type	Convergence, %	Optimal convergence, %	Optimal placement (x,y)	Optimal gain	Cost function J
Continuous	100	100	(0.50,0.50)	0.425	3.244
Discrete location	85	55	(3/5, 3/5)	0.470	3.564
Percent change					9.8 %

Single actuator/sensor for 11 modes. The optimal location for the local minima is shown in Fig.2.11, which is consistent with results of Xu et al.. Note that the optimal discrete location of the grid is not the one closest to that minimum; in fact, it is closer to another local minimum. Fig.2.10 is a plot of the cost function for a constant gain. This plot is not as simple as the plot for one mode. It was necessary to search all of the local

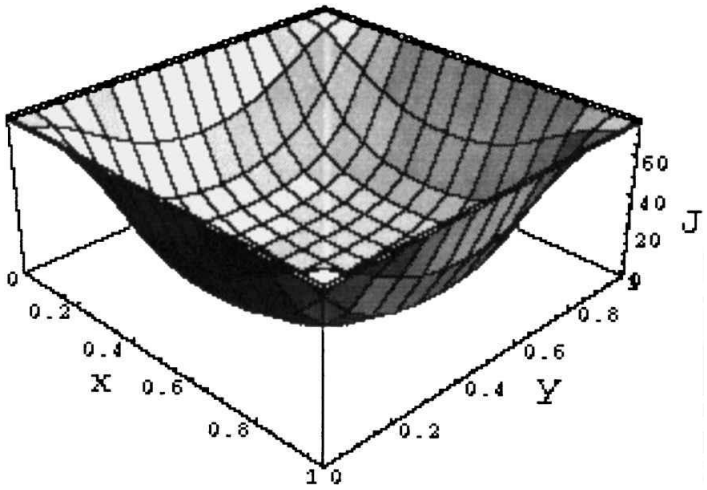

Figure 2.8: Cost function J with respect to single actuator/sensor placement, 1 mode, gain = 0.160.

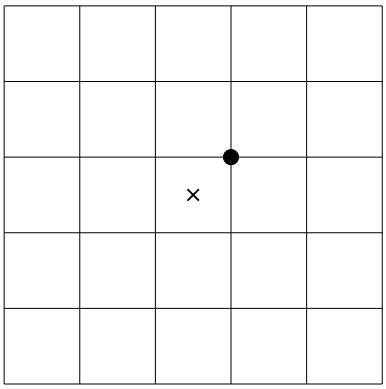

Figure 2.9: Actuator/sensor placement for one mode: •, $J(0.6,0.6) = 3.564$ and gain = 0.106; ×, $J(0.5,0.5) = 3.244$ and gain = 0.125.

minima to find the optimal grid-line solution, and it does not necessarily exist around the absolute minimum.

Table 2.2: One actuator/sensor, 11-mode case

Design type	Convergence, %	Optimal convergence, %	Optimal placement (x,y)	Optimal gain	Cost function J
Continuous	100	40	(0.79,0.82)	0.264	45.468
Discrete location	75	45	(4/5, 3/5)	0.279	45.775
Percent change					0.6 %

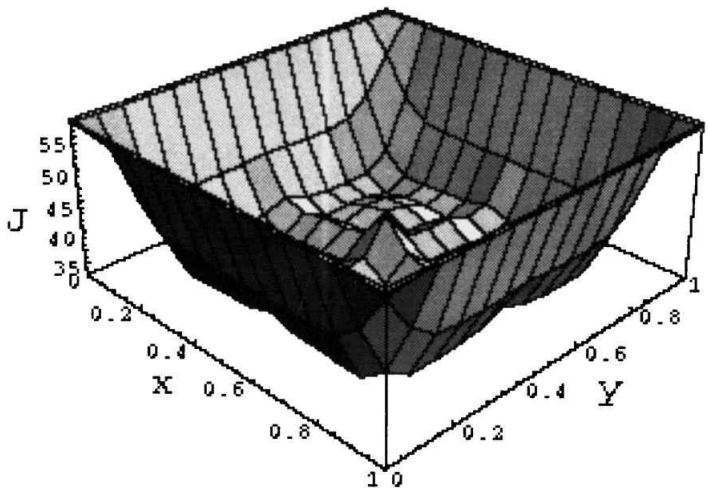

Figure 2.10: Cost function J with respect to single actuator/sensor placement, 11 mode, gain = 0.160.

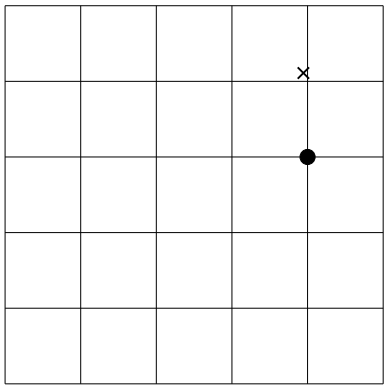

Figure 2.11: Actuator/sensor placement for one mode: •, $J(0.8,0.6) = 45.775$ and gain = 0.279; ×, $J(0.790,0.825) = 45.468$ and gain = 0.264.

11 actuators/sensors for 11 modes. The number of actuators is equal to the number of modes in the structural model. This problem was chosen because it is the case with the most variables to optimize. There are 33 optimization variables, 22 of which are integer variables. As in the preceding example, the control penalty is $R = 10$. The nonlinear-programming algorithm is executed with 20 computer-generated random initial values for the optimization variables. The noninteger example shown in Fig.2.12 is again consistent with Xu et al.. For this example, the algorithm converged to the grid pattern 9 of 20 times. Because of the increasing number of combinations and 100 possible interior points to choose from, the optimal discrete location, as shown in Fig.2.13 was found only once. Because of the restrictions on ac-

tuators/sensors placement, the range of gains was increased. In general, it is advantageous for controllers not to fall on mode lines where a mode would be uncontrollable and unobservable; this greatly affected the placement and gains of the present controllers, because several mode lines come very close to the grid lines.

Table 2.3: Case of 11 actuators/sensors, 11 modes

Design type	Convergence, %	Optimal convergence, %	Optimal placement (x,y)	Optimal gain	Cost function J
Continuous	100	10	(0.20,0.20)	0.190	5.873
			(0.20,0.79)	0.192	
			(0.79,0.20)	0.192	
			(0.81,0.80)	0.192	
			(0.16,0.50)	0.199	
			(0.84,0.50)	0.195	
			(0.50,0.84)	0.192	
			(0.50,0.16)	0.199	
			(0.48,0.58)	0.192	
			(0.53,0.53)	0.208	
			(0.58,0.48)	0.192	
Discrete location	40	5	(1/11, 2/11)	0.281	7.614
			(2/11, 9/11)	0.178	
			(9/11, 8/11)	0.168	
			(9/11, 2/11)	0.221	
			(5/11, 1/11)	0.275	
			(4/11, 9/11)	0.221	
			(9/11, 4/11)	0.246	
			(1/11, 5/11)	0.215	
			(6/11, 5/11)	0.206	
			(8/11, 6/11)	0.194	
			(4/11, 3/11)	0.227	
Percent change					29.6 %

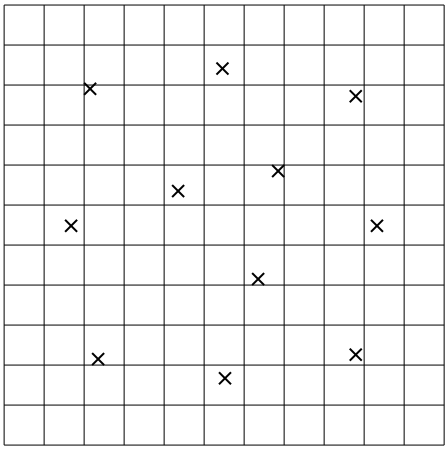

Figure 2.12: Optimal placement for 11 actuators/sensors for 11 modes where $J = 5.873$ and gains = {0.190, 0.192, 0.192, 0.192, 0.192, 0.192, 0.195, 0.195, 0.199, 0.199, 0.208}.

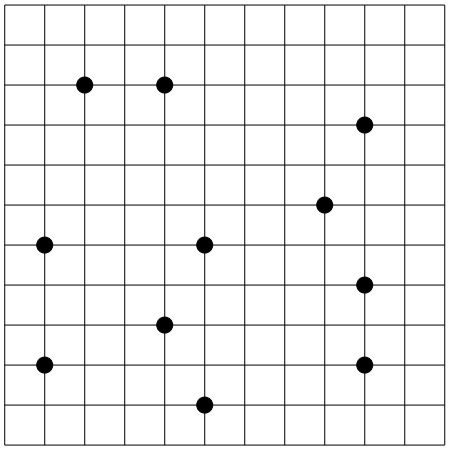

Figure 2.13: Optimal placement for 11 actuators/sensors for 11 modes where $J = 7.614$ and gains = {0.168, 0.178, 0.194, 0.206, 0.215, 0.221, 0.221, 0.227, 0.246, 0.275, 0.281}.

Chapter 3

Problem statement

VARIOUS control strategies can be used to control the vibration of plates. They can be aimed specifically at controlling the kinetic energy of the plate (active vibration control, AVC) or the sound radiation (active structural acoustic control, ASAC). If a reference signal is not available, control strategies are limited to the use of feedback controllers.These can vary greatly in complexity.
Decentralized, static gain control is the simplest form of feedback control. If it is applied in a stable system where the sensors and actuators are colocated and dual, then stability is, in theory, guaranteed. In a practical situation, it can have the extra advantage that no connections are required between different control locations and/or a central processing unit and that actuator, sensor and controller could be produced as identical modular units.
It is also known that direct feedback from velocity sensors to collocated ideal force actuators adds damping to a structure and is unconditionally stable, even for multiple channels. While velocity signals may be derived relatively easily from accelerometers above a certain frequency, the notion of an ideal point force is rarely realizable since there is generally no other structure to react such a force off.
However, as there are sensors and actuators with a very fast dynamics, such as piezoceramics, model of instantaneous force can be justified, and since the purpose of the research is to find the optimal locations on the structure where these forces have to be applied, a model that excludes the dynamics of sensors and actuators is fully accounted for by this type of analysis.

In light of this, consider the following hypothesis:

(i) The number of sensors is equal to the number of actuators. Call it N_{sa}.

(ii) Sensors and actuators are collocated.

(iii) The control is decentralized, so $\mathbf{G} = \text{diag}\{g_i\}$.

The controllers will be optimized for difference performance measures: the kinetic energy of the plate or the sound power radiated into the far field. The actuators are assumed to be ideal point force actuators, and the sensors ideal velocity sensors.

So, according to what stated in Eq.(1.3), the purpose is to find

$$\min J(\mathbf{x}_{sa}, \mathbf{G}) \rightarrow \mathbf{x}^*_{sa}, \mathbf{G}^* \tag{3.1}$$

where $\mathbf{x}_{sa}$ are now the coordinates of the collocated sensors/actuators.

3.1 Structural model

The model of the structure is fully described by Dozio [3], exployting a Ritz-based approach, due to its conceptual simplicity, wide flexibility, high reliability and computational efficiency. The Ritz tecnique has been developed with the aim of providing an unified framework for general plate analysis which can be accurate, efficient and easy for computer implementation. The goal is to investigate the dynamic response of plates which may be subject to various complicating factors, thus extending the potential of the method. Several effects representing practical situations are considered, including in-plane loads, elastically restrained edges, rigid/elastic concentrated masses, intermediate line and point supports or their combinations.

3.1.1 Ritz formulation

Consider a thin rectangular orthotropic plate of Fig.3.1, with length a and width b lying in the (x, y) plane. The plate may be subjected to various complicating external conditions. Normal displacement of the plate is indicated by $w = w(x, y, t)$, where the origin of the (x, y) coordinate system is located at the plate center.

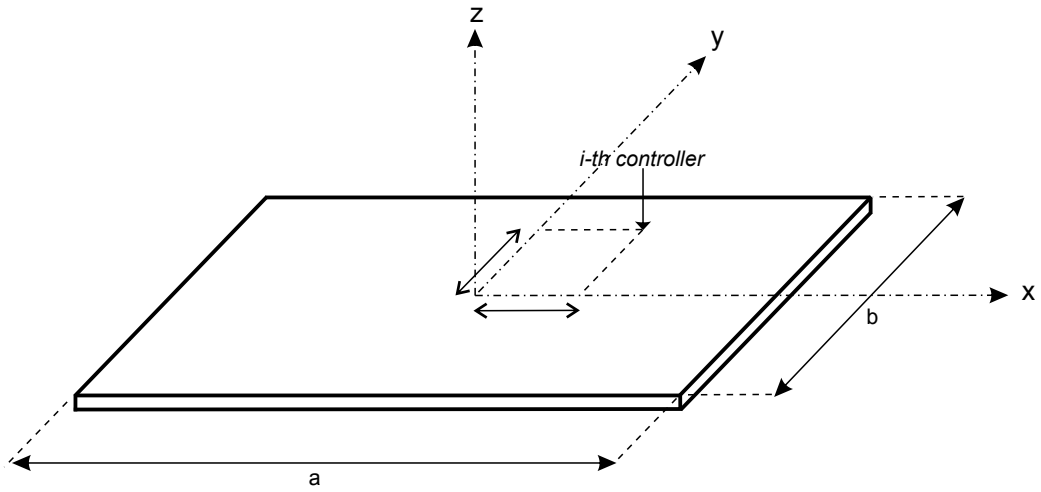

Figure 3.1: Rectangular plate lying in the (x, y) plane.

Throughout the remainder of the thesis, the counterclockwise four-letter symbolic notation introduced by Leissa [7], is used for describing classical boundary conditions for each edge:

(i) S = simply supported: zero deflection and free rotation.

(ii) C = clamped: zero deflection and zero rotation.

(iii) F = free: free deflection and free rotation.

Consider now the non-dimensional coordinates:

$$\xi = \frac{2x}{a}, \quad \eta = \frac{2y}{b}, \tag{3.2}$$

The Ritz approximation is employed by assuming the following solution:

$$w(\xi, \eta, t) = W(\xi, \eta)\mu(t) \tag{3.3}$$

where

$$W(\xi, \eta) = \sum_{m=1}^{M} \sum_{n=1}^{N} \Phi_m(\xi)\Phi_n(\eta) \tag{3.4}$$

with the admissible functions proposed by Beslin and Nicolas [2]:

$$\Phi_m(\xi) = sin(a_m\xi + b_m)sin(c_m\xi + d_m) \tag{3.5}$$

where the coefficients a_i, b_i, c_i and d_i can be selected according the boundary conditions, as proposed by Dozio [3]. The functions $\Phi_n(\eta)$ are defined accordingly to Eq. (3.5), where ξ and m are replaced by η and n, respectively.
Equation (3.3) can be conveniently vritten in matrix form as the scalar product of a line vector of Ritz shapes at position (ξ, η),

$$\mathbf{W}(\xi, \eta) = \lfloor W_{11}(\xi, \eta) \quad W_{12}(\xi, \eta) \quad \dots \quad W_{MN}(\xi, \eta) \rfloor \tag{3.6}$$

and a column vector with the generalized coordinates

$$\boldsymbol{\mu}(t) = [\mu_{11} \quad \mu_{12} \quad \dots \quad \mu_{MN}]^T \tag{3.7}$$

thus:

$$w(\xi, \eta, t) = \mathbf{W}(\xi, \eta)\boldsymbol{\mu}(t) \tag{3.8}$$

3.1.2 Dynamic Equations

Once selected the material properties, the plate dimensions, the boundary conditions and the other complicating factors on the plate (look Appendix A), the model ends up with the complete Mass and Stiffness matrices of the plate.

$$\mathbf{M}_s \qquad \mathbf{K}_s \tag{3.9}$$

This matrices have dimensions of $(M \cdot N \times M \cdot N)$, where M and N are the orders of the series expansion for the Ritz functions on x and y direction. After selecting the number of sensor/actuators with which perform the numerical optimization, N_{sa}, is possible to write the dynamic equation in matricial form, for the generalized coordinates $\boldsymbol{\mu}$, including the ideal point force $F(\xi, \eta, t)$, acting on the plate, induced by the actuators at points (ξ_{sa},η_{sa}). According the Principle of Virtual Work, the equation of motion can be written as:

$$\mathbf{M}_s \ddot{\boldsymbol{\mu}}(t) + \mathbf{K}_s \boldsymbol{\mu}(t) = \mathbf{F}(\xi, \eta, t) = \mathbf{b}\mathbf{u}(t) \tag{3.10}$$

where $\mathbf{u}(t)$ is the vector of actuator forces, $\mathbf{M}_s$ and $\mathbf{K}_s$ are sparse matrix resulting from the routine, and $\mathbf{b}$ is the matrix containing the Ritz functions evaluated at the controllers locations:

$$\mathbf{b}_{(M \cdot N, N_{sa})} = \begin{bmatrix} \mathbf{W}(\xi_1, \eta_1)^T & \mathbf{W}(\xi_2, \eta_2)^T & \dots & \mathbf{W}(\xi_{N_{sa}}, \eta_{N_{sa}})^T \end{bmatrix} \tag{3.11}$$

The problem is transformed in modal coordinates in order to diagonalize and simplify the numerical calculations.
The resulting eigenproblem, even when it is large since many functions are used in the Ritz approximation, Eq.(3.4), can be solved numerically in a very efficient way with a MATLAB function. [1]

[1] Using, for example, iterative projection methods of Arnoldi type. An algorithmic

After computing eigenvalues and eigenvectors, a small amount of damping, ζ, is included in the response of the modes. Beeing $\mathbf{q}(t)$ the vector of modal coordinates, the new matrix formulation of the problem becomes:

$$\ddot{\mathbf{q}}(t) + \mathrm{Diag}\{2\zeta_i\omega_i\}\dot{\mathbf{q}}(t) + \mathrm{Diag}\{\omega_i^2\}\mathbf{q}(t) = \mathbf{U^T b u}(t) \tag{3.12}$$

where ω_i are the eigenvalues of the plate, $\mathbf{U}$ is the mass-normalized eigenvectors matrix, and $\mathbf{q}$, $\dot{\mathbf{q}}$ and $\ddot{\mathbf{q}}$ are, respectively, vectors of the modal amplitude, modal velocity and modal acceleration, such that $\boldsymbol{\mu}(t) = \mathbf{U}\mathbf{q}(t)$.

For direct output velocity feedback control, the n-dimensional measurement vector $\mathbf{y}(t)$ is given by

$$\mathbf{y}(t) = \mathbf{c}\dot{\boldsymbol{\mu}}(t) = \mathbf{c}\mathbf{U}\dot{\mathbf{q}}(t) \tag{3.13}$$

where $\mathbf{c}$ is the placement matrix

$$\mathbf{c}_{(N_{sa}, M\cdot N)} = \begin{bmatrix} \mathbf{W}(\xi_1, \eta_1) \\ \mathbf{W}(\xi_2, \eta_2) \\ \vdots \\ \mathbf{W}(\xi_{N_{sa}}, \eta_{N_{sa}}) \end{bmatrix} = \mathbf{b^T} \tag{3.14}$$

The control force is proportional to the output measurements

$$\mathbf{u}(t) = -\mathbf{G}\mathbf{y}(t) \tag{3.15}$$

where $\mathbf{G}$ is the unknown time-invariant gain matrix.

variant of the Arnoldi process called the Implicity Restarted Arnoldi method is used as implemented in MATLAB via the built-in *eigs* function. To have a look of the computation efficiency of the method refer to Dozio [3], where density of the mass and stiffness matrices and execution effort taken for calculating the first ten frequencies of the mated eigenproblem are presented.

The kinetic energy of the plate at any particular point in time, can be calculated as:

$$\begin{aligned} E_k = \frac{1}{2}\int_0^a \int_0^b \rho h \dot{w}(x,y)^2 \, dA &= \frac{1}{2}\frac{\rho hab}{4}\int_0^1 \int_0^1 \dot{w}(\xi,\eta)^2 \, d\xi \, d\eta \\ &= \frac{1}{2}\frac{\rho hab}{4}\int_0^1 \int_0^1 \dot{\boldsymbol{\mu}}^{\boldsymbol{T}} \mathbf{W}^{\mathbf{T}} \mathbf{W} \dot{\boldsymbol{\mu}} \, d\xi \, d\eta \\ &= \frac{1}{2}\dot{\mathbf{q}}^{\mathbf{T}} \mathbf{U}^{\mathbf{T}} \underbrace{\frac{\rho hab}{4}\int_0^1 \int_0^1 \mathbf{W}^{\mathbf{T}} \mathbf{W} \, d\xi \, d\eta}_{\mathbf{M_s}} \mathbf{U}\dot{\mathbf{q}} \\ &= \frac{1}{2}\dot{\mathbf{q}}^{\mathbf{T}} \underbrace{\mathbf{U}^{\mathbf{T}} \mathbf{M_s} \mathbf{U}}_{\mathbf{I}} \dot{\mathbf{q}} \end{aligned} \tag{3.16}$$

So, for the chosen mode shape rapresentation, as the matrix $\mathbf{U}$ contains mass-normalized eigenvectors, the performance index for the vibration of the plate can be calculated as the sum of the squared modal velocities.

$$J_{ke} = \frac{1}{2}\dot{\mathbf{q}}^{\mathbf{T}}(t)\dot{\mathbf{q}}(t) \tag{3.17}$$

3.1.3 State space representation of the structural model

It is convenient at this point to express Eqs.(3.12) to (3.15) as a first-order state space equation:

$$\begin{Bmatrix} \dot{\mathbf{q}} \\ \ddot{\mathbf{q}} \end{Bmatrix} = \underbrace{\begin{bmatrix} 0 & \mathbf{I} \\ -\text{Diag}\{\omega_i^2\} & -\text{Diag}\{2\zeta_i\omega_i\} \end{bmatrix}}_{\mathbf{A_s}} \begin{Bmatrix} \mathbf{q} \\ \dot{\mathbf{q}} \end{Bmatrix} + \underbrace{\begin{bmatrix} 0 \\ \mathbf{U^T b} \end{bmatrix}}_{\mathbf{B_s}} \mathbf{u} \tag{3.18}$$

$$\mathbf{y}(t) = \underbrace{\begin{bmatrix} 0 & \mathbf{cU} \end{bmatrix}}_{\mathbf{C_s}} \begin{Bmatrix} \mathbf{q} \\ \dot{\mathbf{q}} \end{Bmatrix} \tag{3.19}$$

Summarizing:

$$\begin{cases} \dot{\mathbf{x}}_\mathbf{s}(t) = \mathbf{A_s x_s}(t) + \mathbf{B_s u}(t) \\ \mathbf{y}(t) = \mathbf{C_s x_s}(t) \\ \mathbf{u}(t) = -\mathbf{G y}(t) \end{cases} \tag{3.20}$$

3.2 Radiation model

For the purpose of estimating their sound radiation characteristics, many structures of practical interest may be modelled sufficiently accurately as rectangular, uniform, flat plates. For example, consider walls and floor of buildings, machinery casings, part of vehicle, plane and satellite shells and hulls and bulkheads of ships. The natural modes of vibration of such plates vary in shape and frequency with their edge conditions and it is not strictly correct to consider the modes of isolated panels when they are dynamically coupled to contiguous structures, except in a purely mathematical sense as component modes of larger systems. However, the isolated rectuangular panel forms a useful starting point for modeling the radiation behaviour.
The modeling of sound radiation of a plate in an infinite baffle is usually done in one or two ways, either by analyzing modal radiation or the so-called radiation modes.

3.2.1 Sound Radiation formulation

Referring to the book by Fahy and Gardonio, the time-averaged total sound power radiation of a baffled plate can be formulated in terms of the far-field sound intensity over a hemisphere surface positioned with reference to the centre of the panel. For harmonic vibration,

$$\bar{P}(\omega) = \frac{1}{2}\int_0^a \int_0^b \mathrm{Re}\left(v(x,y,\omega)^* \tilde{p}(x,0,y,\omega)\right)\, dx\, dy \tag{3.21}$$

where v is the transverse velocity of the plate determined through mode shape terms $v(x,y) = \lfloor \boldsymbol{\phi}(x,y) \rfloor \{\mathbf{v}\}$, $*$ denotes the complex conjugate, and the surface acoustic pressure $\tilde{p}$ can be written in terms of the normal surface velocity through the Rayleigh integral as

$$p(x,0,y,\omega) = \frac{j\omega\rho_0}{2\pi}\int_0^a \int_0^b v(x',y',\omega)\frac{e^{-jkR}}{R}\, dx'\, dy' \tag{3.22}$$

where, $R = \sqrt{(x-x')^2 + (y-y')^2}$ is the distance between the point (x,y) where the sound pressure is estimated and the vibrating surface element at (x', y'). Substituting Eq.(3.22) into Eq.(3.21), the time-average total sound power is given by the quadruple integral, which, using the vector expression

for $v(x,y)$ becomes

$$\bar{P}(\omega) = \frac{1}{2}\Re\Big\{\frac{j\omega\rho_0}{2\pi}\int_0^a\int_0^b\int_0^a\int_0^b \{\mathbf{v}\}^H \lfloor\boldsymbol{\phi}(x,y)\rfloor^T \times\frac{e^{-jkR}}{R}\lfloor\boldsymbol{\phi}(x',y')\rfloor\{\mathbf{v}\}\Big\}\,dx'\,dy'\,dx\,dy \tag{3.23}$$

where H denotes the Hermitian transpose (transpose and conjugate). Since $je^{-jkR}/R = j(\cos kR - j\sin kR)/R$, and because $\{\mathbf{v}\}^H\{\mathbf{v}\}$ is bound to be real positive, this expression can be rewritten as

$$\bar{P}(\omega) = \frac{\omega\rho_0}{4\pi}\{\mathbf{v}\}^H\left(\int_0^a\int_0^b\int_0^a\int_0^b \lfloor\boldsymbol{\phi}(x,y)\rfloor^T\frac{\sin kR}{R}\lfloor\boldsymbol{\phi}(x',y')\rfloor\,dx'\,dy'\,dx\,dy\right)\{\mathbf{v}\} \tag{3.24}$$

or, alternatively, in matrix form

$$\bar{P}(\omega) = \{\mathbf{v}\}^H[\mathbf{A}(\omega)]\{\mathbf{v}\} \tag{3.25}$$

where $[\mathbf{A}]$ is an $(n\times n)$ matrix (n represents the number of structural modes), which is normally referred to as the Power Transfer Matrix.

3.2.2 Formulation in terms of Elementary Radiators

Although the formulation presented above seems to be quite simple and neat, the derivation of the quadruple integrals for the elements in the power transfer matrix $[\mathbf{A}]$ is relatively complex and involver. An alternative non-modal approach based on the elementary radiators is therefore presented as described by Fahy and Gardonio [5].

As shown in Fig.3.2, the baffled panel is divided into a grid of R rectangular elements whose transverse vibrations are specified in terms of the

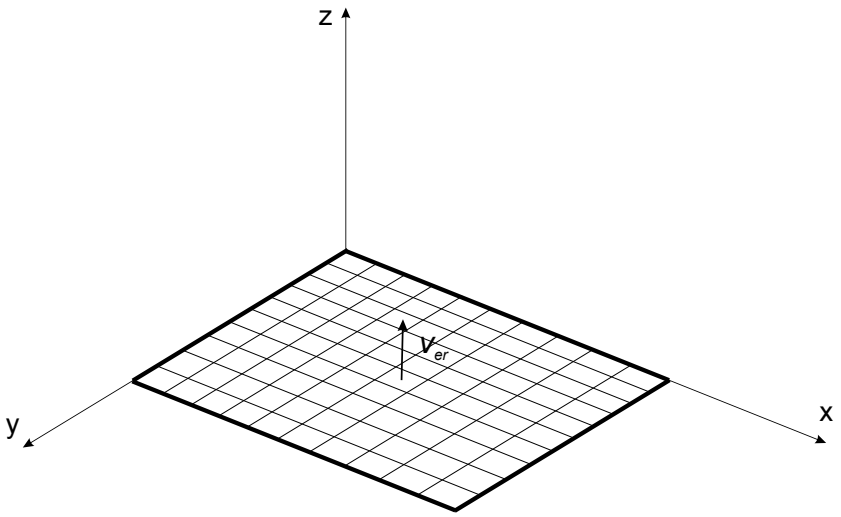

Figure 3.2: Subdivision of a panel into elementary radiators.

velocities v_{er} at their centre positions so that, assuming time-harmonic motion, the overall vibration of the panel can be described by the following column vector of complex amplitudes:

$$\{\mathbf{v}_e\} = \lfloor v_{e1} \quad v_{e2} \quad \dots \quad v_{eR} \rfloor^T \tag{3.26}$$

If the amplitudes of the sound pressures acting on each element are also grouped into a column vector, as

$$\{\mathbf{p}_e\} = \lfloor p_{e1} \quad p_{e2} \quad \dots \quad p_{eR} \rfloor^T , \tag{3.27}$$

assuming that the dimensions of the element are small compared with both the structural wavelength and the acoustic wavelength, the total radiated sound power can then be expressed as the summation of the powers radiated by each element expressed as $\bar{P}_{er} = 1/2 A_e \mathrm{Re}\left(v_{er}^* p_{er}\right)$, so that

$$\bar{P}(\omega) = \sum_{r=1}^{R} \frac{1}{2} A_e \mathrm{Re}\left(v_{er}^* p_{er}\right) = \frac{S}{2R} \mathrm{Re}\left(\{\mathbf{v_e}\}^H \{\mathbf{p_e}\}\right) \tag{3.28}$$

where A_e and S are respectively the areas of eah element and of the whole panel. The pressure on each element is generated by the vibrations of all elements of the panel. Assuming that $\sqrt{A_e} \ll \lambda$, where λ is the acoustic wavelength, Eq.(3.22) gives

$$p_{ei}(x_i, y_i) = \frac{j\omega\rho_0 A_e e^{-jkR_{ij}}}{2\pi R_{ij}} v_{ej}(x_j, y_j) \tag{3.29}$$

with R_{ij} the distance between the centres of the i-th and j-th elements. The vector of sound pressures can therefore be expressed by the impedence matrix relation

$$\{\mathbf{p_e}\} = [\mathbf{Z}]\{\mathbf{v_e}\} \tag{3.30}$$

where $[\mathbf{Z}]$ is the matrix incorporating the point and transfer acoustic impedence terms over the grid of elements into which the panel has been subdivided: $Z_{ij}(\omega) = (j\omega\rho_0 A_e/2\pi R_{ij})e^{-jkR_{ij}}$. Note that, because of reciprocity, the impedance matrix $[\mathbf{Z}]$ is symmetric, in which case $[\mathbf{Z}] = [\mathbf{Z}]^T$. Substituting Eq.(3.30) into the expression for the total radiated sound power given in Eq.(3.28), we obtain

$$\bar{P}(\omega) = \frac{S}{2R}\mathrm{Re}\left(\{\mathbf{v_e}\}^H [\mathbf{Z}]\{\mathbf{v_e}\}\right) \tag{3.31}$$

which, because $[\mathbf{Z}]$ is symmetric, can be rewritten as

$$\bar{P}(\omega) = \frac{S}{4R}\{\mathbf{v_e}\}^H \left([\mathbf{Z}] + [\mathbf{Z}]^H\right)\{\mathbf{v_e}\} = \{\mathbf{v_e}\}^H [\mathbf{R}]\{\mathbf{v_e}\} \tag{3.32}$$

The matrix [**R**] is defined as the Radiation Resistance Matrix for the elementary radiators which, for the baffled panel, is given by

$$[\mathbf{R}] = \frac{S}{2R}\mathrm{Re}\left([\mathbf{Z}]\right) = \frac{S}{4R}\left([\mathbf{Z}] + [\mathbf{Z}]^H\right)$$
$$= \frac{\omega^2\rho_0 A_e^2}{4\pi c}\begin{bmatrix} 1 & \frac{\sin(kR_{12})}{kR_{12}} & \cdots & \frac{\sin(kR_{1R})}{kR_{1R}} \\ \frac{\sin(kR_{21})}{kR_{21}} & 1 & & \\ \vdots & \cdots & \ddots & \cdots \\ \frac{\sin(kR_{R1})}{kR_{R1}} & & & 1 \end{bmatrix} \tag{3.33}$$

where ω is the circular frequency in rad/s , ρ_0 is the density of the air, A_e is the area associated with the discretized radiator, c is the speed of sound in air, k is the wave number (ω/c), and R_{ij} is the distance between the center of the i-th and j-th velocity locations.
Since $R_{ij} = R_{ji}$, the radiation matrix is symmetric, and as found for the power transfer matrix [**A**], it is also positive definite since the quadratic expression for the power radiation in Eq.(3.32) is bound to be positive.

The agreement between the two models is generally good provided that the dimensions of the discrete elements are both much less than the acoustic wavelength and the modal wavelengths in the panel, i.e., much greater than the Cartesian components of the plate modal wavenumber vectors.
In general, the modal approach can be used for regular shapes and common boundary conditions such that analytical expressions can be derived for the mode shapes. In the elementary radiator model, the velocities of the elementary radiators can be derived using general Ritz functions (or Finite Elements analysis) which enables the study of non-uniform, baffled plates of complex geometry having non-classic boundary conditions which can result from interfaces with other flexible structures, that are the basis of this work.

3.2.3 Radiation modal expansion (RME)

Before assembling the augmented plant model, a model which incorporates the physics associated with the structural acoustic coupling must be developed. This dynamic model is used to "filter" the discrete velocity measurements such that the rms sound power radiated from the structure can be estimated.
Since the radiation matrix is also a function of frequency, a singular value

decomposition can be performed to determine the dominant radiation modes of the system at each frequency. Singular value decomposition is performed at frequency ω_i as follows:

$$\mathbf{R}(\omega_i) = \mathbf{u}\mathbf{\Sigma}\mathbf{u}^{\mathbf{H}} \tag{3.34}$$

where $\mathbf{u}$ is an $(R \times R)$ matrix whose columns are the normalized radiations modes of the matrix at frequency ω_i, and $\mathbf{\Sigma}$ is an $(R \times R)$ diagonal matrix whose elements are the singular values, decreasing monotonically along the diagonal. The magnitude fo the j-th diagonal element, σ_j, of $\mathbf{\Sigma}$ determines the relative importance of the j-th radiation mode compared to other radiation modes.

In order to predict the total power radiated over some bandwidth, the characteristics of the $\mathbf{R}$ matrix must be modeled over the bandwidth. Thus, for an $(R \times R)$ matrix, a total of R^2 transfer functions must be modeled fitting the trend of the singular values versus frequency. This level of complexity is impractical for control system design, since the order of the dynamic compensator is typically the same order as the augmented plant. "Optimal" controllers cannot be improved by going to higher orders.

A special curve fitting technique, called Radiation Modal Expansion (RME) is introduced, as presented by Gibbs et al. [6], which provides a reasonable approximation to the dynamics of the $\mathbf{R}$ matrix using a small fraction of the original number of states. This technique exploits the "nesting" property of the radiation modes: the space spanned by the *significant* radiating modes at frequency below some arbitrary maximum frequency of the bandwidth ω_{max} is a subspace of the space spanned by the radiating modes at the frequency ω_{max}. Thus, the set of singular vectors at ω_{max} corresponding to the significant radiating modes can be used as a basis to describe the radiation at any frequency below ω_{max}.

The key to incorporating the essential physics of structural acoustic coupling rests in curve fitting the dominant radiating modes over the bandwidth, which is performed using the RME techinque outlined in this section. In this technique, the significant radiation modes at the upper frequency of the bandwidth of interest are used as a basis to curve fit the properties of the $\mathbf{R}$ matrix over the entire bandwidth. The amplitude-weighting coefficients are determined by the radiated power of each respective normalized radiation mode shape at each frequency ω over the bandwidth as follows:

$$\Psi_i^2(\omega) = \mathbf{u^H}_{i,max}\mathbf{R}(j\omega)\mathbf{u}_{i,max} \tag{3.35}$$

where $\Psi_i^2(\omega)$ is the radated power of the i-th radiating mode (shape determined at ω_{max}), and $\mathbf{u}_{i,max}$ is the i-th radiating mode shape determined at ω_{max}. A plot of the amplitude-weighting coefficients $\Psi_i(\omega)$ for the first six radiation modes is shown in Fig. 3.3.

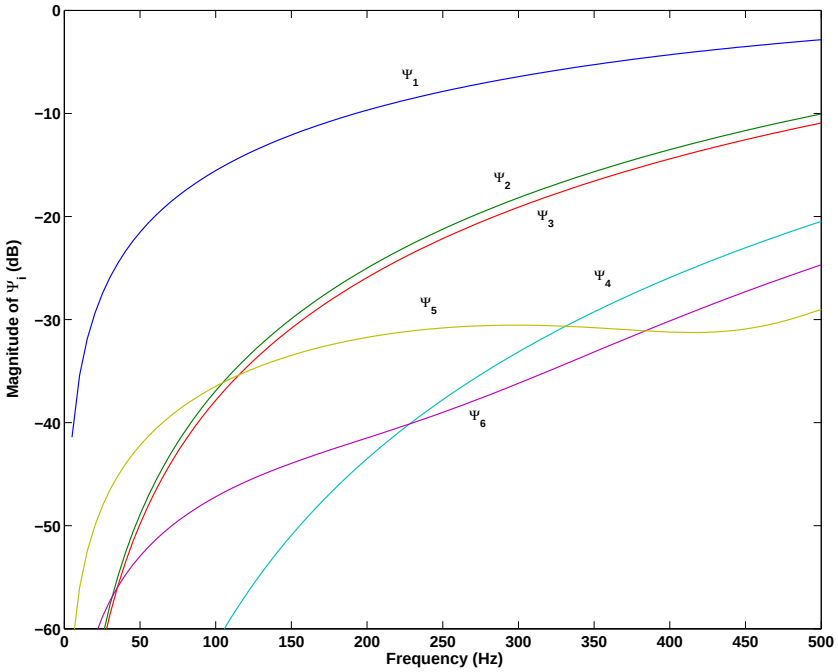

Figure 3.3: Radiation modal expansion coefficients (Ψ_i) for the first six radiation modes. The model is calculated with a generic rectangular geometry in air at standard conditions, up to 500 Hz.

In order to create a model of the RME system it is only necessary to curve fit in frequency [2] the dynamics described by the RME coefficients, Ψ_i, shown in Fig.3.3. An example of curve fitting with the *fitmagfrd* function of MATLAB is shown in Fig.3.4.
Comparing the two figures do not notice visible differences between the trend

[2]The curve fitting of the frequency response is performed with a MATLAB function *fitmagfrd* that needs as input the frequencies and the magnitude of the response and returns the corresponding sate space matrices . For more details refer to the help of MATLAB.

of the model and the MATLAB fitting, despite using relatively low order transfer functions: for the first 6 radiation modes, until 500 Hz, 3$^{\text{rd}}$ order transfer functions are sufficient.

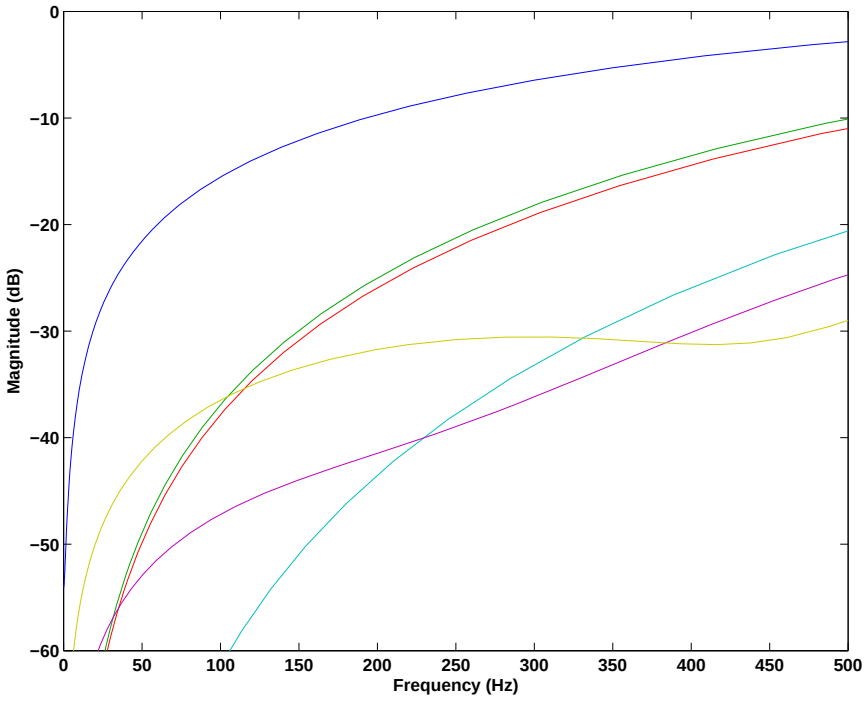

Figure 3.4: Fitting of the radiation modal expansion coefficients (Ψ_i) for the first six radiation modes, up to 500 Hz, with 3$^{\text{rd}}$ order radiation filters.

3.2.4 State space representation of the acoustic model

At the end of the fitting operation, the MATLAB routine eds up with the following state space matrix for the radiation filters, one for wach filter, which dimensions depends from the order of the transfer functions adopted in the *fitmagfrd* procedure:

$$\mathbf{A}_{rf} \quad \mathbf{B}_{rf} \quad \mathbf{C}_{rf} \quad \mathbf{D}_{rf} \tag{3.36}$$

But in order to rewrite the radiation model in a state space representation, the input to each radiation mode has to be calculated as a function of the modal velocities as:

$$\{\mathbf{v}_e\} = \mathbf{cU}\dot{\mathbf{q}}(t) \tag{3.37}$$

where $\mathbf{c}$ is the placement matrix of Eq.(3.14), evaluated in the coordinates of each elementary radiatior velocity (ξ_e, η_e). At this point, applying the frequency dependent filters, the sate space model can be derived for each radiation filter:

$$\begin{cases} \dot{\mathbf{a}}_{rfi} = \mathbf{A}_{rfi}\mathbf{a}_{rfi} + \mathbf{B}_{rfi}\mathbf{u^H}_i\mathbf{cU}\dot{\mathbf{q}} \\ \mathbf{y}_{rfi} = \mathbf{C}_{rfi}\mathbf{a}_{rfi} + \mathbf{D}_{rfi}\mathbf{u^H}_i\mathbf{cU}\dot{\mathbf{q}} \end{cases} \tag{3.38}$$

and then, incorporating all the radiation modes considered in the model, the representation becomes:

$$\begin{Bmatrix} \dot{\mathbf{a}}_{rf1} \\ \dot{\mathbf{a}}_{rf2} \\ \vdots \\ \dot{\mathbf{a}}_{rfN} \end{Bmatrix} = \underbrace{\begin{bmatrix} \mathbf{A}_{rf} & 0 & \dots & 0 \\ 0 & \mathbf{A}_{rf2} & & \vdots \\ \vdots & & \ddots & 0 \\ 0 & \dots & 0 & \mathbf{A}_{rfN} \end{bmatrix}}_{\mathbf{A}_{ac}} \begin{Bmatrix} \mathbf{a}_{rf1} \\ \mathbf{a}_{rf2} \\ \vdots \\ \mathbf{a}_{rfN} \end{Bmatrix} + \underbrace{\begin{bmatrix} \mathbf{B}_{rf1}\mathbf{u^H}_1\mathbf{cU} \\ \mathbf{B}_{rf2}\mathbf{u^H}_2\mathbf{cU} \\ \vdots \\ \mathbf{B}_{rfN}\mathbf{u^H}_N\mathbf{cU} \end{bmatrix}}_{\mathbf{B}_{ac}} \dot{\mathbf{q}} \tag{3.39}$$

$$\mathbf{y_{ac}} = \begin{Bmatrix} \mathbf{y}_{rf1} \\ \mathbf{y}_{rf2} \\ \vdots \\ \mathbf{y}_{rfN} \end{Bmatrix} \underbrace{\begin{bmatrix} \mathbf{C}_{rf} & 0 & \dots & 0 \\ 0 & \mathbf{C}_{rf2} & & \vdots \\ \vdots & & \ddots & 0 \\ 0 & \dots & 0 & \mathbf{C}_{rfN} \end{bmatrix}}_{\mathbf{C}_{ac}} \begin{Bmatrix} \mathbf{a}_{rf1} \\ \mathbf{a}_{rf2} \\ \vdots \\ \mathbf{a}_{rfN} \end{Bmatrix} + \underbrace{\begin{bmatrix} \mathbf{D}_{rf1}\mathbf{u^H}_1\mathbf{cU} \\ \mathbf{D}_{rf2}\mathbf{u^H}_2\mathbf{cU} \\ \vdots \\ \mathbf{D}_{rfN}\mathbf{u^H}_N\mathbf{cU} \end{bmatrix}}_{\mathbf{D}_{ac}} \dot{\mathbf{q}} \tag{3.40}$$

which, written in a more compact form becomes:

$$\begin{cases} \dot{\mathbf{a}}_{ac} = \mathbf{A}_{ac}\mathbf{a}_{ac} + \mathbf{B}_{ac}\dot{\mathbf{q}} \\ \mathbf{y}_{ac} = \mathbf{C}_{ac}\mathbf{a}_{ac} + \mathbf{D}_{ac}\dot{\mathbf{q}} \end{cases} \tag{3.41}$$

where $\mathbf{a}_{ac}$ are the states of the radiation filters, the matrix $\mathbf{B_{ac}}$ describes the excitation of the filters as a function of the modal velocities, and $\mathbf{A_{ac}}$ describes the dynamics, $\mathbf{C_{ac}}$ describes the relation between the states of each filter and its output and $\mathbf{D_{ac}}$ is a direct feedthrough matrix of the structural modal velocities to the cost variables.
At this point, an estimation of the sound radiation J_{ac} is possible:

$$J_{ac} = \mathbf{y_{ac}^T}(t)\mathbf{y_{ac}}(t) \tag{3.42}$$

3.3 Global state space representation

An efficient way to simultaneously deal with the structural and the acoustic model, as they are coupled, is embedding them in a global state space representation with a state vector which includes structural modes and acoustic modes. Combining Eqs.(3.20) and (3.46), obtain:

$$\begin{Bmatrix} \dot{\mathbf{q}} \\ \ddot{\mathbf{q}} \\ \dot{\mathbf{a}}_{ac} \end{Bmatrix} = \underbrace{\begin{bmatrix} 0 & \mathbf{I} & 0 \\ -Diag\{\omega_i^2\} & -Diag\{2\zeta_i\omega_i\} & 0 \\ 0 & \mathbf{B}_{ac} & \mathbf{A}_{ac} \end{bmatrix}}_{\mathbf{A}} \begin{Bmatrix} \mathbf{q} \\ \dot{\mathbf{q}} \\ \mathbf{a}_{ac} \end{Bmatrix} + \underbrace{\begin{bmatrix} 0 \\ \mathbf{U^T b} \\ 0 \end{bmatrix}}_{\mathbf{B}} \mathbf{u} \quad (3.43)$$

$$\mathbf{y}_v(t) = \underbrace{\begin{bmatrix} 0 & \mathbf{cU} & 0 \end{bmatrix}}_{\mathbf{C_1}} \begin{Bmatrix} \mathbf{q} \\ \dot{\mathbf{q}} \\ \mathbf{a}_{ac} \end{Bmatrix} \quad (3.44)$$

$$\mathbf{y}_{ac}(t) = \underbrace{\begin{bmatrix} 0 & \mathbf{D}_{ac} & \mathbf{C}_{ac} \end{bmatrix}}_{\mathbf{C_2}} \begin{Bmatrix} \mathbf{q} \\ \dot{\mathbf{q}} \\ \mathbf{a}_{ac} \end{Bmatrix} \quad (3.45)$$

that summarizing become:

$$\begin{cases} \dot{\mathbf{x}}(t) = \mathbf{A}\mathbf{x}(t) + \mathbf{B}\mathbf{u}(t) \\ \mathbf{y}_v(t) = \mathbf{C}_1\mathbf{x}(t) \\ \mathbf{y}_{ac}(t) = \mathbf{C}_2\mathbf{x}(t) \\ \mathbf{u}(t) = -\mathbf{G}\mathbf{y}_v(t) \end{cases} \quad (3.46)$$

Chapter 4

Optimization problem

In the following, an optimal design procedure is developed of the actuator and sensor placements (ξ_{sa}, η_{sa}), and the feedback gains $\mathbf{G}$, that for the *Decentralized constant gain control* considered, constitute a total of $3 \times N_{sa}$ optimization variables.
First, a performance function is chosen that includes both the structural response and the control effort. The standard performance function is

$$J = \frac{1}{2} \int_0^\infty \left(\mathbf{x^T Q x} + \mathbf{u^T R u} \right) \, dt \tag{4.1}$$

where $\mathbf{Q}$ is chosen according to the type of optimization performed, kinetic energy or radiated sound power (look Appendix A for reference), while the control penalty matrix $\mathbf{R}$ is the symple diagonal matrix

$$\mathbf{R} = R \begin{bmatrix} \mathbf{I} & 0 \\ 0 & \mathbf{I} \end{bmatrix}. \tag{4.2}$$

where R varies depending on the type of optimization performed.
Eq.4.1 can be expressed as function of the state vector by substituting the expression $\mathbf{u} = -\mathbf{GCx}$, obtaining

$$J = \frac{1}{2} \int_0^\infty \mathbf{x^T} \underbrace{\left(\mathbf{Q} + \mathbf{C^T G^T R G C} \right)}_{\mathbf{W_G}} \mathbf{x} \, dt \tag{4.3}$$

Introducing the closed loop matrix $\bar{\mathbf{A}} = \mathbf{A} - \mathbf{BGC}$, the state vector can be expressed as function of the initial conditions $\mathbf{x}(0) = \mathbf{x_0}$

$$\mathbf{x}(t) = e^{\bar{\mathbf{A}}t}\mathbf{x_0} \tag{4.4}$$

so obtain a performance index as function of the initial state vector

$$J = \frac{1}{2}\mathbf{x_0^T}\underbrace{\left[\int_0^\infty (e^{\bar{\mathbf{A}}t})^T \mathbf{W_G} e^{\bar{\mathbf{A}}t}\, dt\right]}_{\mathbf{P}}\mathbf{x_0} = \frac{1}{2}\mathbf{x_0^T P x_0} = \frac{1}{2}\,\mathrm{tr}[\mathbf{x_0^T P x_0}] \tag{4.5}$$

which, introducing the property of the trace operator becomes

$$J = \frac{1}{2}\,\mathrm{tr}[\mathbf{P x_0 x_0^T}] = \frac{1}{2}\,\mathrm{tr}[\mathbf{P X_0}] \tag{4.6}$$

At this point, referring to the classical theory of optimal control, the Lagrangian multipliers are introduced, because matrix $\mathbf{P}$ is a solution of a Lyapunov equation. Therefore it must comply with the following constraint:

$$J = \frac{1}{2}\,\mathrm{tr}[\mathbf{P X_0} + \mathbf{\Lambda^T}(\bar{\mathbf{A}}^\mathbf{T}\mathbf{P} + \mathbf{P}\bar{\mathbf{A}} + \mathbf{W_G})] \tag{4.7}$$

This performance function, which is expressed implicitly in terms of actuator and sensor placement vector $\mathbf{x}_{sa}$ (embedded in the matrices $\mathbf{B}$ and $\mathbf{C}$), and the feedback gain matrix $\mathbf{G}$ is used in the following for the optimizaiton problem.
As the optimization variables are non-integer values, the optimization problem can be solved with standard nonlinear-programming techniques. Because the performance function gradients can be found analytically, descent methods can be used to solve this problem. The derivation of the gradients is

shown in the following.
Exploiting the properties of the trace operator, take the partial derivatives of the cost function, and obtain 2 constraint Lyapunov equations (Eq.(4.8)), and 3 equations of gradients with respect to the optimization variables (Eq.(4.9)):

$$\begin{cases} \dfrac{\partial J}{\partial \mathbf{\Lambda}} = \bar{\mathbf{A}}^{\mathbf{T}}\mathbf{P} + \mathbf{P}\bar{\mathbf{A}} + \mathbf{W_G} = 0 \\ \dfrac{\partial J}{\partial \mathbf{P}} = \mathbf{X_0} + \bar{\mathbf{A}}\mathbf{\Lambda} + \mathbf{\Lambda}\bar{\mathbf{A}}^{\mathbf{T}} = 0 \end{cases} \tag{4.8}$$

$$\begin{cases} \dfrac{\partial J}{\partial \mathbf{G}} = -\mathbf{B}^{\mathbf{T}}\mathbf{P}\mathbf{\Lambda}\mathbf{C}^{\mathbf{T}} + \mathbf{R}\mathbf{G}\mathbf{C}\mathbf{\Lambda}\mathbf{C}^{\mathbf{T}} = 0 \\ \dfrac{\partial J}{\partial \mathbf{B}} = -\mathbf{P}\mathbf{\Lambda}\mathbf{C}^{\mathbf{T}}\mathbf{G}^{\mathbf{T}} = 0 \\ \dfrac{\partial J}{\partial \mathbf{C}} = -\mathbf{G}^{\mathbf{T}}\mathbf{B}^{\mathbf{T}}\mathbf{P}\mathbf{\Lambda} + \mathbf{G}^{\mathbf{T}}\mathbf{R}\mathbf{G}\mathbf{C}\mathbf{\Lambda} \end{cases} \tag{4.9}$$

The gradients with respect to the adimensional coordinates (ξ_{sa}, η_{sa}), are subsequently obtained by the chain rule as follows:

$$\frac{\partial J}{\partial \xi_i} = \frac{\partial J}{\partial B_{kl}} \frac{\partial B_{kl}}{\partial b_{rs}} \frac{\partial b_{rs}}{\partial W_{mn}(\xi_i)} \frac{\partial W_{mn}(\xi_i)}{\xi_i} \tag{4.10}$$

where

$$\frac{\partial B_{kl}}{\partial b_{rs}} = \begin{cases} 0, & \text{if} \quad 1 \leq k \leq MN \\ \delta_{(k-MN)r}\delta_{ls}, & \text{if} \quad MN+1 \leq k \leq 2MN \end{cases} \tag{4.11}$$

$$\frac{\partial b_{rs}}{\partial W_{mn}(\xi_i)} = U_{(mn,i)} \tag{4.12}$$

$$\frac{\partial W_{mn}(\xi_i)}{\xi_i} = \{a_m[\cos(a_m\xi_i + b_m)\sin(c_m\xi_i + d_m)] + c_m[\cos(c_m\xi_i + d_m)\sin(a_m\xi_i + b_m)]\} \times \sin(a_n\eta_i + b_n)\sin(c_n\eta_i + d_n) \quad (4.13)$$

After substitution and manipulation, it is found that Eq.(4.10) can be simplified to

$$\frac{\partial J}{\partial \xi_i} = \sum_{k=1}^{MN} \frac{\partial J}{\partial B_{(k+mn)i}} U_{(mn,i)}\{a_m[\cos(a_m\xi_i + b_m)\sin(c_m\xi_i + d_m)] + c_m[\cos(c_m\xi_i + d_m)\sin(a_m\xi_i + b_m)]\} \times \sin(a_n\eta_i + b_n)\sin(c_n\eta_i + d_n) \quad (4.14)$$

where $\mathbf{U}$ is the eigenvectors matrix of the structural dynamic model, and a_m, b_m, c_m and d_m, are the coefficients of the series expansion relative to the actual boundary conditions. In similar way, the partial derivative with respect to the η coordinate is obtained. While for the derivative with respect to the gains, simply assume:

$$\frac{\partial J}{\partial g_i} = \frac{\partial J}{\partial \mathbf{G}_{ii}} \quad (4.15)$$

At this point a set of $3 \times N_{sa}$ gradients value is available for the numerical optimization algorithm.

4.1 Gradient-based numerical optimization

One of the most robust gradient-based optimization techniques is the Davidon-Fletcher-Powell (DFP) algorithm (for more in-depth theory refer to [8]), which is summarized by the flow chart in Fig.4.1.

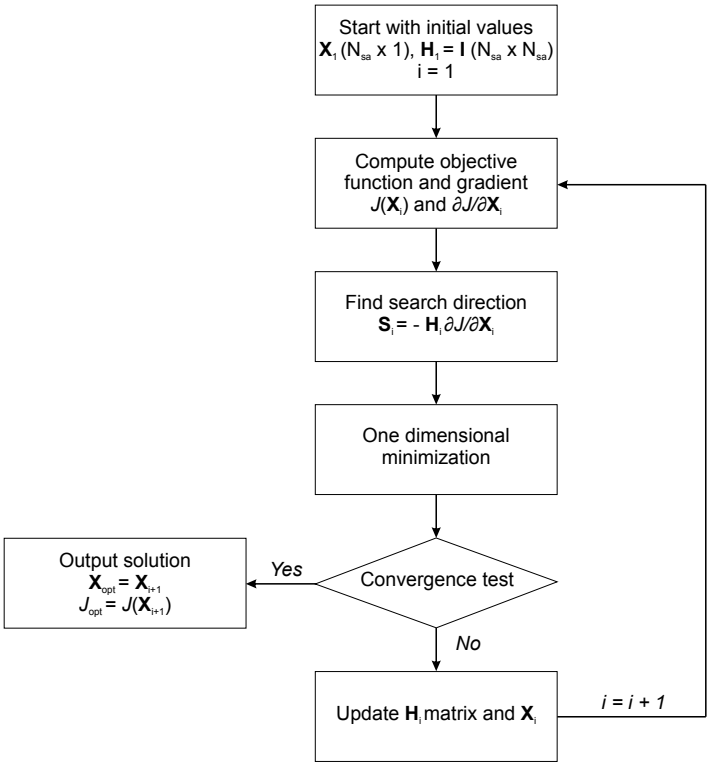

Figure 4.1: Flow chart of the DFP algorithm.

The basic parameters for each iteration i are: the vector of optimization variables $\mathbf{X}_i$, an appropriate inverse of the Hessian matrix, $\mathbf{H}_i$, and a search direction vector $\mathbf{S}_i$. After the search direction vector is computed, the one-dimensional minimization proceeds as follows. An accelerated step size algorithm is used to determine an interval in the search direction which contatins at least one local minimum. Then, within this interval, an interpolation function is used to find a minimum. For a well-defined convex performance function, convergence is rapid, and the metric approaches the inverse of the Hessian at the solution. However, if there are more than one local minima in the searching direction, convergence may be slow.
In the last step of the algorithm, the following convergence tests are used:

$$\left|\frac{J(\mathbf{X}_{i+1}) - J(\mathbf{X}_i)}{J(\mathbf{X}_i)}\right| \leq \varepsilon_1 \tag{4.16}$$

$$\left|\frac{\partial J}{\partial X_j}\right| \leq \varepsilon_2 \qquad j = 1, \ldots, N_{sa} \tag{4.17}$$

where ε_1 and ε_2 are the convergence control parameters, and X_j is the j-th component of vector $\mathbf{X}_i$. In the simulation a value of 1e-7 is used for both the convergence tests.
In the following the step-by-step DFP algorithm is summarized:

1. Choose $\mathbf{X}_1$ positive definite (identity matrix), $[\mathbf{H}_1]$, N_{iter}
   ε_1 and ε_2 (tolerance for stopping criteria)
   Set $i = 1$ (initialize iteration counter)

2. $\mathbf{S}_i = [\mathbf{H}_i]\ \partial J/\partial \mathbf{X}_i(\mathbf{X}_i)$
   $\mathbf{X}_{i+1} = \mathbf{X}_i + \alpha_i \mathbf{S}_i; \quad \Delta\mathbf{X} = \alpha_i \mathbf{S}_i$
   α_i is determined by minimizing $J(\mathbf{X}_{i+1})$

3. If Eq.(4.16) holds $\rightarrow$ stop (function not changing)
   If Eq.(4.17) holds $\rightarrow$ stop (gradient tends to zero)
   If $i + 1 = N_{\text{iter}} \rightarrow$ stop (iteration limit)

   Else

$$\begin{aligned}
\mathbf{Y} &= \partial J/\partial \mathbf{X}_i(\mathbf{X}_{i+1}) - \partial J/\partial \mathbf{X}_i(\mathbf{X}_i);\\
\mathbf{Z} &= [\mathbf{H}_i]\mathbf{Y};\\
[\mathbf{B}] &= \frac{\Delta\mathbf{X}\Delta\mathbf{X}^{\mathbf{T}}}{\Delta\mathbf{X}^{\mathbf{T}}\mathbf{Y}};\\
[\mathbf{C}] &= -\frac{\mathbf{Z}\mathbf{Z}^{\mathbf{T}}}{\mathbf{Y}^{\mathbf{T}}\mathbf{Z}};\\
[\mathbf{H}_{i+1}] &= [\mathbf{H}_i] + [\mathbf{B}] + [\mathbf{C}];\\
i &= i + 1;
\end{aligned}$$

   Go to step 2

In the above the matrices are enclosed by square brackets. The initial choice of the metric is a positive definite matrix. The *identity matrix* is a safe choice.

Chapter 5

Convergence study

FOR the validation of the results obtained (see next chapter), a study of convergence of the method was carried out, without control simulation, both for the structural and the acoustic model. The results were compared with both analytical solutions (where it is possible) of the frequency response, and the solutions coming from literature.
As plate model was adopted the same used by Engels et al. [4], with the purpose to obtain comparable results:

Table 5.1: Variables of the plate used in the simulation.

E	=	7×10^{10} Pa	Young's modulus
ρ	=	2720 kg/m^3	density of the plate
ζ	=	0.01	modal damping factor
f_{max}	=	1 kHz	maximum frequency of interest
h	=	0.001 m	tickness of the plate
a	=	0.247 m	x dimension of the plate
b	=	0.278 m	y dimension of the plate
J	=	h^3/12 m^3	bending stiffness

5.1 Convergence of the structural model

Considering a simply supported plate, a modal model can be easily carried out with the mode shapes defined as:

$$\Psi_{mn}(x, y) = \sin(k_m x) \sin(k_n y) \tag{5.1}$$

with $k_m = m\pi/a$ and $k_n = n\pi/b$. The natural frequency corresponding to the above mode shape can be computed as:

$$\omega_{mn} = \sqrt{\frac{EJ}{\rho h}}(k_m^2 + k_n^2) \tag{5.2}$$

The analytical solution of Eq.(5.2) was compared with a simply supported plate model (SSSS) generated by the routine, varying the number of term adopted in the series expansion for the Ritz functions. Results are obtained by using a square selection strategy, i.e., the same number of terms $M = N$ is adopted in the series.
The resulting frequencies are listed in Table 5.2, for frequencies below $f_{max} =$ 1 kHz.

As one would expect, as the degree of the Ritz functions increases, the solution is getting closer to the exact one, from the top, due to the higher stiffness of the approximated structure. In theory, the exact solution would be achieved with an infinite number of Ritz admissible functions.

A further convergence stuty for the structural model has been done on the frequency response of the kinetic energy. As reference, the spectrum of expected kinetic energy by Engels et al. [4], has been considered. They assumed a modal model of a simply supported plate (which characteritics are listed in Table 5.1), and an excitation by a pressure field $p(x, y)$, with a white spectrum in time, as well in space. In order to plot the same effect, a constat modal distribution of the pressure field was chosen, equal for each modal coordinate.
In the Figure 5.1 the spectra of kinetic energy are shown, without control action, compared with that obtained by Engels et al. for a white noise excitation, increasing the order of the Ritz functions.

Table 5.2: Convergence study of a (SSSS) plate for frequencies below f_{max}. Comparison with the exact solution, for a simply supported input plate reported in Table 5.1.

$f = \omega_{mn}/2\pi$	M=N								
(Hz)	4	8	12	16	20	24	30	40	50
67,47	67.60	67.48	**67.47**	67.47	67.47	67.47	67.47	67.47	67.47
156,76	157.13	156.80	156.77	**156.76**	156.76	156.76	156.76	156.76	156.76
180,59	181.05	180.63	180.60	**180.59**	180.59	180.59	180.59	180.59	180.59
269,88	270.42	269.93	269.89	269.89	**269.88**	269.88	269.88	269.88	269.88
305,59	341.82	306.27	305.74	305.65	305.62	305.60	305.60	**305.59**	305.59
369,11	416.31	370.01	369.31	369.19	369.15	369.13	369.12	**369.11**	369.11
418,71	449.11	419.25	418.83	418.75	418.73	418.72	**418.71**	418.71	418.71
458,41	500.09	459.17	458.58	458.47	458.44	458.42	**458.41**	458.41	458.41
513,94	600.72	515.97	514.45	514.14	514.04	514.00	513.97	513.96	513.95
607,23	666.53	608.23	607.44	607.31	607.27	607.25	607.24	**607.23**	607.23
627,06	705.28	628.81	627.49	627.23	627.14	627.11	627.08	627.07	**627.06**
633,05	744.63	635.67	633.70	633.31	633.18	633.12	633.08	633.06	**633.05**
722,34	826.40	724.72	722.93	722.57	722.46	722.41	722.37	722.35	722.35
781,83	912.75	793.71	783.84	782.53	782.16	782.01	781.92	781.86	781.85
815,58	985.01	817.49	816.02	815.75	815.67	815.63	815.61	815.59	815.59
871,17	1221.18	873.52	871.72	871.38	871.27	871.23	871.20	871.18	**871.17**
894,94		905.91	896.75	895.57	895.23	895.10	895.02	894.97	894.96
972,39		987.62	974.98	973.30	972.82	972.62	972.51	972.44	972.41

Underlined bold numbers denote convergent values to four significant figures.

As can be seen, increasing the order of the Ritz functions, and so gradually refining the model, the frequency response becomes more precise, stabilizing to that computed by Engels et al. [4], with the peaks coincident with the solutions found analitically. It can be noted how (look at Fig. 5.1d), with a relatively low order of approximation, a fairly accurate representation of the frequency response of the structure is obtained.

The convergence of the structural model has been also verified for different boundary conditions, for which there is no analytical solution. As there is no literature in a representation of the spectrum of the kinetic energy, the analysis was performed by comparing the result with a more accurate one, iterating the procedure.
As reference, a fully clamped plate on the four edges was considered (CCCC), with the same characteritics in Table 5.1, excited by the same pressure field $p(x, y)$. In the Figure 5.2 the spectra of kinetic energy are shown, without control action, compared with themself, increasing the number of the Ritz functions.

As can be seen, also for the fully clamped plate, increasing the order of the

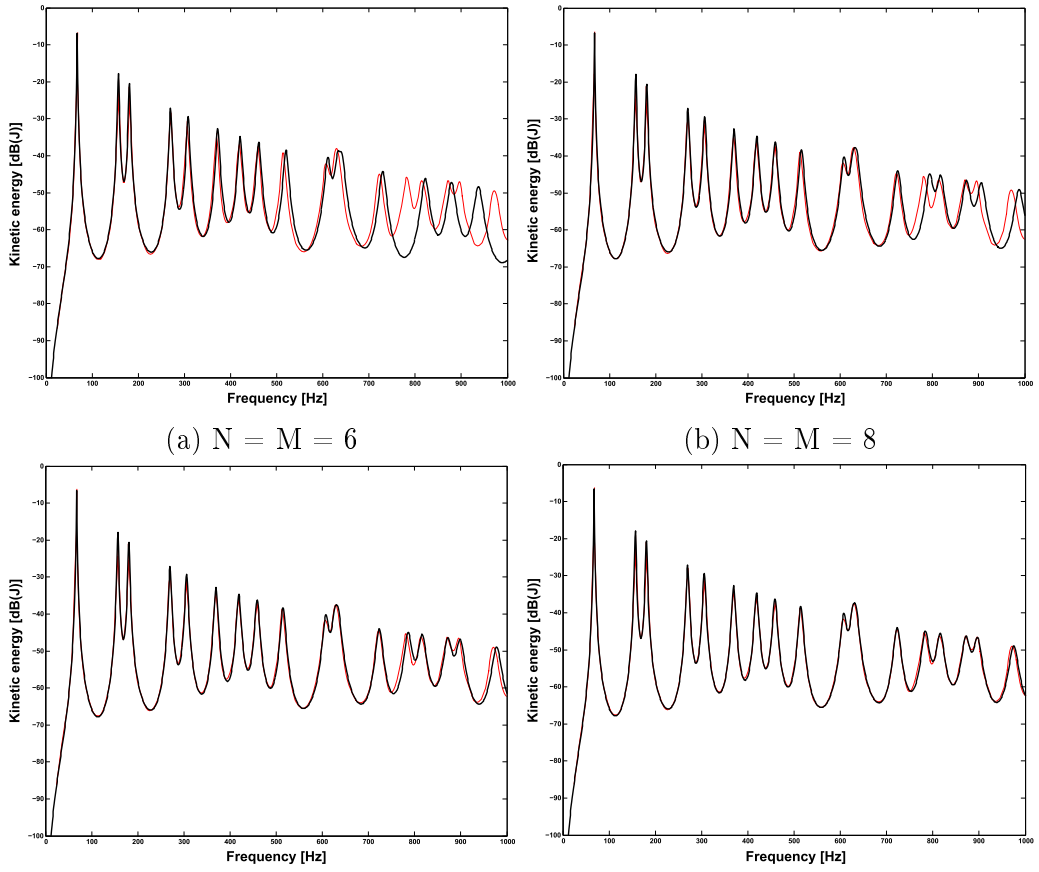

(a) N = M = 6 (b) N = M = 8

(c) N = M = 10 (d) N = M = 12

Figure 5.1: Spectrum of kinetic energy, assuming white noise excitation, varying the order of Ritz functions. With — is plotted as reference the spectrum obtained by Engels et al. taking into account all the mode shapes with a natural frequency up to $f_{max} = 3$ kHz, which results in 60 modes taken into account.

Ritz functions, and so gradually refining the model, the frequency response becomes more precise, stabilizing to a fixed rapresentation. It can be noted how (look at Fig.5.2d), with only 14 admissible Ritz functions, the spectrum is very precise at low frequencies and accurate enough at high frequencies below the frequency of interest.

For completeness, as in the (SSSS) case, in Table 5.3 the frequencies of the structure are reported, varying the terms of the series expansion $M = N$.

Due to the higher complexity of the problem, with respect to the simply supported plate, the convergence is slower, as can be seen from the slower trend of the frequency approximation, but still guaranteed, with a higher

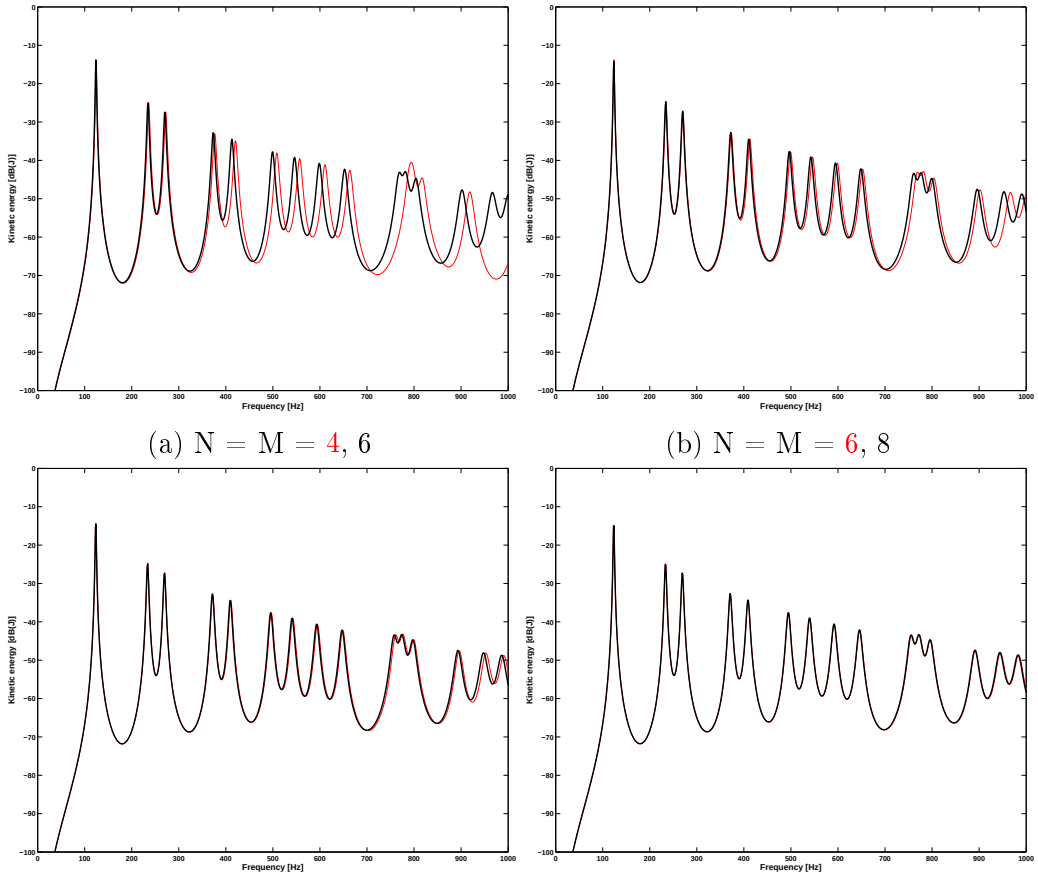

(a) N = M = 4, 6 (b) N = M = 6, 8

(c) N = M = 8, 10 (d) N = M = 12, 14

Figure 5.2: Spectrum of kinetic energy, assuming white noise excitation, varying the order of Ritz functions. With — is plotted the spectrum obtained with a lower order of approximation; with — is plotted the spectrum obtained with a higher order of approximation.

number of Ritz functions.

5.2 Convergence of the acoustic model

Even for the acoustic radiation model an analysis of convergence was made, in order to verify the effectiveness of the method. A good yardstick is the spectrum of the acoustic radiated power, which is an optimization variable of the problem.
In Table 5.4 the input data used for the computation are listed.

Figure 5.3 shows the trend of the spectra keeping fixed the structural ap-

Table 5.3: Convergence study of a (CCCC) plate for frequencies below f_{max}. Input plate variables are reported in Table 5.1.

M=N									
4	6	8	12	16	20	24	30	40	50
124.51	123.87	123.66	123.53	123.49	123.47	123.47	**123.46**	123.46	123.46
236.08	234.49	233.91	233.53	233.41	233.37	233.34	233.33	233.32	233.31
272.23	270.49	269.86	269.44	269.31	269.25	269.23	269.21	**269.20**	269.20
376.48	373.26	372.02	371.16	370.88	370.77	370.71	370.67	370.65	370.64
420.58	412.87	410.49	409.04	408.62	408.46	408.39	408.34	408.31	408.29
508.46	499.30	496.49	494.77	494.29	494.10	494.02	493.96	493.92	493.91
557.00	546.10	542.44	540.06	539.35	539.07	538.93	538.84	538.78	538.76
610.82	598.68	594.70	592.13	591.37	591.07	590.93	590.83	590.76	590.74
663.65	652.56	648.75	646.21	645.43	645.11	644.96	644.85	644.78	644.75
790.89	768.22	760.69	755.80	754.35	753.78	753.51	753.32	753.20	753.16
796.69	782.03	776.70	772.98	771.80	771.31	771.07	770.90	770.79	770.75
817.64	804.27	799.69	796.63	795.69	795.30	795.12	794.99	794.91	794.87
918.60	902.01	896.05	891.91	890.59	890.05	889.79	889.60	889.48	889.43
1028.79	966.51	952.75	945.16	943.09	942.29	941.92	941.67	941.50	941.45
1097.69	1000.87	990.95	984.12	981.98	981.10	980.68	980.38	980.18	980.11

Underlined bold numbers denote convergent values to four significant figures.

Table 5.4: Acoustic data used in the simulation.

ρ	=	1.2754 kg/m^3	air density at standard conditions
c	=	331.3 m/s	speed of sound at standard conditions
f_{max}	=	1 kHz	maximum frequency of interest
E_x	=	6	elementary radiators on the x axis
E_y	=	5	elementary radiators on the y axis
ord	=	4	order of the fitting transfer functions

proximation terms, and varying the number of radiation modes. The graphs are compared with themeself until reaching a stable rapresentation.

Also the radiated acoustic power shows a clear convergence trend with a relatively low number of radiation modes. In Fig.5.3d the rapresentation reaches a sufficient accuracy so as to allow the implementation of the model for further optimization analysis.

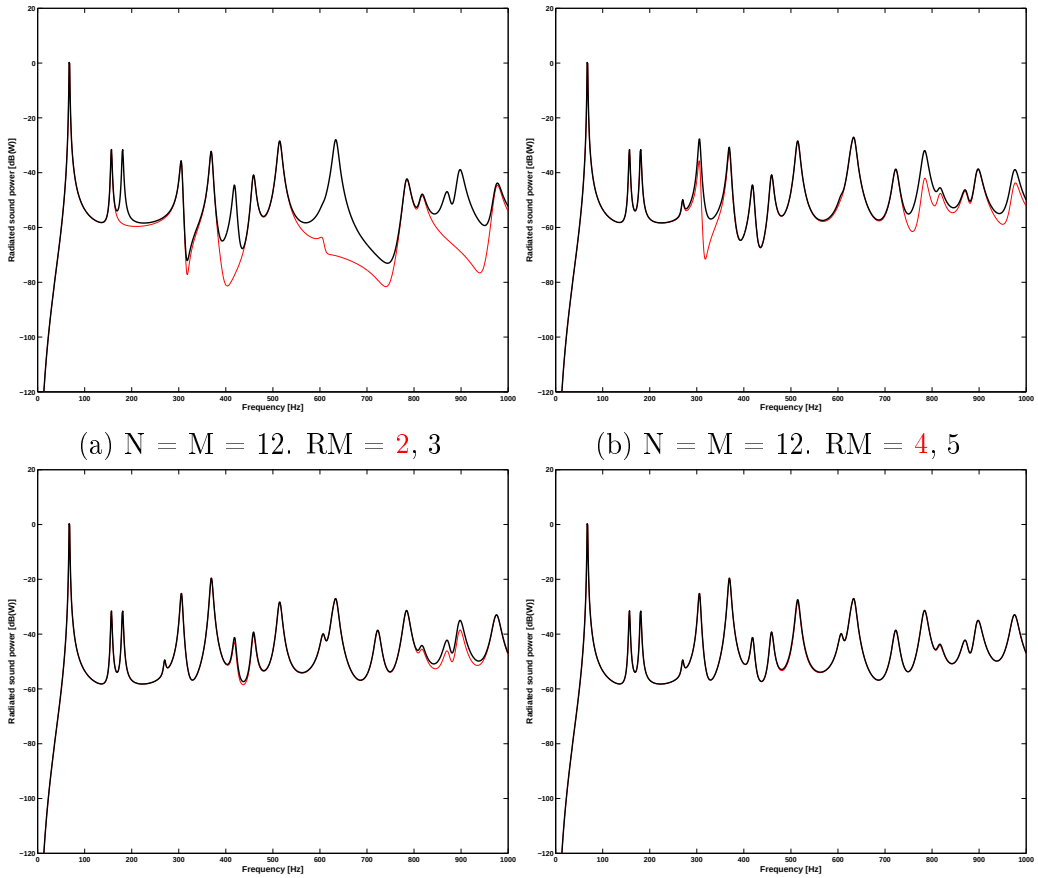

(a) N = M = 12. RM = 2, 3

(b) N = M = 12. RM = 4, 5

(c) N = M = 12. RM = 6, 8

(d) N = M = 12. RM = 8, 10

Figure 5.3: Spectrum of the radiated sound power, assuming white noise excitation, varying the number of radiation modes. With — is plotted the spectrum obtained with less radiation modes; with — is plotted the spectrum obtained with more radiation modes.

Chapter 6

Analysis and Results

In this chapter the most interesting part of the job is presented and discussed. Particular cases were taken into account, which differ for the input parameters assigned, in order to highlight the differences between the various scenarios. As starting point, the study of Engels et al. [4] is reproduced, for a plate equipped with ideal actuators and senors in fixed positions, for the minimization of its kinetic energy and acoustic radiated power. Once one understood the differences between the results obtained and how they are influenced by the input parameters, it is possible to further research into the optimal locations to be assigned to sensors and actuators, for plates subjected to different boundary conditions and different loading conditions.

6.1 Optimization of gains with a fixed grid of controllers (Engels [4])

To carry out the same type of optimization a modified version of the routine has been used, which maintains a fixed position of the sensors and actuators, performing the minimization of gains only, for a *Decentralized constant gain controller*.

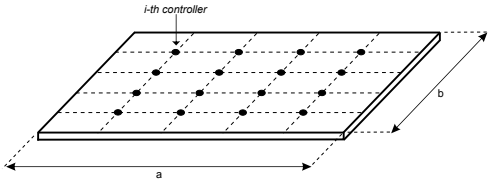

Figure 6.1: Equally spaced sensors and actuators as adopted by Engels et al. [4]. Each dot represents colocated velocity sensors and point force actuator pair.

In this study 16 equally spaced control locations are used, as indicated in Fig.6.1 and 6.2. At each control locations, ideal velocity sensors are assumed that are colocated with ideal force actuators.

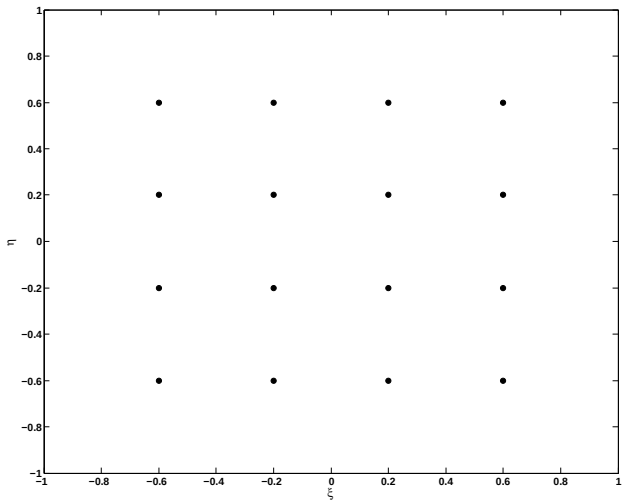

Figure 6.2: Equally spaced sensors and actuators as as adopted by Engels et al. [4]. 2D view.

Figure 6.3 shows the resulting spectrum of the kinetic energy and acoustic radiation with a control action optimized for kinetic energy. A white noise excitation is assumed and the control effort weighting was adjusted such that the expected controller effort was equal to 300 N^2 for each controller ($R = 1/300$).

The kinetic energy around the first resonance frequency is reduced by about 25 dB dropping off to about 10 dB reduction at other resonances. Look at [4] for more details and comparison whith other type of control action.
From the Figure 6.3 you can note that at certain frequencies (780 Hz, 900 Hz, 980 Hz) there is no attenuation of both energy and sound radiation. This result was also obtained by Engels et al., which performed also a further analysis with a red noise excitation on the plate obtaining the conclusion that such frequencies could not be mitigated by any type of control strategy adopted in the simulation.
In Figure 6.4 the same analysis are shown with the same grid of sensors and actuators, but with a stronger control action. The result is always the same: those frequencies are unaffected by the action of controllers. *Why?*

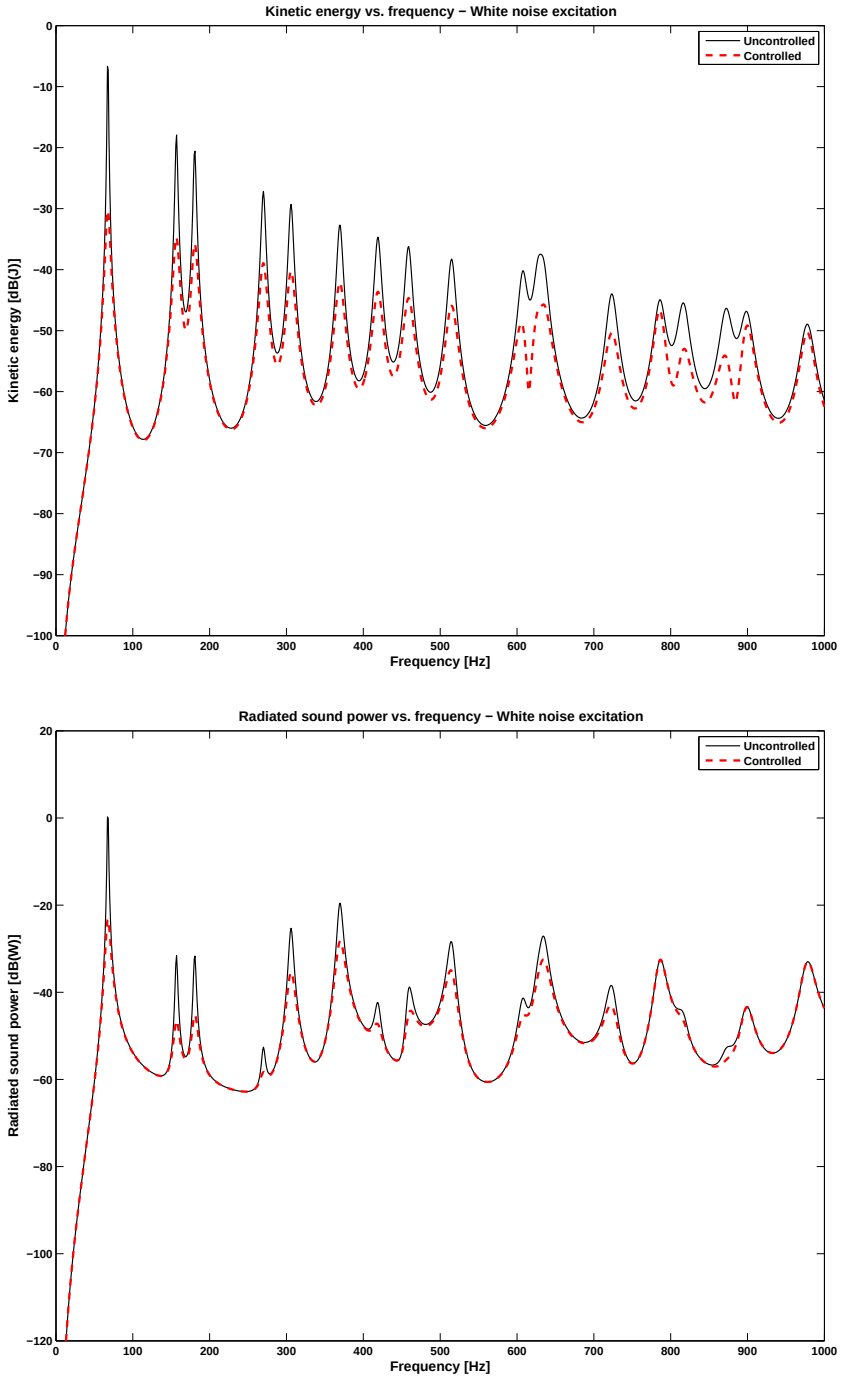

Figure 6.3: Spectrum of kinetic energy and radiated sound power assuming white noise excitation, before and after control, using decentralized constant gain controller. The average control effort for each controller was limited to 300 N^2.

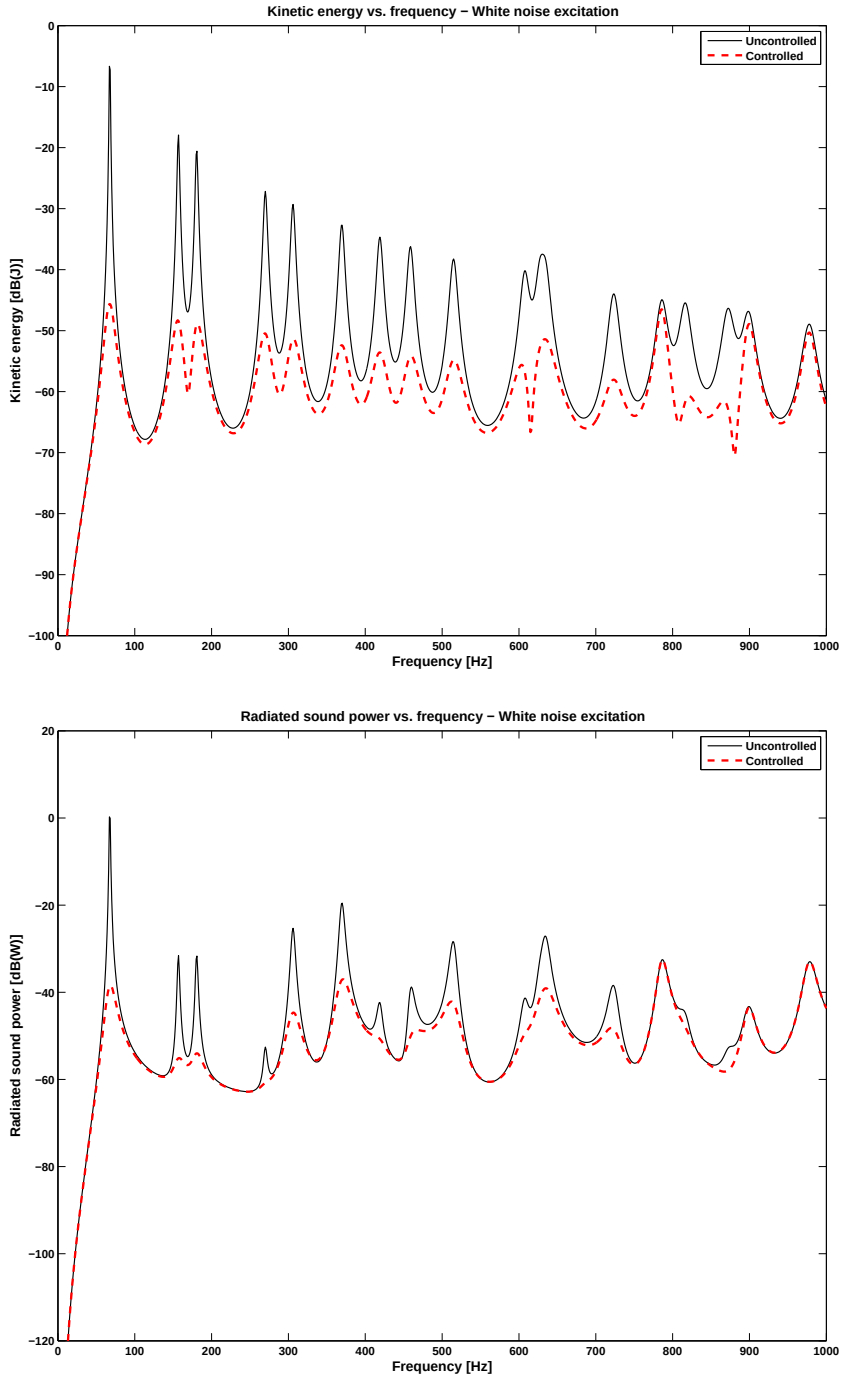

Figure 6.4: Spectrum of kinetic energy and radiated sound power assuming white noise excitation, before and after control, using decentralized constant gain controller. The average control effort for each controller was limited to 1000 N^2.

6.1.1 Emprovement of the grid arrangement

In order to answer this question, a second slightly different grid formed by the same number of sensors and actuators was assumed. In Figure 6.5 they are compared.

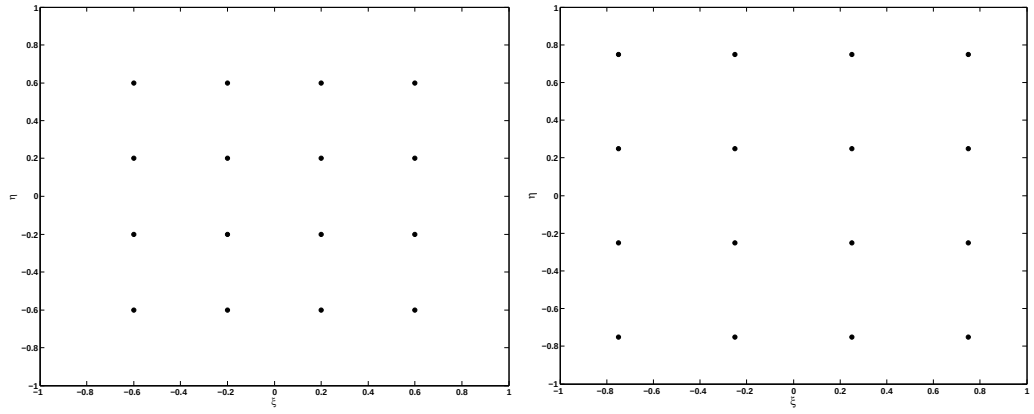

(a) Old configuration [4]. (b) Emproved configuration.

Figure 6.5: Equally spaced sensors and actuators in the old and the new emproved arrangement. Each dot represents colocated velocity sensors and point force actuator pair.

Looking at the results in Figure 6.6 we can find the answer. The reason lies in the fact that such a grid of sensors and actuators arranged in the initial manner (Fig.6.2) is not able to mitigate those particular frequencies. From this fact comes the need to find an optimum arrangement of the actuators, so that the whole spectrum of frequencies of interest may be attenuated. In Fig.6.6 is possible to note that with the same control effort of 300 N^2, the overall spectrum is attenuated, and the force of the actuators is more spanned and better distributed over the plate for a global but lower attenuation.

Finding an *optimum solution* is the purpose of the next results. This solution will optimize both the arrangement of sensors and actuators on the plate and the attenuation of the performance, once selected an appropriate control effort weighting coefficient.

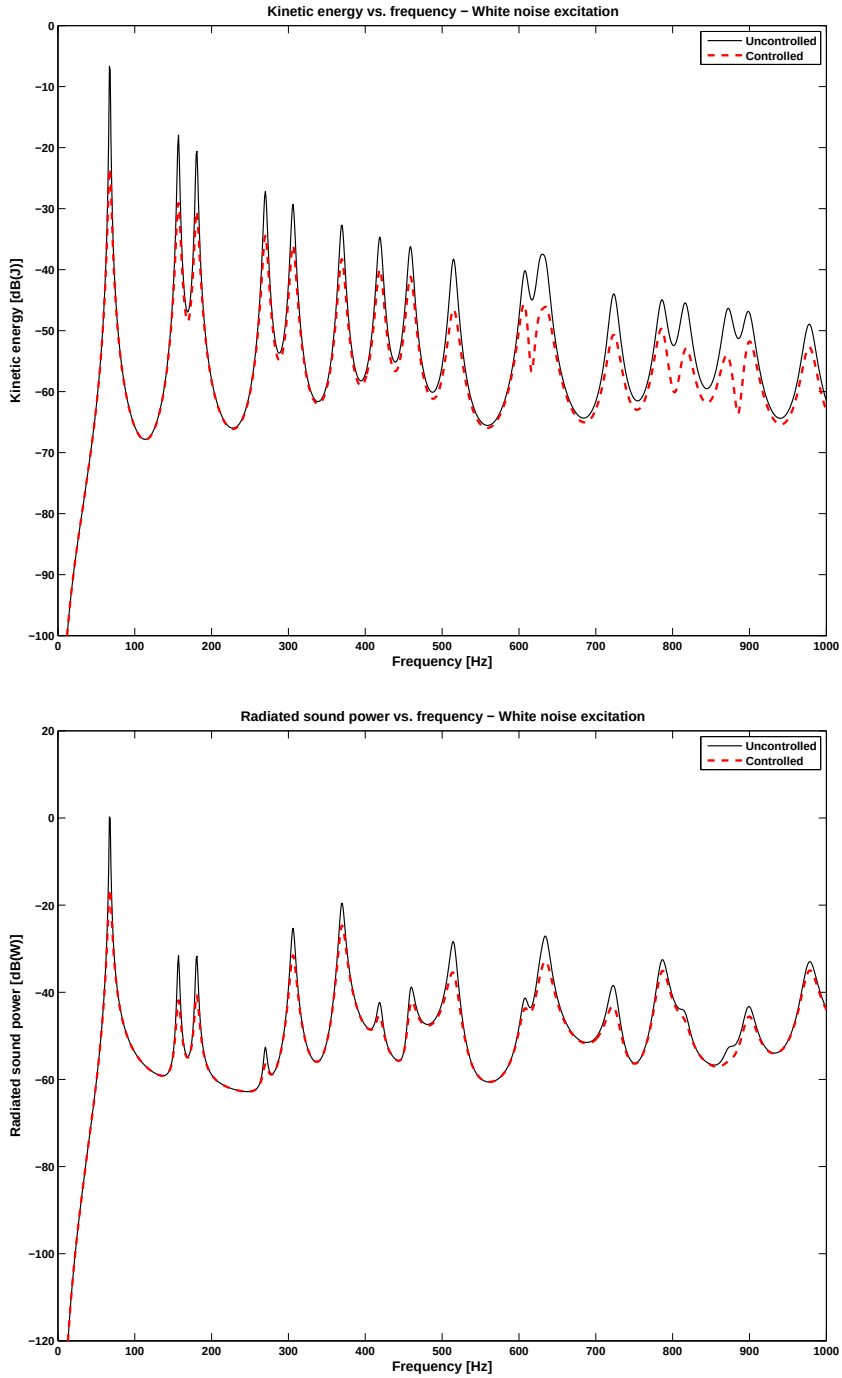

Figure 6.6: Spectrum of kinetic energy and radiated sound power assuming white noise excitation, before and after control, using decentralized constant gain controller. The average control effort for each controller was limited to 300 N^2.

6.2 Differences in minimizing Kinetic energy or Radiated sound power

In the previous section, cases optimized for kinetic energy were considered. In fact, as has been noted, for the same control effort, the attenuation of radiated sound power is lower. *What happens performing the optimization for the sound power?*
Holding the same grid of sensors and actuator of Fig.6.2 some analysis are performed for both the kinetic energy and acoustic power optimizations, changing che control effort parameter. Figure 6.7 and Eq.(6.1) show the results in terms of frequency response and minimum gains for an optimization of the radiated sound power, keeping the control effort weighting $R = 1/300$, such that the expected average control effort is limited to 300 N^2. As one can see, also for the acoustic optimization, is clearly visible the ineffectiveness of this type of configuration for the frequencies around 780 Hz, 900 Hz and 980 Hz.

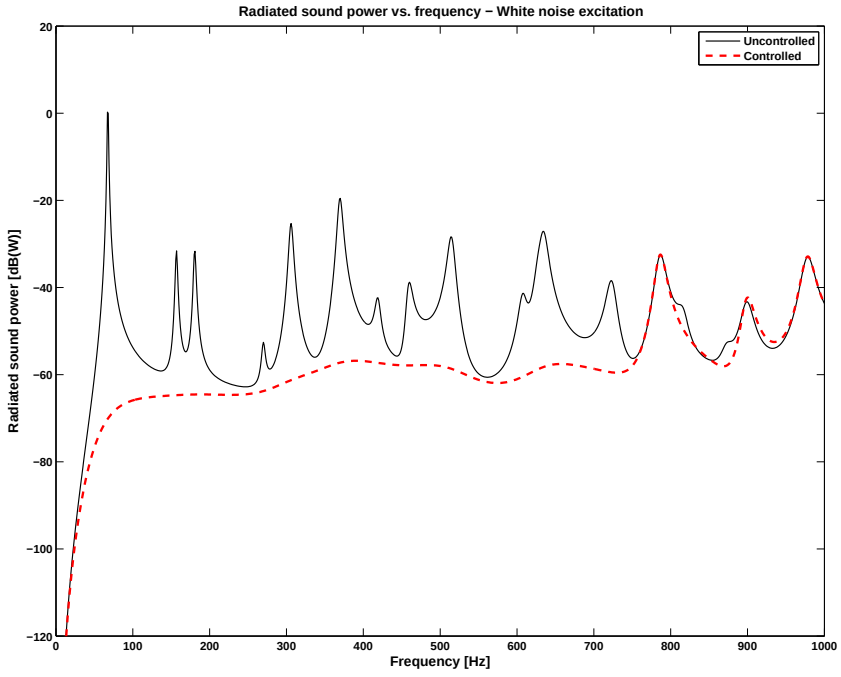

Figure 6.7: Spectrum of radiated sound power assuming white noise excitation, before and after control, using decentralized constant gain controller. The average control effort for each controller was limited to 300 N^2.

$$\mathbf{G}_{300} = \text{diag}\{6.78 \quad 4.60 \quad 4.60 \quad 6.78 \quad 4.93 \quad 3.81 \quad 3.81 \quad 4.93 \quad 4.93 \quad 3.81 \quad 3.81 \quad 4.93 \quad 6.78 \quad 4.60 \quad 4.60 \quad 6.78\} \tag{6.1}$$

The attenuation is much more pronounced than that obtained with an optimization of the kinetic energy. The reason for this lies in the value of the functional J. For both cases, it is given by the equations:

$$J_{ke} = \frac{1}{2}\left[\dot{\mathbf{q}}^T(t)\dot{\mathbf{q}}(t) + \mathbf{u}^T(t)\mathbf{R}\mathbf{u}(t)\right] \tag{6.2}$$

$$J_{ac} = \left[\mathbf{y}_{ac}^T(t)\mathbf{y}_{ac} + \mathbf{u}^T(t)\mathbf{R}\mathbf{u}(t)\right] \tag{6.3}$$

where $\mathbf{u}$ is the vector of control signals applied by the controller and $\mathbf{R}$ is the weighting matrix of the control effort.
Taking as an example the two simulations for the optimization of the kinetic energy and the radiated sound power, made with $R = 1/300$, we get the following values for the performance indices:

$$J_{ke} = 2.214 \times 10^7 \tag{6.4}$$

$$J_{ac} = 1.327 \times 10^9 \tag{6.5}$$

As one can see, J_{ac} is much higher with respect to J_{ke}, so $\mathbf{R}$ should be tuned in such a way to yields an effective control for that particular index. Accordingly, for the optimization of the radiated sound power, R should be higher, with respect to the kinetic energy optimization, due to the greater magnitude of the acoustic index. In Figure 6.8 a new acoustic optimization is performed, keeping the control penalty $R = 1/30$. In this case the sound power density around the first resonance frequency is reduced by about 40 dB, that is a more realistic result, and the optimum static gains of the control matrix are much lower (Eq.(6.6)), that is a very important result in terms of control power saving.

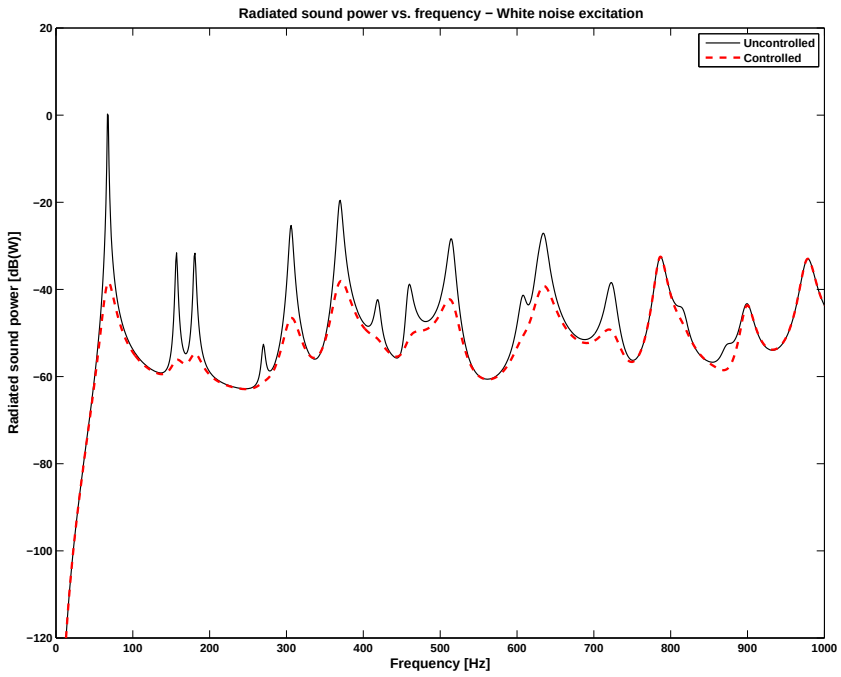

Figure 6.8: Spectrum of radiated sound power assuming white noise excitation, before and after control, using decentralized constant gain controller. The average control effort for each controller was limited to 30 N^2.

$$\mathbf{G}_{30} = \text{diag}\{1.02 \quad 0.78 \quad 0.78 \quad 1.02 \quad 0.67 \quad 0.56 \quad 0.56 \quad 0.66 \quad 0.67 \quad 0.56 \quad 0.56 \quad 0.67 \quad 1.02 \quad 0.78 \quad 0.78 \quad 1.02\} \tag{6.6}$$

The overall difference in the cost function is difficult to see from these plots and it is not clear whether a level of effort is more appropriate than another. Therefore, the overall reduction in the expected kinetic energy and sound radiation should be examined as a function of control effort. Still higher control efforts can be achieved by using higher gains in the control loops, but this results in worse, rather than better performance.

6.3 Comparison between fixed locations and optimized ones

This section will analyze the most interesting results of this work: the differences between a grid of sensors and actuators fixed a priori, and an optimized one through an objective function.
In the following, three numerical studies are presented: optimal placement and gains for 1, 16 and 100 actuators, with variable terms of the series expansion $M = N$ and with 6 most significan radiation modes. All the simulation are performed for a simply supported plate (SSSS) with characteristics listed in Tab. 5.1, and for both kinetic energy and acoustic power optimization.

6.3.1 Optimal placement and gains for a single controller - Kinetic energy optimization

The simplest optimal design problem is for a single actuator and collocated sensor. There are only three optimization variables: the velocity gain, and the ξ and η coordinates of the controller. The control penalty is set to $R = 1/500$, and the terms of the series expansion are $M = N = 4$, which involves an excellent approximation for the first four characteristic frequencies, with an error of about 0.2%, and a bad approximation for the higher frequencies with errors gradually increasing.
If the coordinates of the controller are fixed, there is only a single value for the velocity gain which minimezes the performance function. However, with the three optimizazion variables, there are many local minima. To obtain as many different local minima as possible, the nonlinear programming algorithm is executed more times, with random generated initial values for the optimization variables. In Figure 6.9 is represented the solution with the velocity gain optimized for kinetic energy, with a fixed central position for the actuator placement. It is compared with the placement optimized soultions from Fig. 6.10 to 6.13.

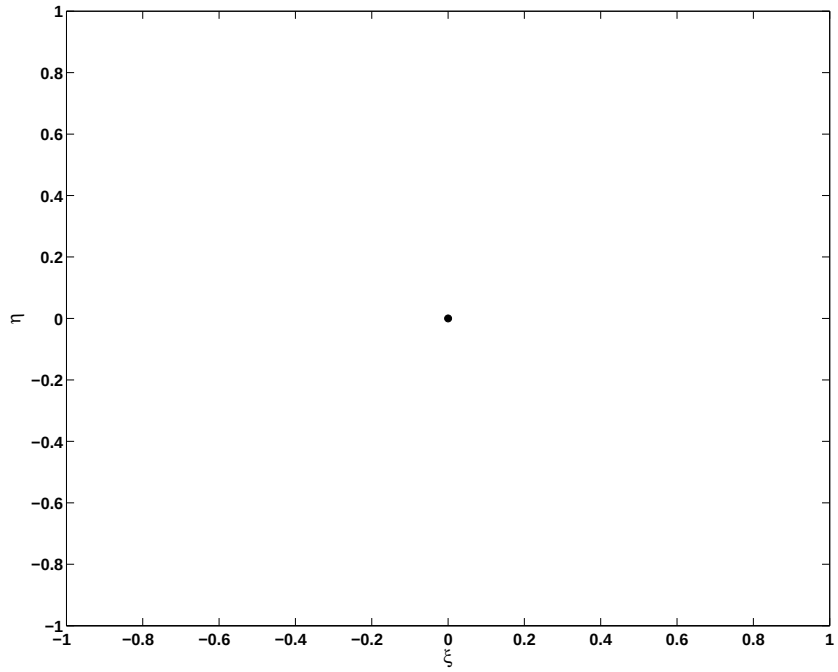

(a) $J_{ke} = 6.866 \times 10^5$, $g_{opt} = 1.69$.

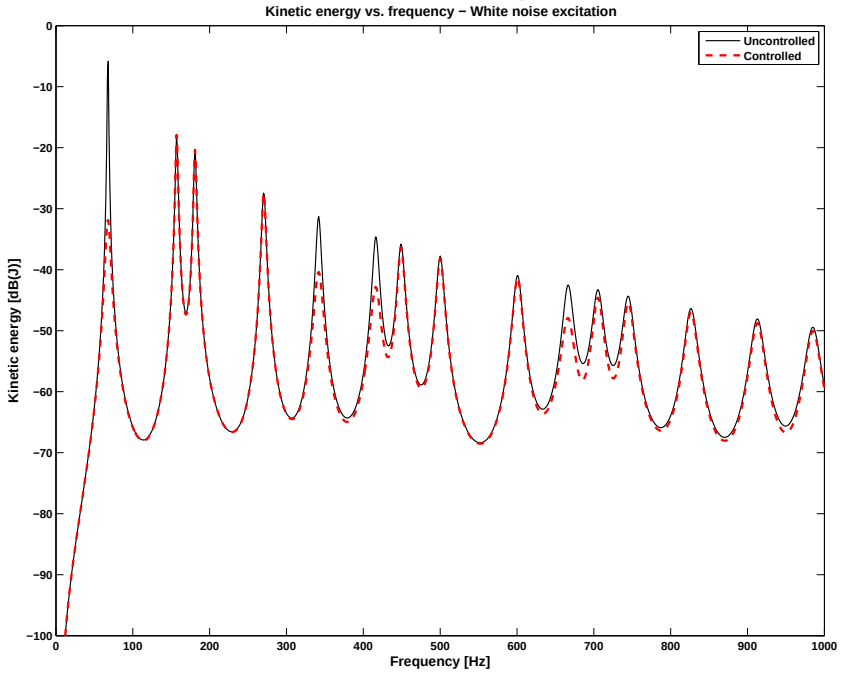

(b) Spectrum of kinetic energy assuming white noise excitation, before and after control. The average control effort for the controller was limited to 500 N^2.

Figure 6.9: Fixed central position - Placement and frequency responce for the single controller case. Single gain optimization for kinetic energy.

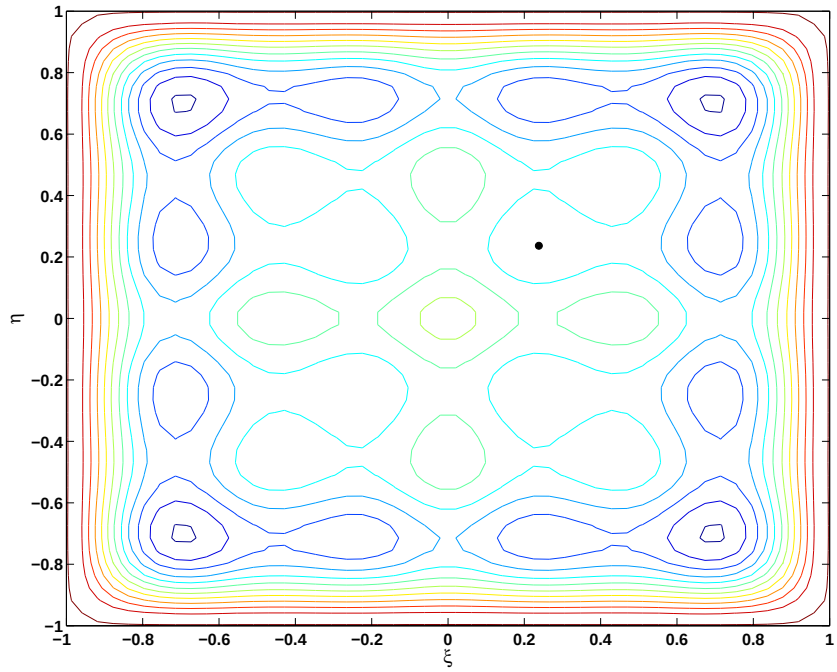

(a) $J_{ke} = 6.705 \times 10^5$, $g_{opt} = 1.38$.

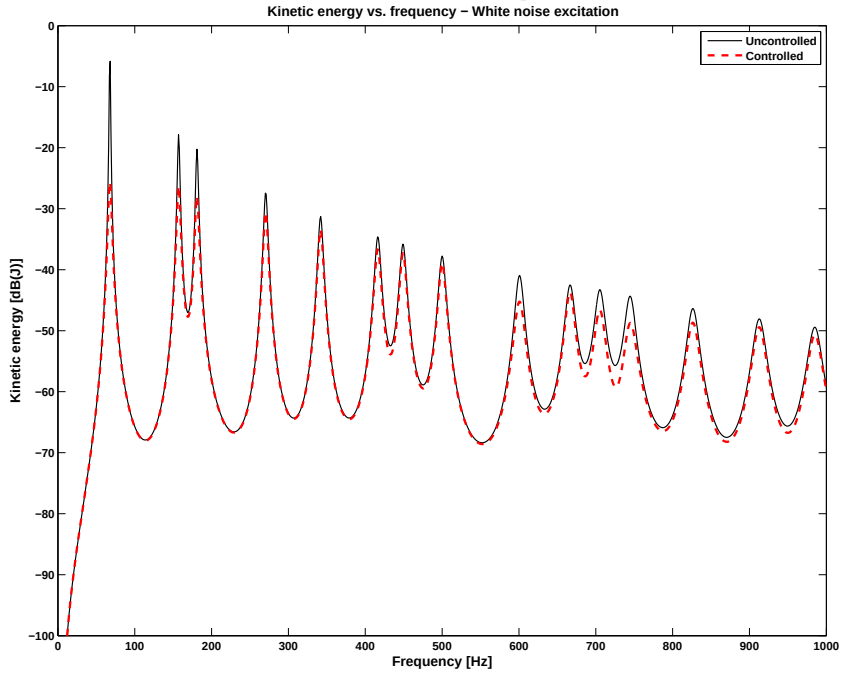

(b) Spectrum of kinetic energy assuming white noise excitation, before and after control. The average control effort for the controller was limited to 500 N^2.

Figure 6.10: Solution 1 - Placement and frequency responce for the single controller case.

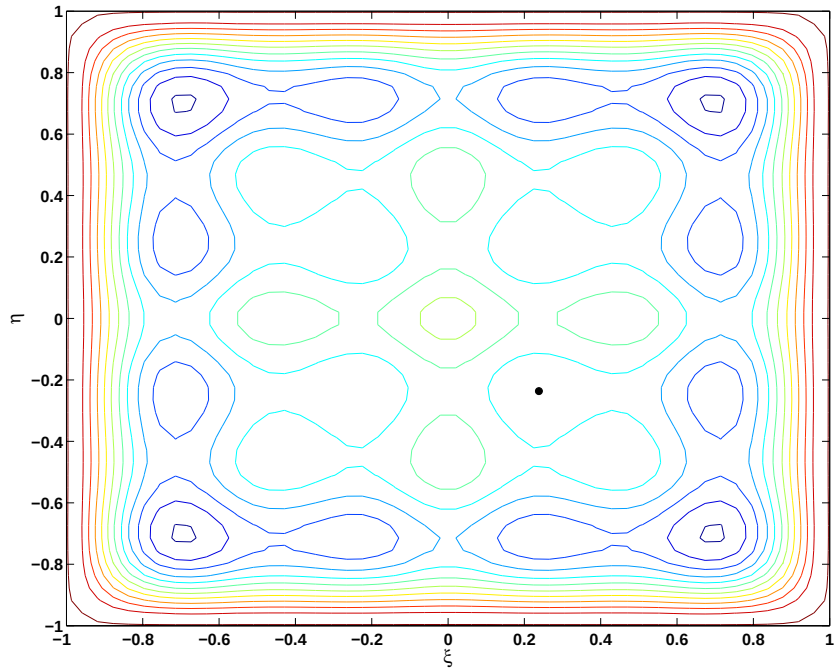

(a) $J_{ke} = 6.705 \times 10^5$, $g_{opt} = 1.38$.

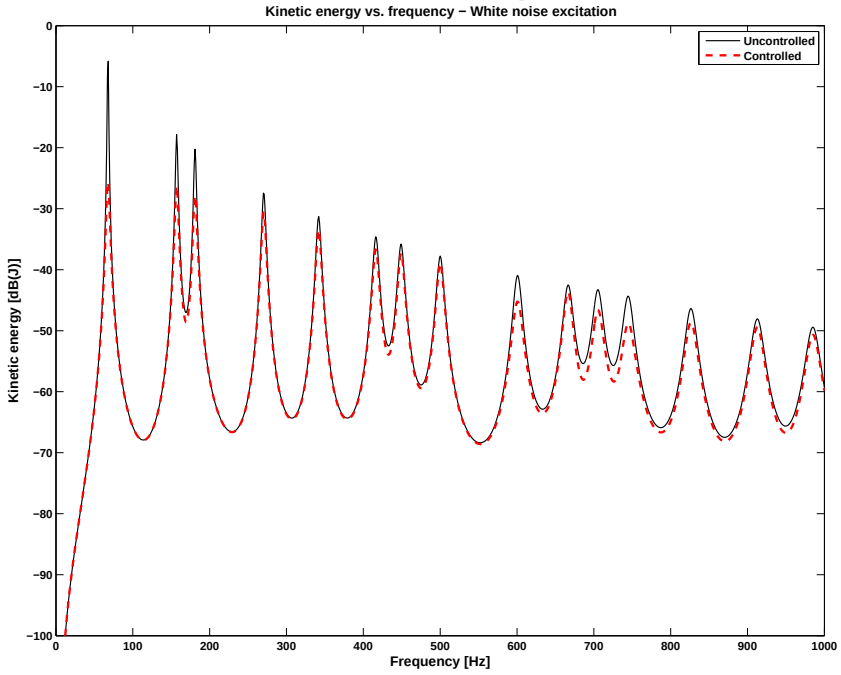

(b) Spectrum of kinetic energy assuming white noise excitation, before and after control. The average control effort for the controller was limited to 500 N^2.

Figure 6.11: Solution 2 - Placement and frequency responce for the single controller case.

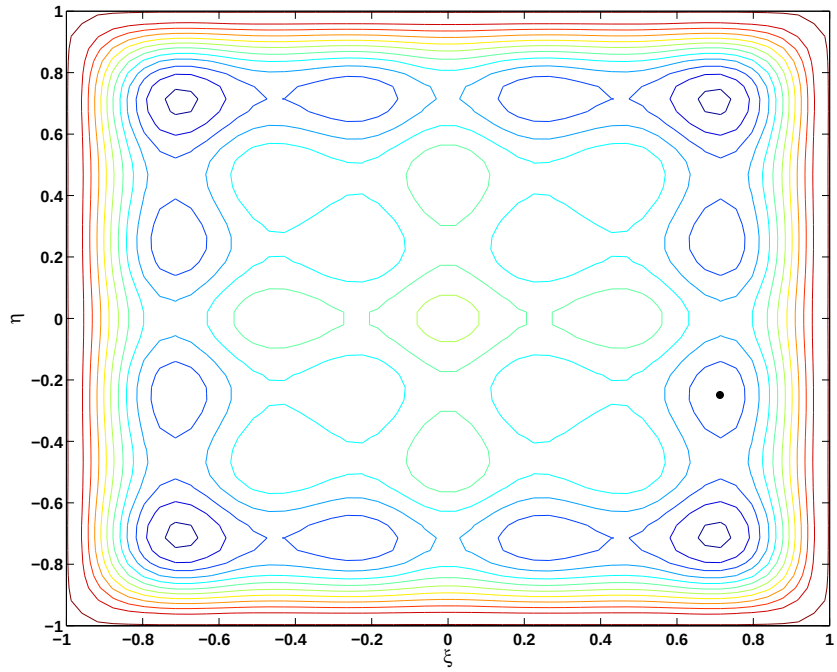

(a) $J_{ke} = 6.613 \times 10^5$, $g_{opt} = 1.28$.

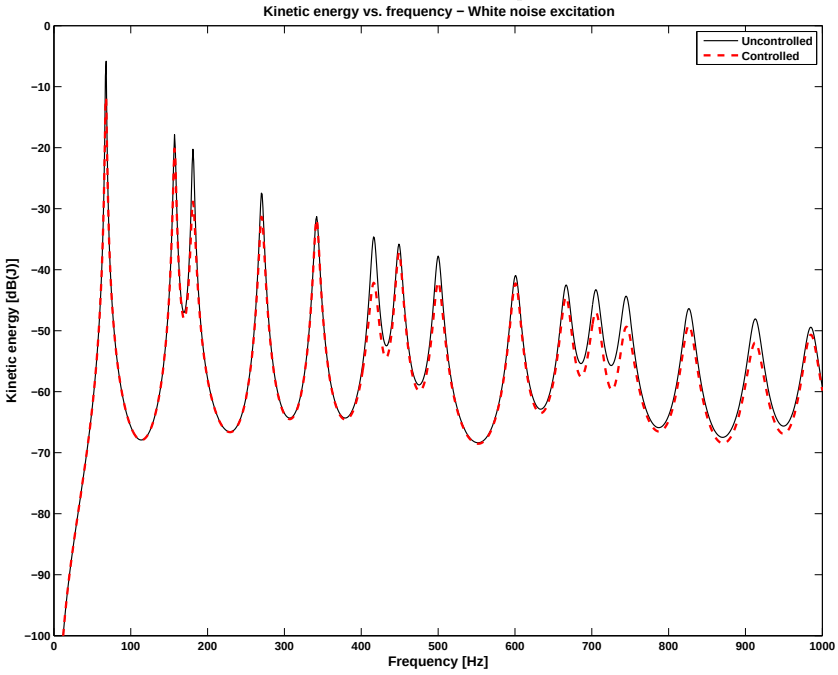

(b) Spectrum of kinetic energy assuming white noise excitation, before and after control. The average control effort for the controller was limited to 500 N^2.

Figure 6.12: Solution 3 - Placement and frequency responce for the single controller case.

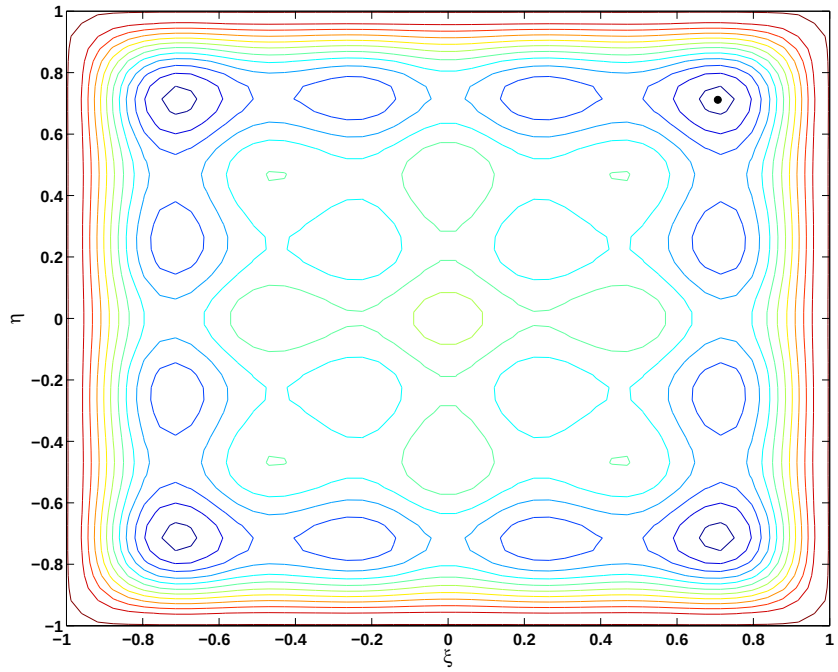

(a) $J_{ke} = 6.533 \times 10^5$, $g_{opt} = 1.21$.

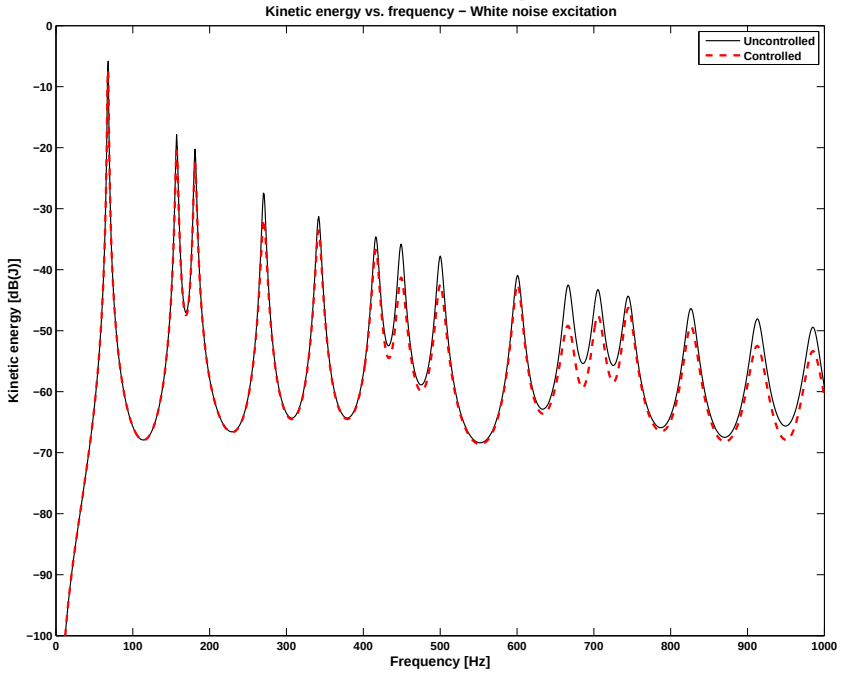

(b) Spectrum of kinetic energy assuming white noise excitation, before and after control. The average control effort for the controller was limited to 500 N^2.

Figure 6.13: Solution 4 - Placement and frequency responce for the single controller case.

Four distinct solution are shown, for the kinetic energy optimization. The placement of the actuators, and the corresponding values for the performance function J_{ke}, and gains g_{opt}, are attached to the figures.
Comparing the solution with the fixed central position for the actuator and the others optimized, it can be noted the purpose of the optimization. Even if in the fixed position solution there is a pronounced attenuation of the first frequency (of about 25 dB), it has the largest values of J_{ke} and g_{opt}. The optimized solutions instead, even if in smaller amounts, act on the entire spectrum of frequencies considered.
The first optimized solution (Fig.6.10), contrary to what you might imagine, yields the largest performance value and largest gain, but it has a higher level of attenuation at low frequency; instead the last solution yields the lowest performance value and lowest gain, and it has a higher level of attenuation at high frequency. In a certain way, it can be deduced that the position of the actuator on the plate is also linked to the frequency band that is able to handle.
In the figures the level curves of the performance function are visible, and they somehow remaind to the "nodal lines" of the open-loop Ritz-function approximation. The figures show that the placement of the actuators lie away from this lines, as expected from controllability theory. Such "nodal lines" bound some empty regions. In each of these regions, local minima exist, and therefore can be occupied by actuators.
Figure 6.14 shows a 3D representation of the cost function with respect to placement coordinates.

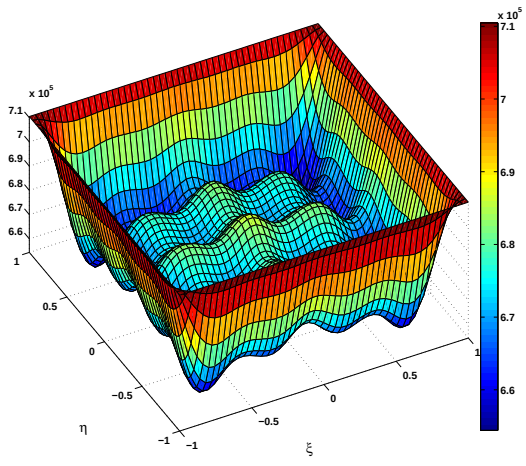

Figure 6.14: Cost function J_{ke} with respect to single actuator/sensor placement, $N = M = 4$, $g = 1.38$.

6.3.2 Optimal placement and gains for a single controller - Acoustic power optimization

Also in this case there are only three optimization variables: the velocity gain, and the ξ and η coordinates of the controller. The control penalty is set to $R = 1/200$, the terms of the series expansion are $M = N = 4$, and the most significan radiation modes taking into account are 6, which involve a good level of approximation, as seen in Chapter 5.
As for the kinetic energy optimization case, with the three optimizazion variables, there are many local minima. To obtain as many different local minima as possible, the nonlinear programming algorithm is executed more times, with random generated initial values for the optimization variables. In Figure 6.16 is represented the solution with the velocity gain optimized for acoustic radiation, with a fixed central position for the actuator placement. It is compared with the optimized placement soultions from Fig.6.17 to 6.20. Also in this case, comparing the solution with the fixed central position for the actuator and the others optimized, a pronounced attenuation of the first frequency can be appreciated (of about 25 dB). It has the largest values of J_{ac} and a small g_{opt}, but is less powerful than the optimized solutions regard to the frequency response.
Figure 6.15 shows the 3D plot of J_{ac} with respect to placement coordinates.

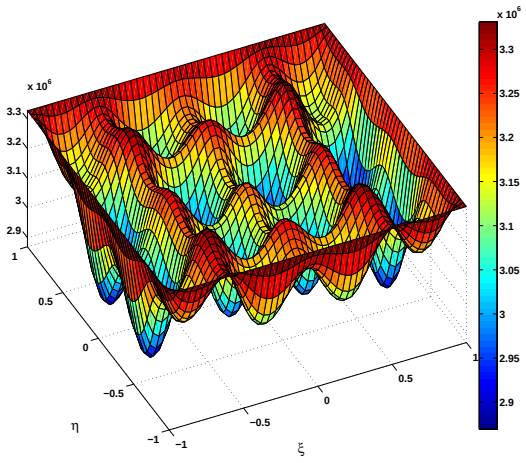

Figure 6.15: Cost function J_{ac} with respect to single actuator/sensor placement, $N = M = 4$, $RM = 6$, $g = 2.87$.

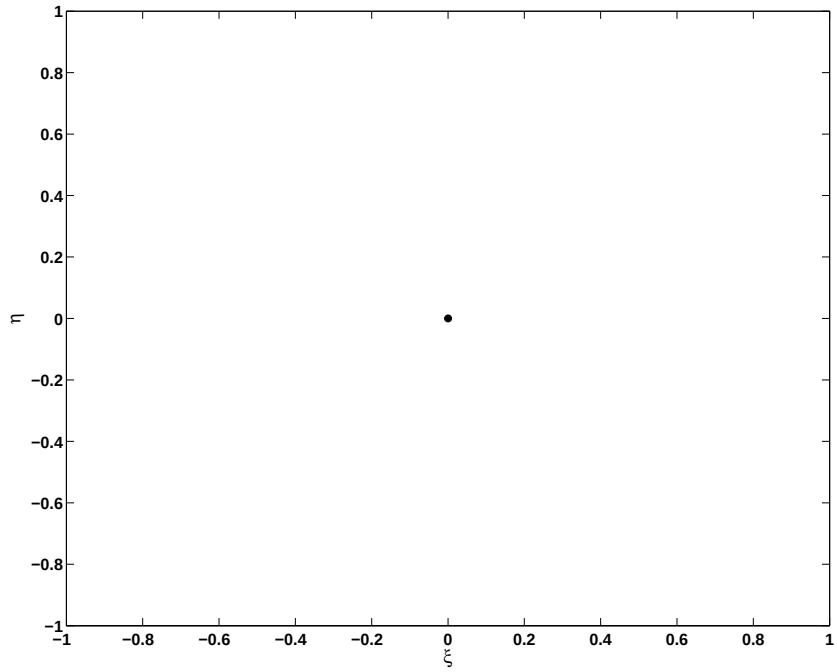

(a) $J_{ac} = 3.234 \times 10^6$, $g_{opt} = 2.07$.

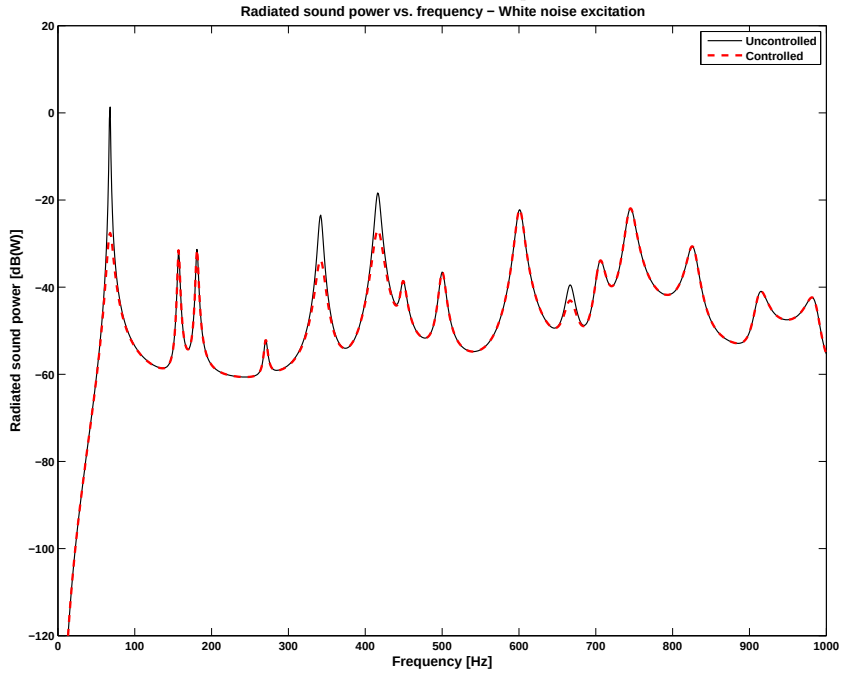

(b) Spectrum of radiated sound power assuming white noise excitation, before and after control. The average control effort for the controller was limited to 200 N^2.

Figure 6.16: Fixed central position - Placement and frequency responce for the single controller case. Single gain optimization for radiated sound power.

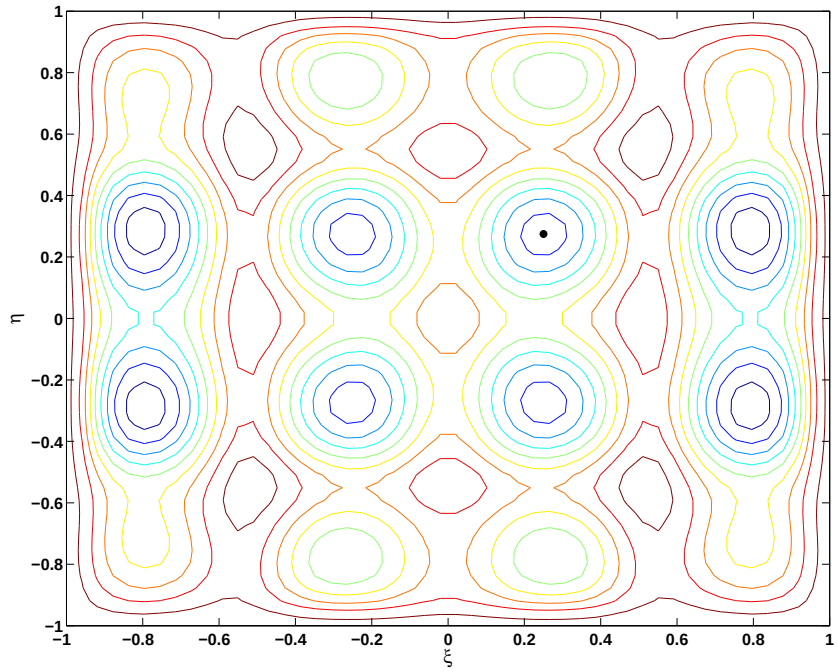

(a) $J_{ac} = 2.920 \times 10^6$, $g_{opt} = 2.87$.

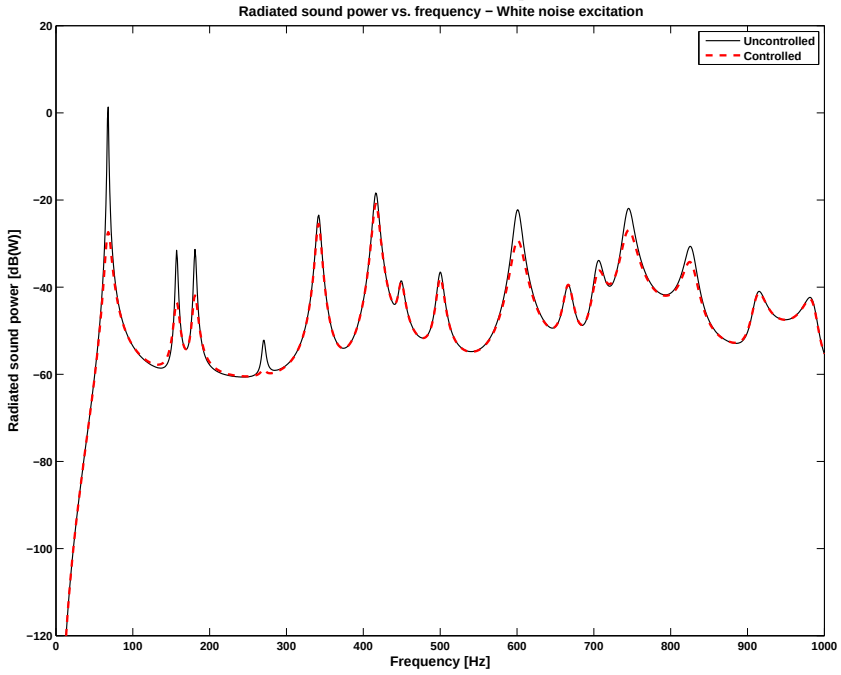

(b) Spectrum of radiated sound power assuming white noise excitation, before and after control. The average control effort for the controller was limited to 200 N^2.

Figure 6.17: Solution 1 - Placement and frequency responce for the single controller case.

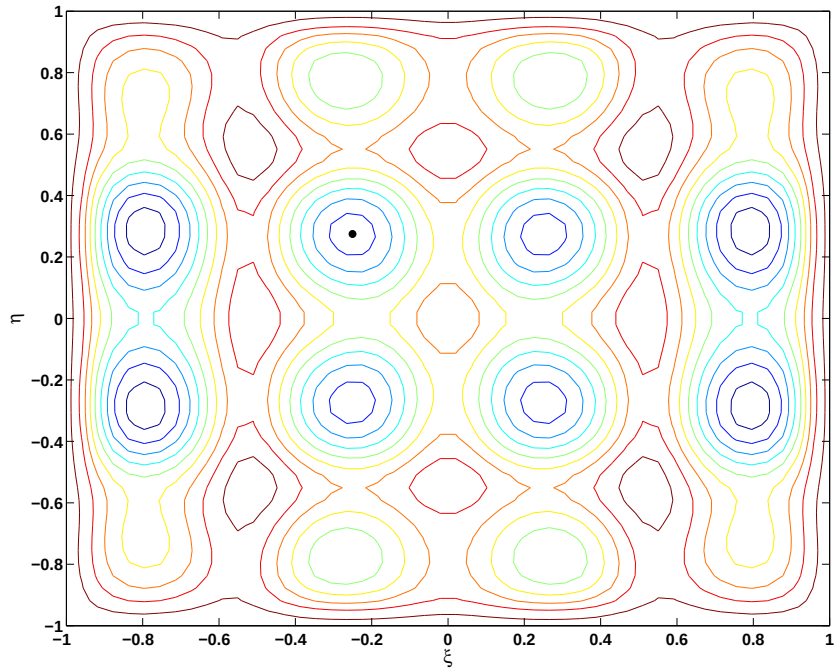

(a) $J_{ac} = 2.920 \times 10^6$, $g_{opt} = 2.87$.

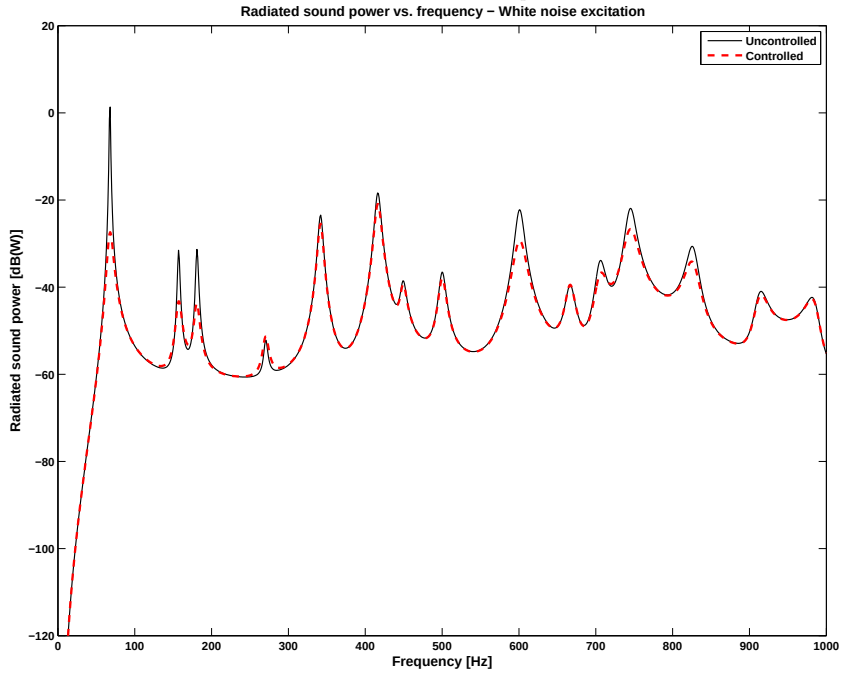

(b) Spectrum of radiated sound power assuming white noise excitation, before and after control. The average control effort for the controller was limited to 200 N^2.

Figure 6.18: Solution 2 - Placement and frequency responce for the single controller case.

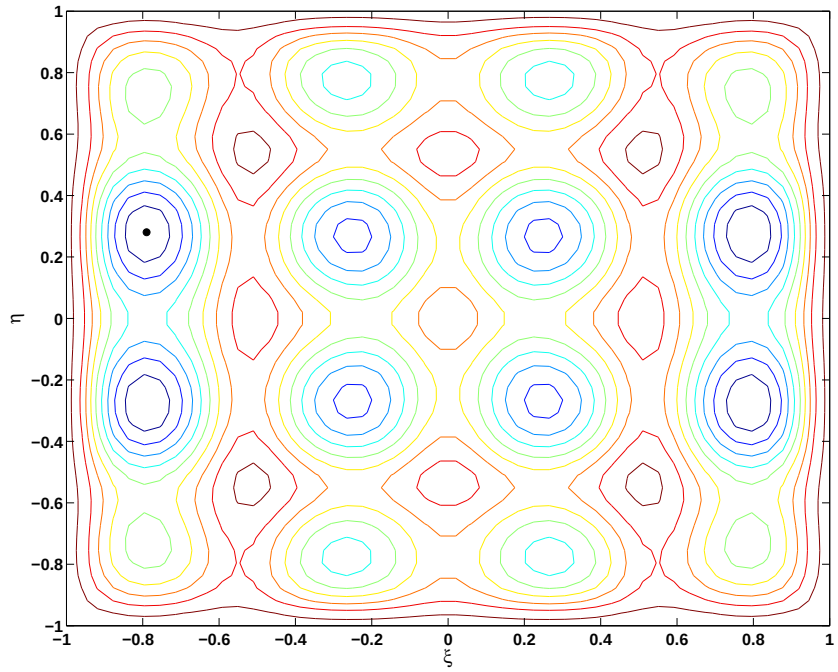

(a) $J_{ac} = 2.856 \times 10^6$, $g_{opt} = 2.40$.

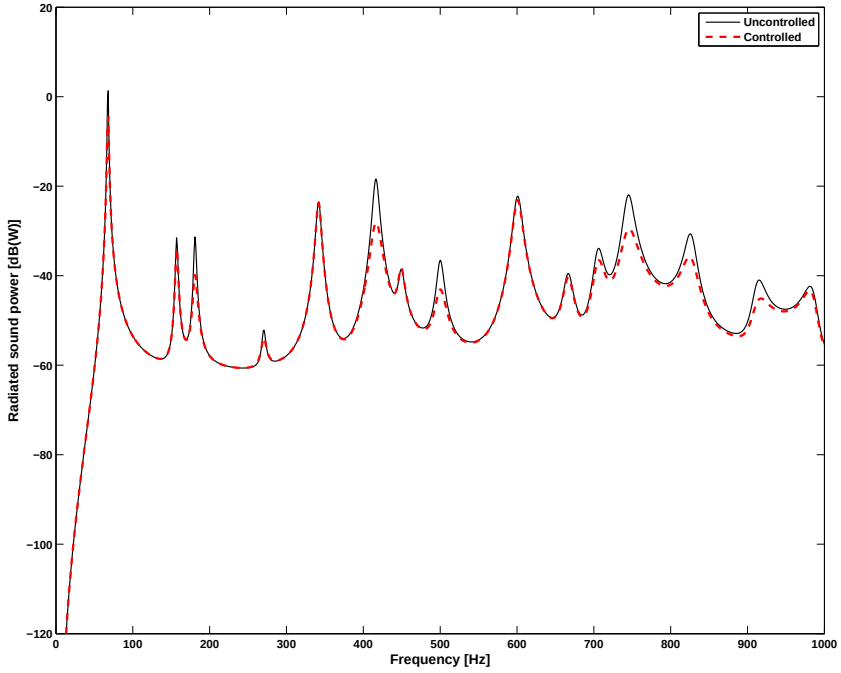

(b) Spectrum of radiated sound power assuming white noise excitation, before and after control. The average control effort for the controller was limited to 200 N^2.

Figure 6.19: Solution 3 - Placement and frequency responce for the single controller case.

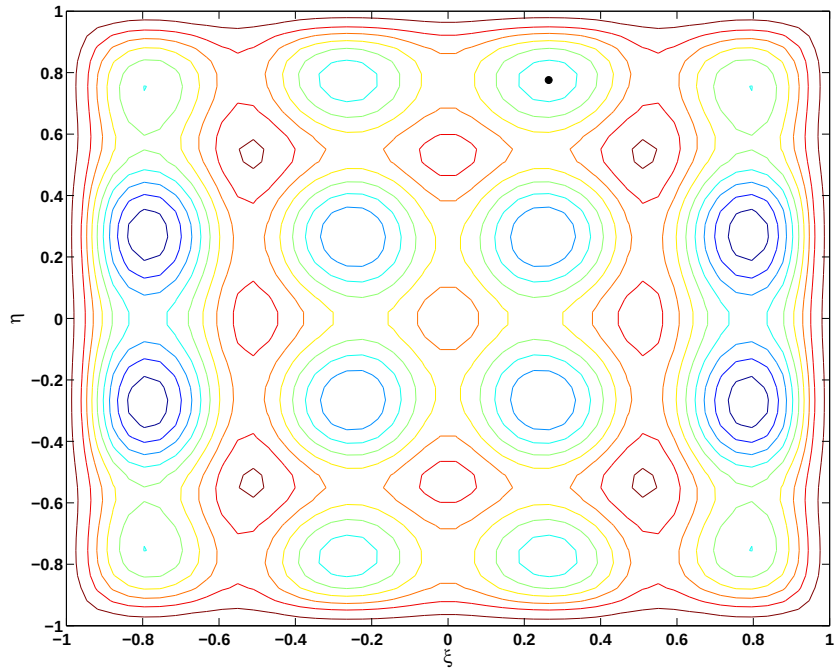

(a) $J_{ac} = 3.018 \times 10^6$, $g_{opt} = 2.02$.

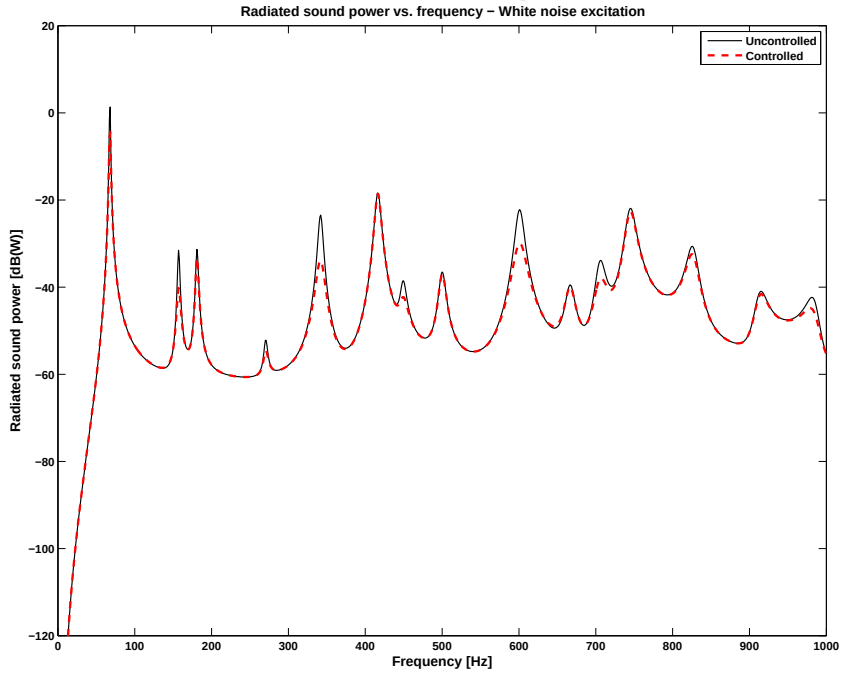

(b) Spectrum of radiated sound power assuming white noise excitation, before and after control. The average control effort for the controller was limited to 200 N^2.

Figure 6.20: Solution 4 - Placement and frequency responce for the single controller case.

6.3.3 Optimal placement and gains for 16 controllers. Kinetic energy and acoustic optimization

In this case the order of the series expansion is increased, until to have a very good approximation (with a maximum error of 0.5%) of the first 8 frequencies $M = N = 6$. The number of the most significant radiating modes is kept costant. At this time there are 48 optimization variables: three for each controller. The control penalty is $R = 1/1000$ for kinetic energy optimization and $R = 1/100$ for the acoustic optimization. For both the situations a comparison is made with a fixed grid of sensors and actuators as schematized in Fig.6.5b. The best frequency responce plots of each optimization procedure are shown, comparable with those of the fixed configuration.

Results of kinetic energy optimization. As you can see comparing the two frequency response of Fig.6.21b and Fig.6.24 the spectrum of the kinetic energy is almost the same, also for such a badly distributed optimal solution, but the velocity gains are lower for the optimized one.

Results of acoustic power optimization. Also in this case comparing the two frequency response of Fig.6.25b and Fig.6.28 the spectra of the radiated sound power are very similar, the optimal solution seems to be well distributed over the plate, and the velocity gains are lower with respect to the fixed grid optimization.

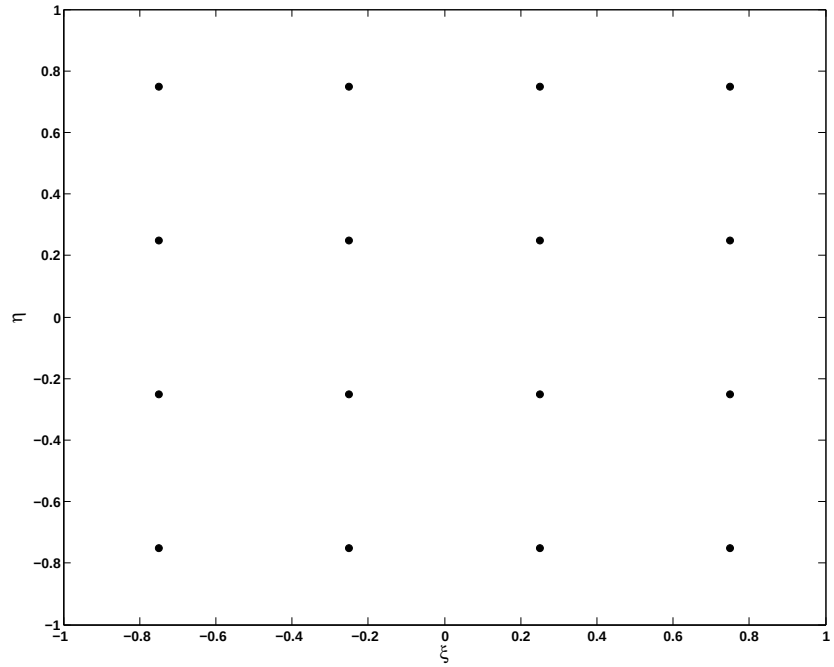

(a) $J_{ke} = 2.527 \times 10^6$, $\mathbf{G}_{opt} = \text{diag}\{1.043 \quad 1.056 \quad 1.056 \quad 1.040 \quad 1.047 \quad 1.036 \quad 1.036 \quad 1.052 \quad 1.052 \quad 1.030 \quad 1.031 \quad 1.047 \quad 1.037 \quad 1.057 \quad 1.060 \quad 1.043\}$.

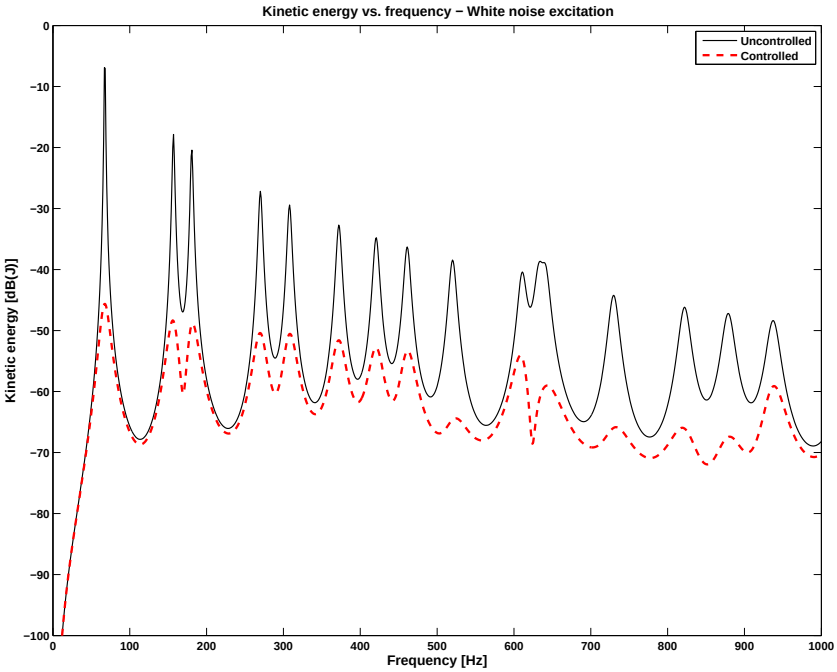

(b) Spectrum of kinetic energy assuming white noise excitation, before and after control. The average control effort for the controller was limited to 1000 N^2.

Figure 6.21: Fixed cconfiguration - Placement and frequency responce 16 controllers case. Gains optimization for kinetic energy.

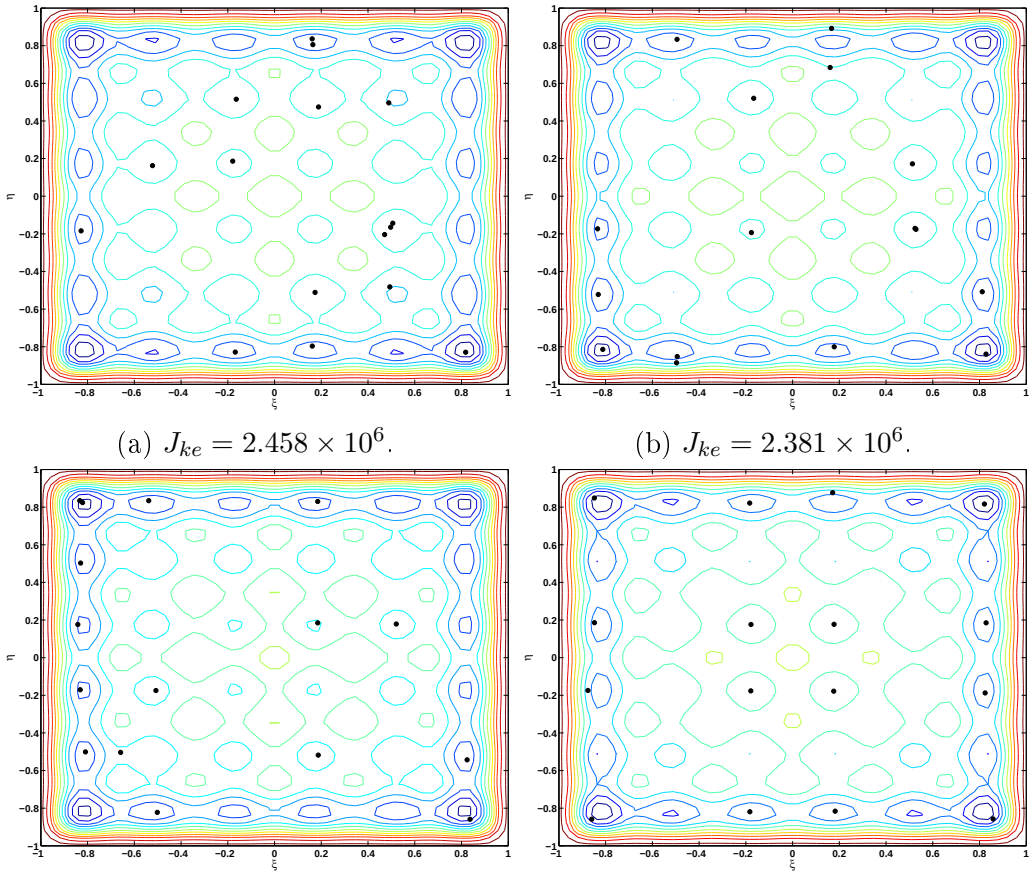

(a) $J_{ke} = 2.458 \times 10^6$.

(b) $J_{ke} = 2.381 \times 10^6$.

(c) $J_{ke} = 2.337 \times 10^6$.

(d) $J_{ke} = 2.374 \times 10^6$.

Figure 6.22: Optimized placements for the 16 controller case. Kinetic energy optimization

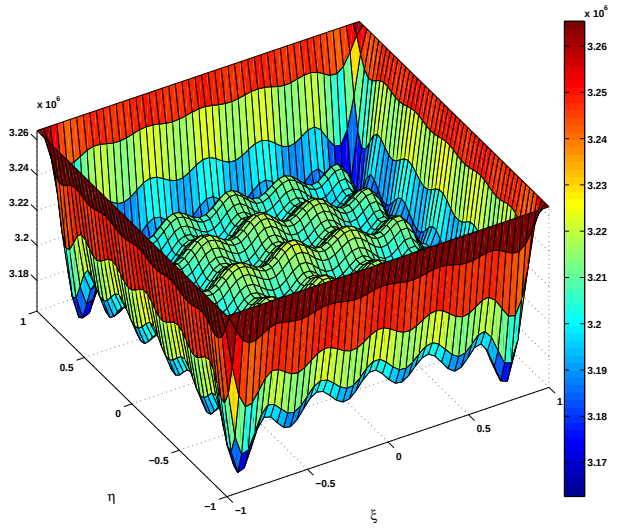

Figure 6.23: Cost function J_{ke} with respect to 16 actuator/sensor placement, $N = M = 6$, $g = 0.62$.

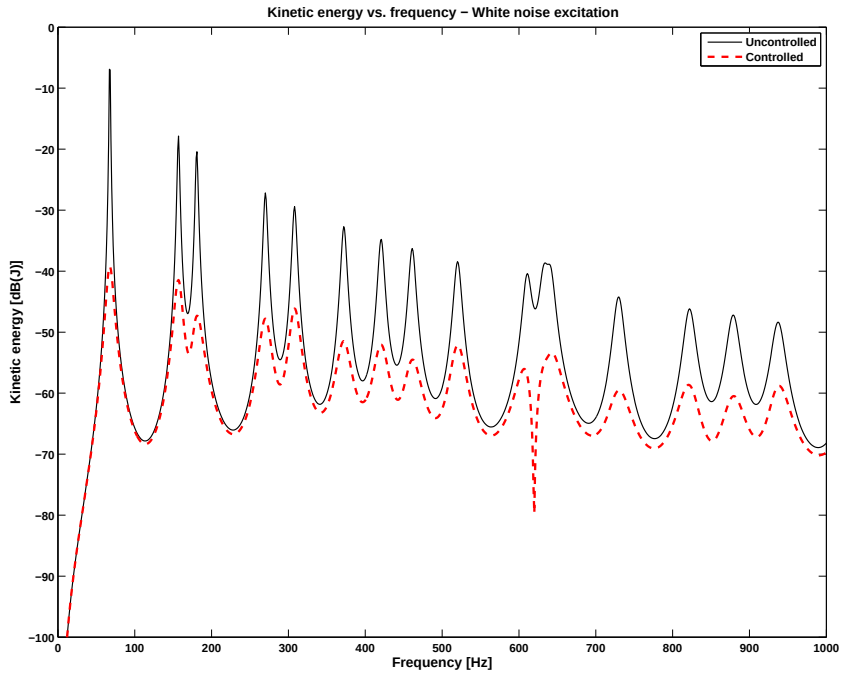

Figure 6.24: Spectrum of kinetic energy assuming white noise excitation, before and after control, for the optimum solution of Fig.6.22c. The average control effort for the controller was limited to 1000 N^2. $\mathbf{G}_{opt} = \mathrm{diag}\{0.820 \quad 1.123 \quad 0.880 \quad 0.899 \quad 1.100 \quad 0.886 \quad 1.056 \quad 0.938 \quad 0.871 \quad 0.803 \quad 0.974 \quad 0.838 \quad 0.939 \quad 1.012 \quad 1.008 \quad 0.879\}$.

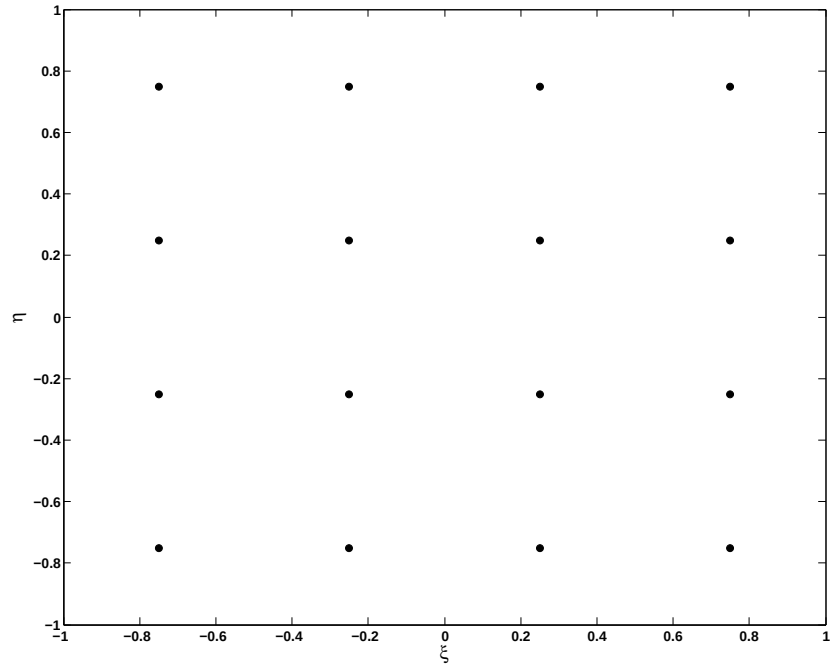

(a) $J_{ac} = 5.639 \times 10^7$, $\mathbf{G}_{opt} = \text{diag}\{1.507 \quad 1.776 \quad 1.770 \quad 1.501 \quad 2.040 \quad 2.787 \quad 2.798 \quad 2.045 \quad 2.038 \quad 2.783 \quad 2.793 \quad 2.044 \quad 1.513 \quad 1.766 \quad 1.772 \quad 1.508\}$.

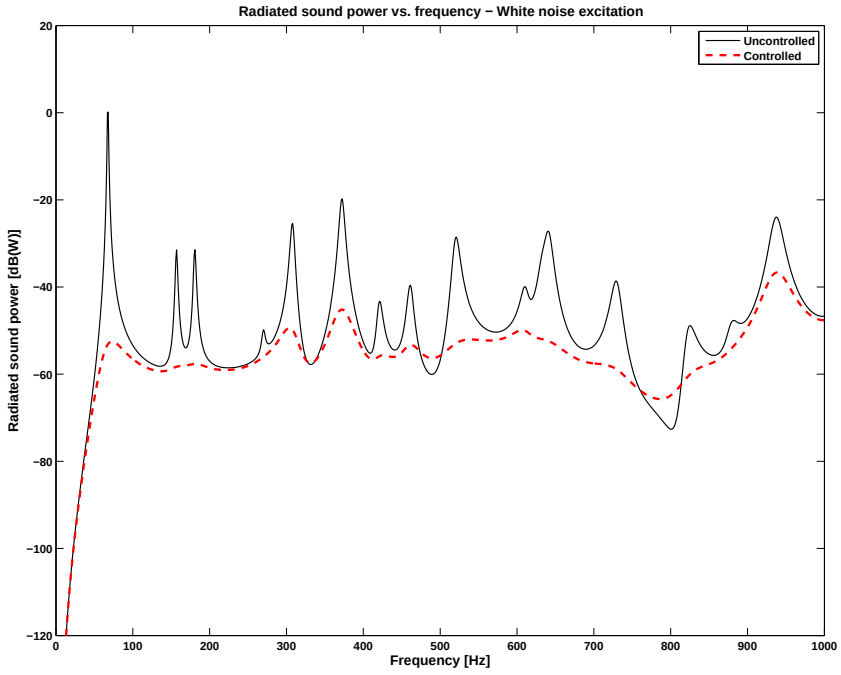

(b) Spectrum of radiated sound power assuming white noise excitation, before and after control. The average control effort for the controller was limited to 100 N^2.

Figure 6.25: Fixed cconfiguration - Placement and frequency responce 16 controllers case. Gains optimization for radiated soun power.

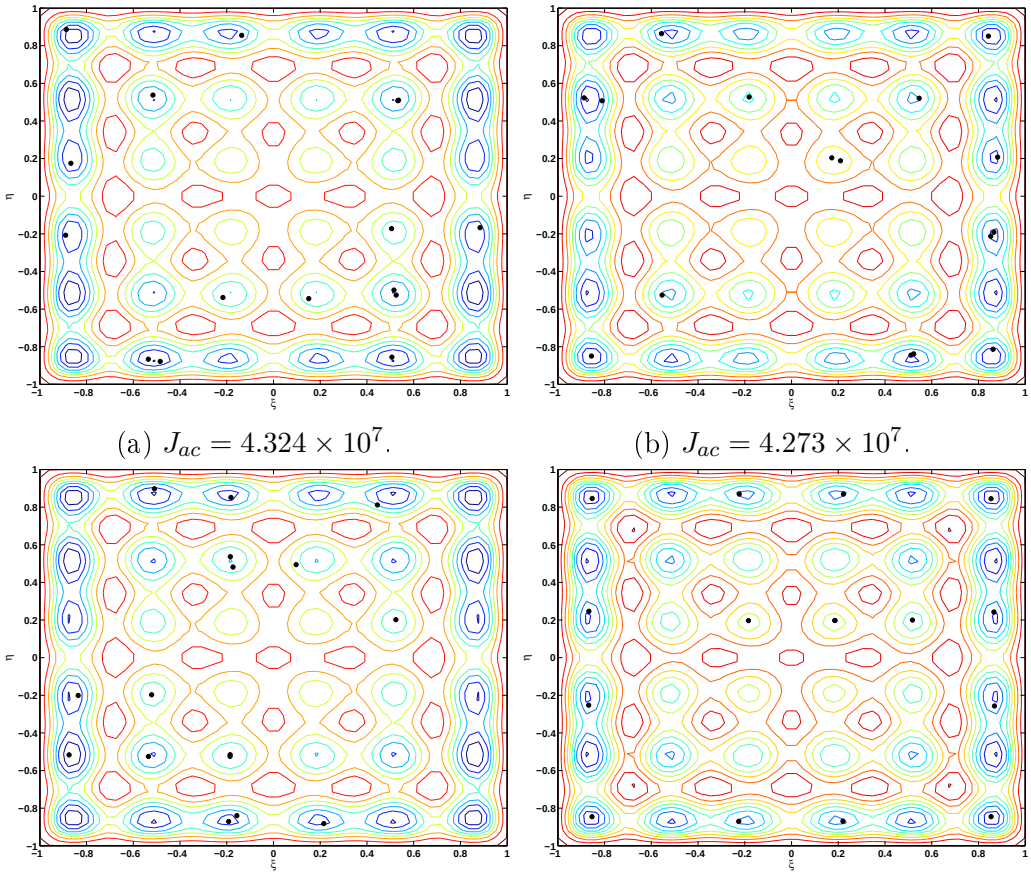

(a) $J_{ac} = 4.324 \times 10^7$.

(b) $J_{ac} = 4.273 \times 10^7$.

(c) $J_{ac} = 4.536 \times 10^7$.

(d) $J_{ac} = 4.222 \times 10^7$.

Figure 6.26: Optimized placements for the 16 controller case. Radiated sound power optimization.

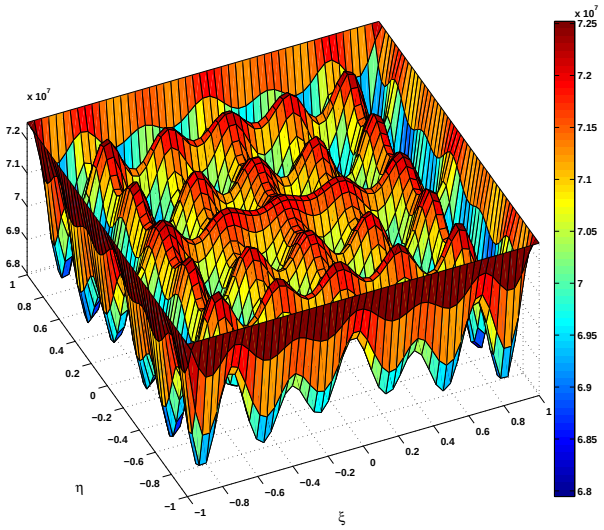

Figure 6.27: Cost function J_{ac} with respect to 16 actuator/sensor placement, $N = M = 6$, $RM = 6$, $g = 1.43$.

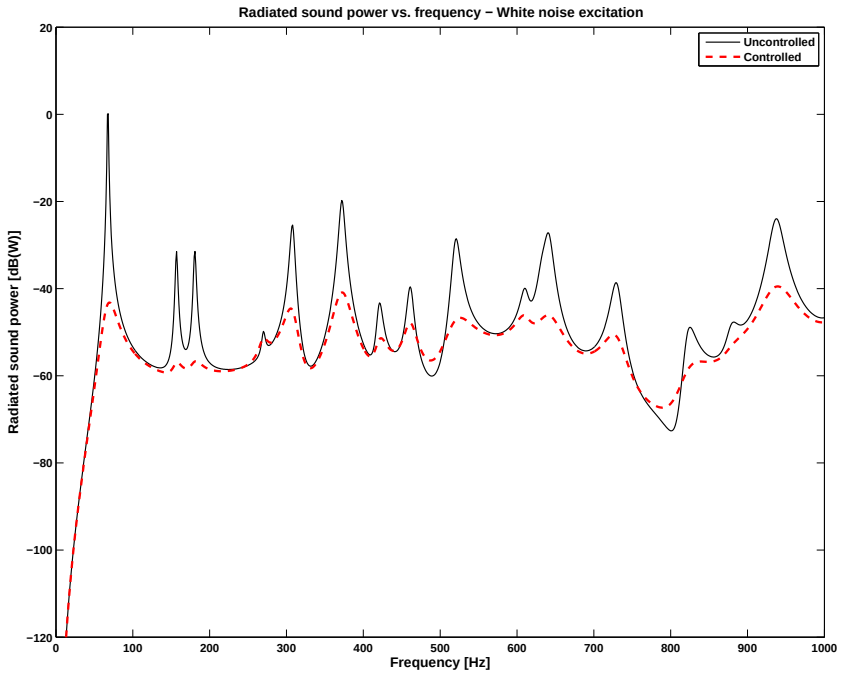

Figure 6.28: Spectrum of radiated sound power assuming white noise excitation, before and after control, for the optimum solution of Fig. 6.26d. The average control effort for the controller was limited to $100\,\mathrm{N}^2$. $\mathbf{G}_{opt} = \mathrm{diag}\{1.419 \quad 1.728 \quad 1.693 \quad 1.420 \quad 1.965 \quad 1.725 \quad 1.725 \quad 1.975 \quad 1.836 \quad 1.730 \quad 1.880 \quad 1.833 \quad 1.434 \quad 1.706 \quad 1.672 \quad 1.437\}$.

6.3.4 Optimal placement and gains for 100 controllers. Kinetic energy and acoustic optimization

Simulation are done with with an increasing order of the series expansion $N = M = 7$, and the same number of radiation modes $RM = 6$. The optimal placement of controllers is shown in Fig.6.29 for kinetic energy optimization and in Fig.6.31 for acoustic optimization. As expected, the placement results uniformly distributed throughout the plate, in such a way that all the local minima of the function are identified. This optimization problem is a simple study of distributed control, which have wide potential applications. The problem is also a demonstration of how easy the nonlinear programming algorithm can handle 300 variables.
Figures 6.30 and 6.32 show di results in terms of the frequency response. The attenuation at this time is very strong over the whole band of interest. The final optimal results for the gains are plotted as a function over the plate in Fig.6.33 and 6.34. The gain levels assume a sort of symmetrical distribution with respect to the structure geometry, and are nearly constant. This indicates that for distributed control, spatially constant gains may be an appropriate design strategy.

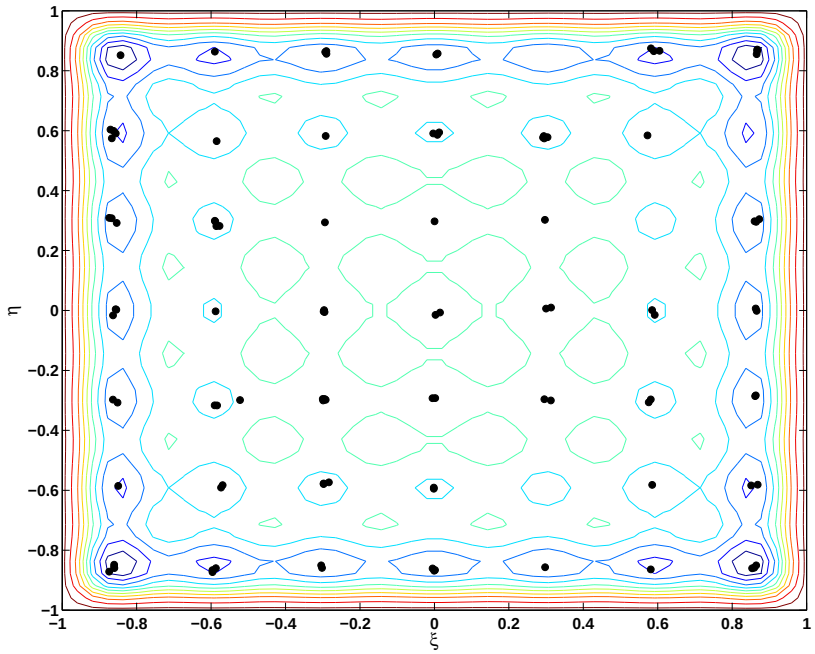

Figure 6.29: Placement of 100 controllers - Kinetic energy optimization

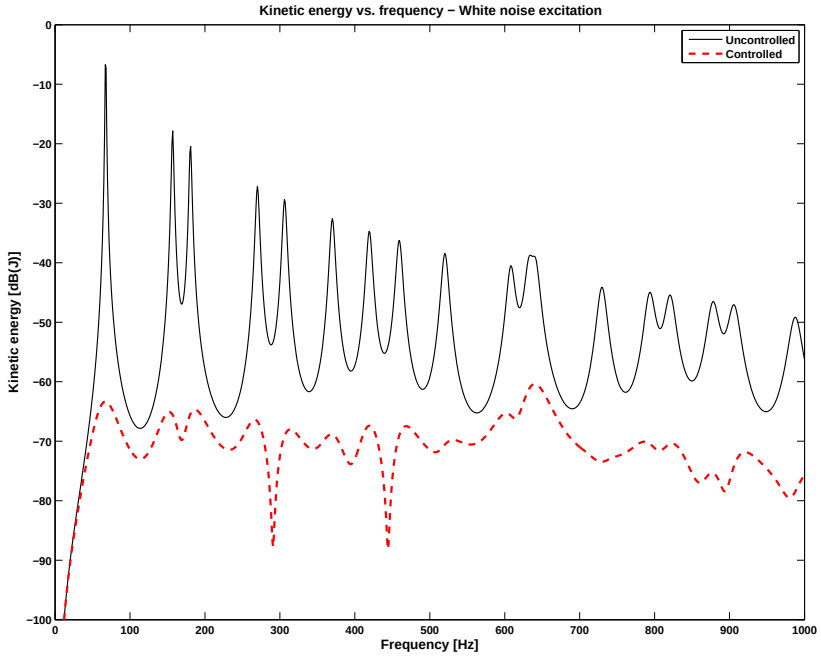

Figure 6.30: Spectrum of kinetic energy assuming white noise excitation, before and after control. The average control effort for the controller was limited to 900 N^2

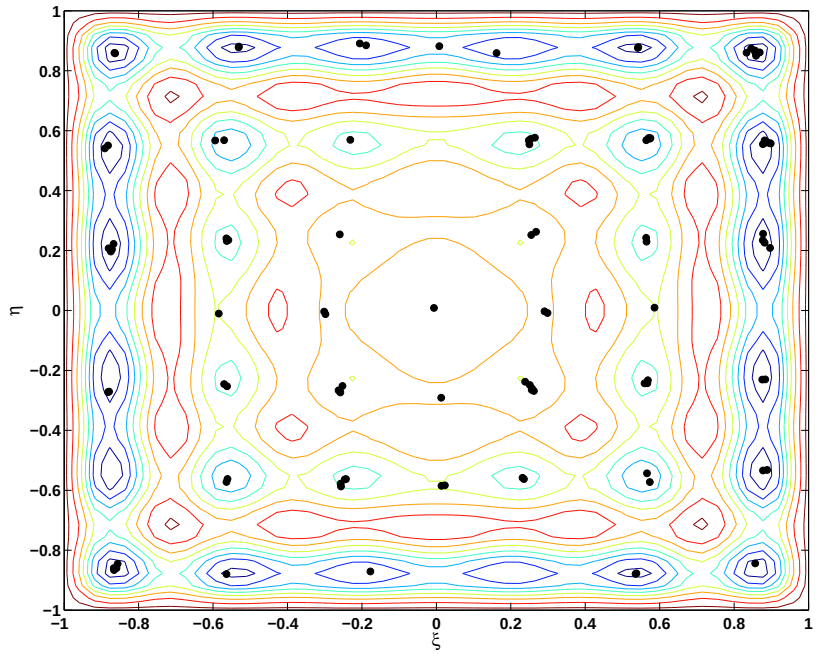

Figure 6.31: Placement of 100 controllers - Radiated sound power optimization

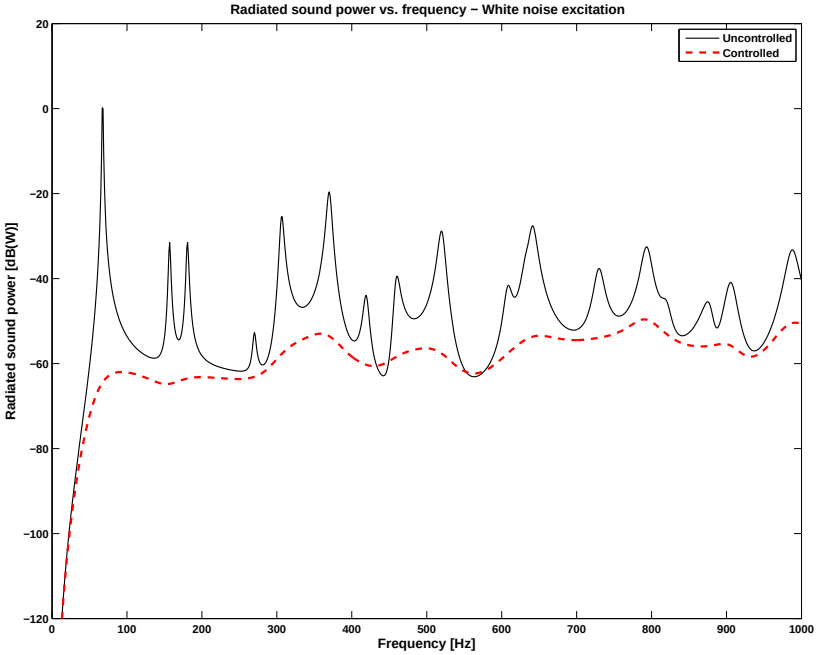

Figure 6.32: Spectrum of radiated sound power assuming white noise excitation, before and after control. The average control effort for the controller was limited to 100 N^2

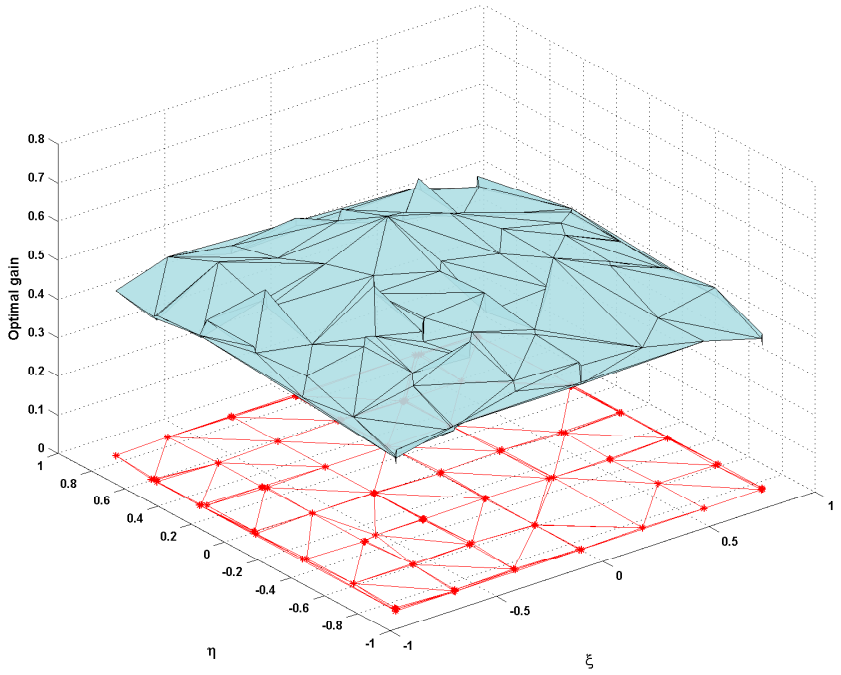

Figure 6.33: Optimal gains for the 100 controllers' case - Kinetic energy optimization.

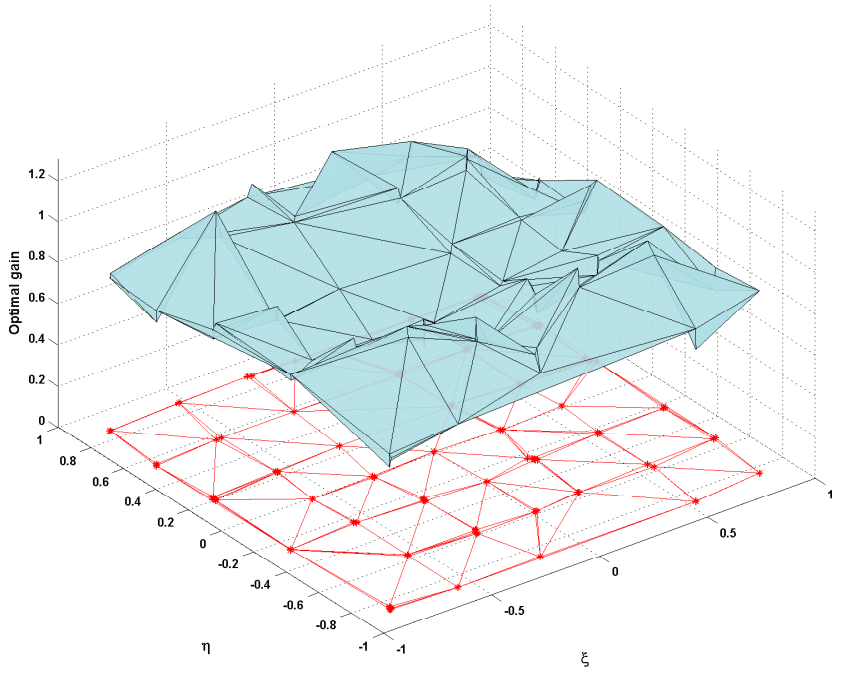

Figure 6.34: Optimal gains for the 100 controllers' case - Acoustic optimization.

6.4 Results for different boundary conditions

In the following, significant results are presented, with the aim of showing that there are differences by applying optimization to structures with different boundary conditions. Some standard and simple results are shown for demonstration purposes, performing only kinetic energy optimization. These results, together with those that follow, represent the final goal of this thesis.

6.4.1 Fully clamped plate (CCCC)

A fully clamped plate with zero deflection and rotation on all four edges. The control effort weighting coefficient is set to $R = 1/500$. In Figure 6.36 four optimal solution are presented, and at the end the frequency response for the best one is plotted in Fig.6.37. The reported plots show the expected results: with a fully clamped plate, the optimal positions are more displaced toward the center of the plate, because of the greater rigidity of the plate near the edges (null displacement and rotation).

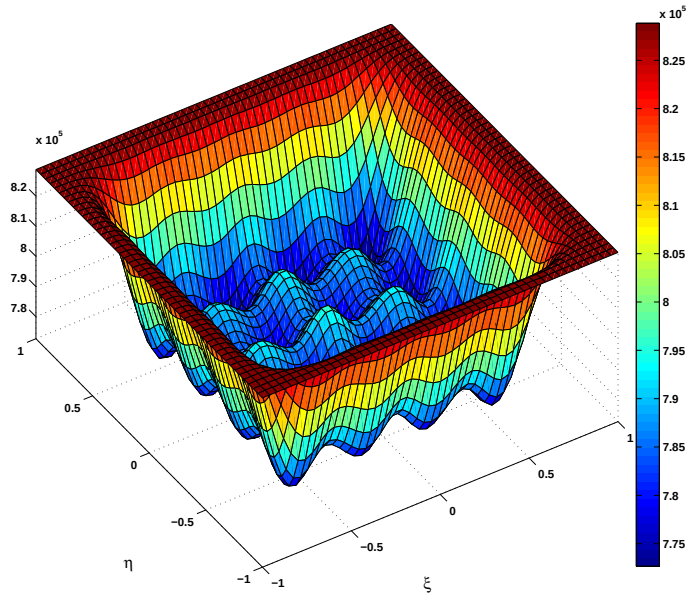

Figure 6.35: Cost function J_{ke} with respect to 8 actuator/sensor placement, $N = M = 4$, $RM = 6$, $g = 0.86$.

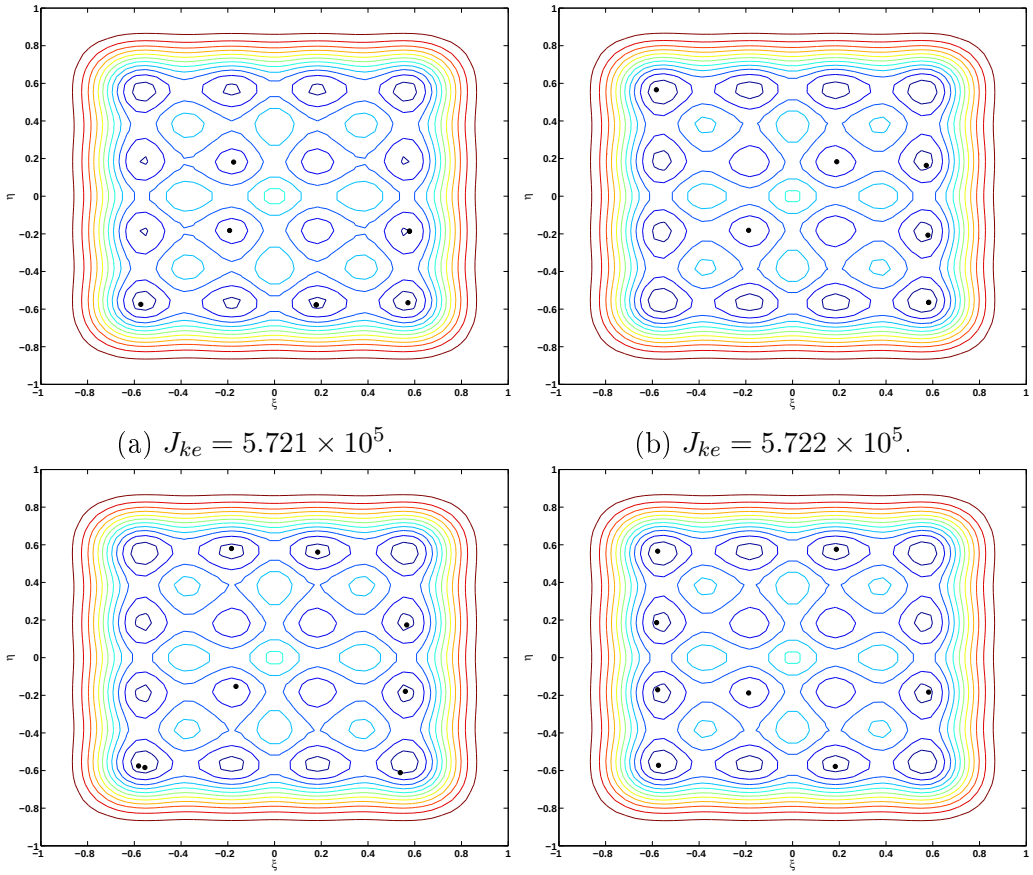

(a) $J_{ke} = 5.721 \times 10^5$.

(b) $J_{ke} = 5.722 \times 10^5$.

(c) $J_{ke} = 5.725 \times 10^5$.

(d) $J_{ke} = 5.676 \times 10^5$.

Figure 6.36: Optimized placements for 8 controllers. (CCCC) plate. Kinetic energy optimization.

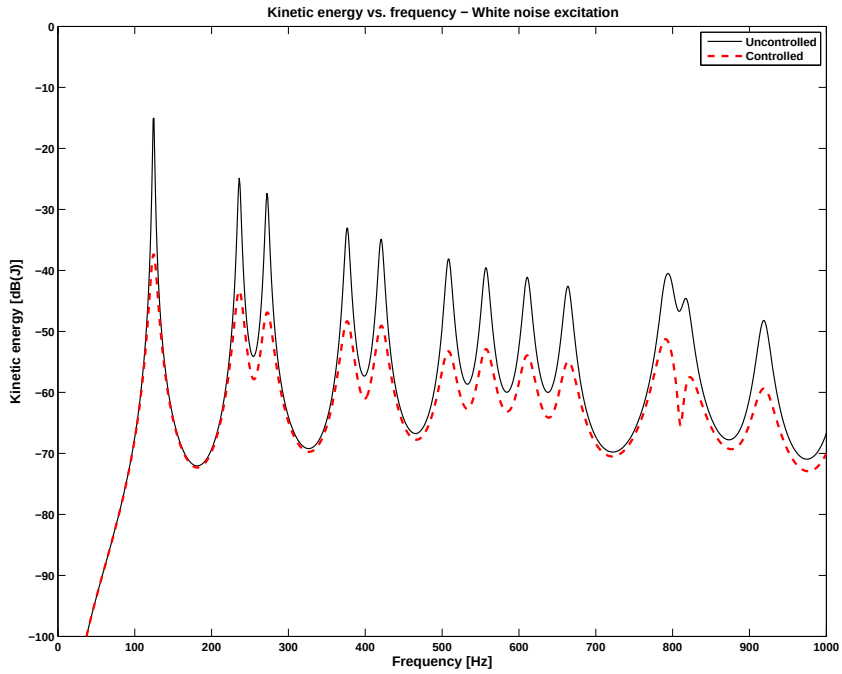

Figure 6.37: Spectrum of kinetic energy assuming white noise excitation, before and after control, for the optimum solution of Fig.6.36d. The average control effort for the controller was limited to $500\,\mathrm{N}^2$. $\mathbf{G}_{opt} = \mathrm{diag}\{0.842 \quad 0.876 \quad 0.850 \quad 0.817 \quad 0.848 \quad 0.829 \quad 0.826 \quad 0.868\}$.

6.4.2 Half clamped, half simply supported plate (CCSS)

This is a plate with zero deflection and rotation on 2 adjacent edges and zero deflection and free rotation on the other 2 adjacent edges. The control effort weighting coefficient is set to $R = 1/500$. In Figure 6.38 four optimal solution are presented, and at the end the frequency response for the best one is plotted in Fig.6.40. Also in this case the plots show the expected results: the CCSS plate has non-symmetric boundary conditions, so the placement of controllers should comply with the same geometry. In fact the edges with a simply supported conditions show controllers located closer to those edges.

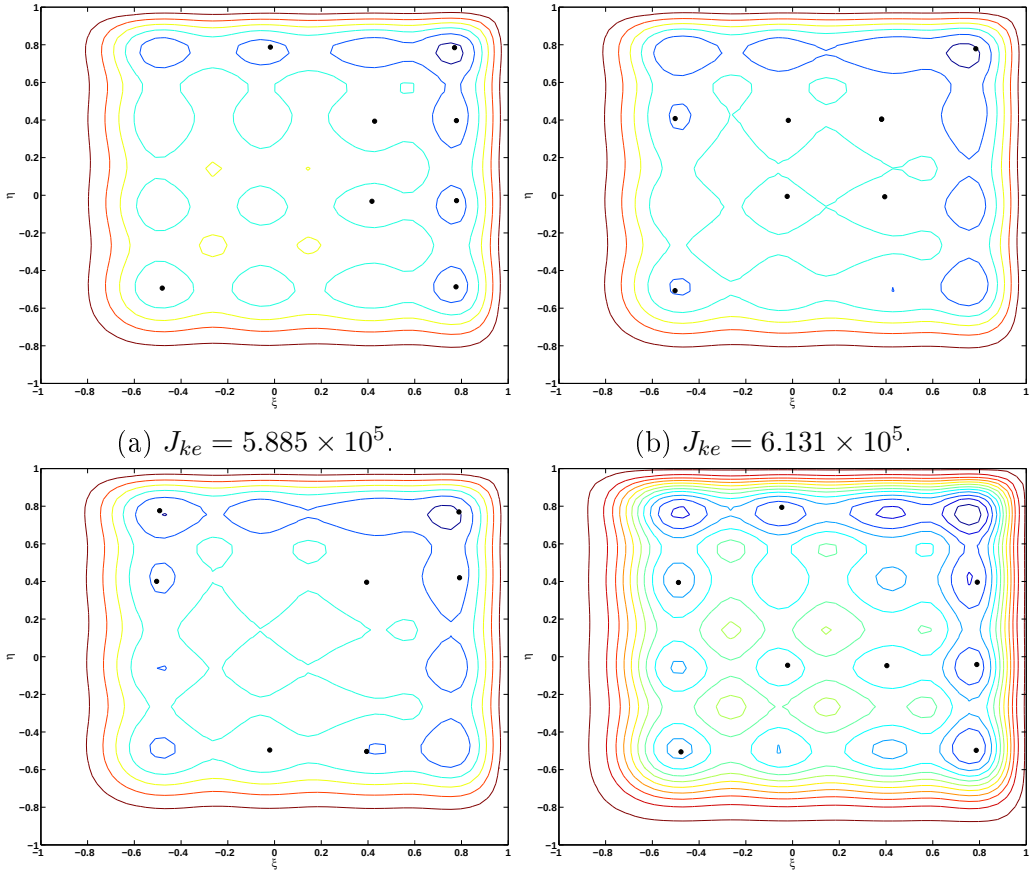

(a) $J_{ke} = 5.885 \times 10^5$.

(b) $J_{ke} = 6.131 \times 10^5$.

(c) $J_{ke} = 5.946 \times 10^5$.

(d) $J_{ke} = 5.992 \times 10^5$.

Figure 6.38: Optimized placements for 8 controllers. (CCSS) plate. Kinetic energy optimization.

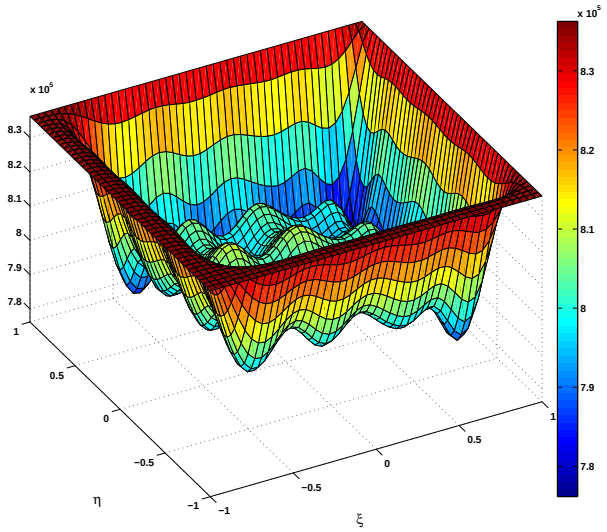

Figure 6.39: Cost function J_{ke} with respect to 8 actuator/sensor placement, $N = M = 4$, $RM = 6$, $g = 0.79$.

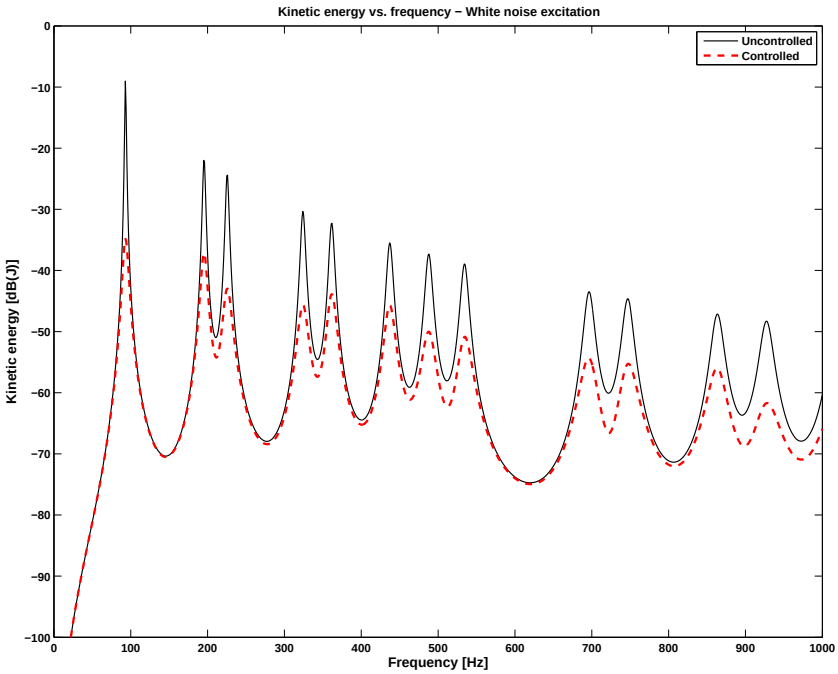

Figure 6.40: Spectrum of kinetic energy assuming white noise excitation, before and after control, for the optimum solution of Fig.6.38a. The average control effort for the controller was limited to $500\,\mathrm{N}^2$. $\mathbf{G}_{opt} = \mathrm{diag}\{1.055 \quad 0.670 \quad 0.819 \quad 0.818 \quad 0.863 \quad 0.759 \quad 0.724 \quad 0.790\}$.

6.4.3 Clamped free plate (CCCF)

This plate has zero deflection and rotation on 3 adjacent edges and free deflection and free rotation on one edge. The control effort weighting coefficient is set to $R = 1/300$. In Figure 6.41 four optimal solution are presented, and at the end the frequency response for the best one is plotted in Fig.6.43. In this case the results are particularly significant: as it should be, the minimum of the function J is concentrated around the free edge of the plate. This is because it is the only side that has complete freedom to move and through which, then, it is easier to control the entire structure. Other local minima are visible in the central areas, which provide alternative optimal solutions.

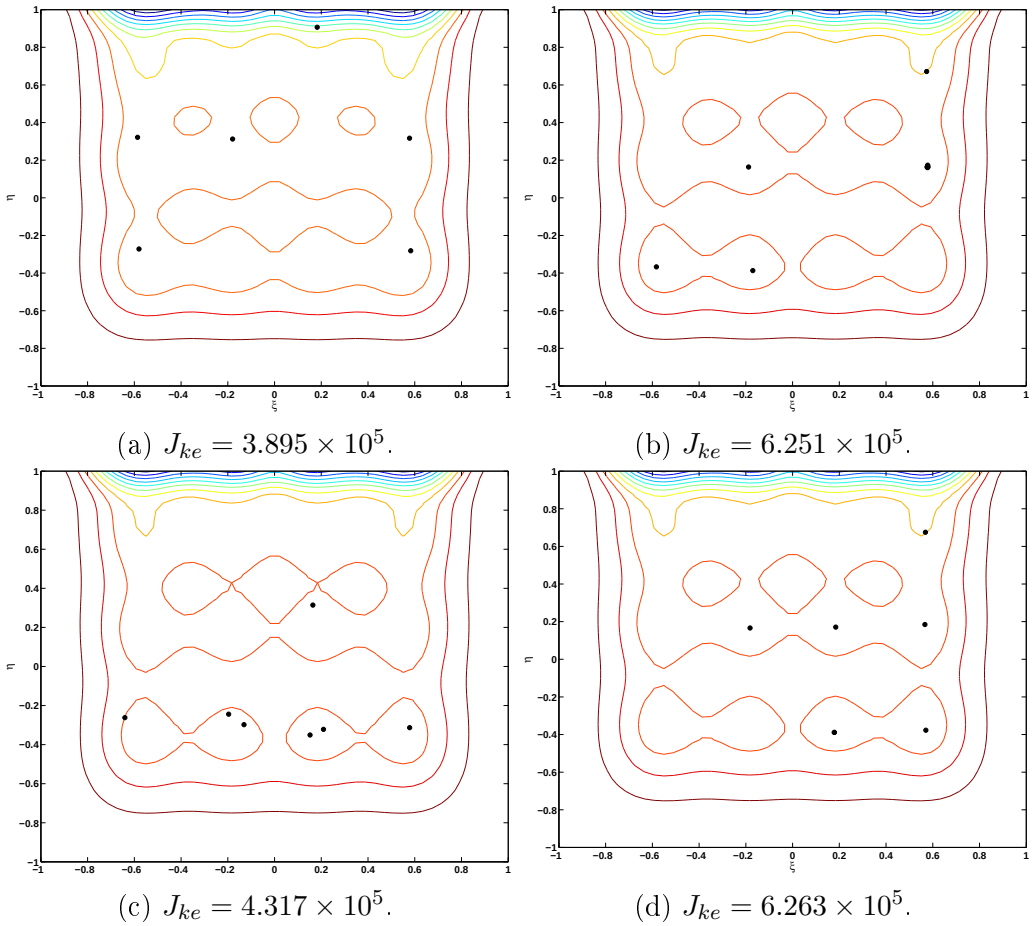

(a) $J_{ke} = 3.895 \times 10^5$. (b) $J_{ke} = 6.251 \times 10^5$.

(c) $J_{ke} = 4.317 \times 10^5$. (d) $J_{ke} = 6.263 \times 10^5$.

Figure 6.41: Optimized placements for 8 controllers. (CCCF) plate. Kinetic energy optimization.

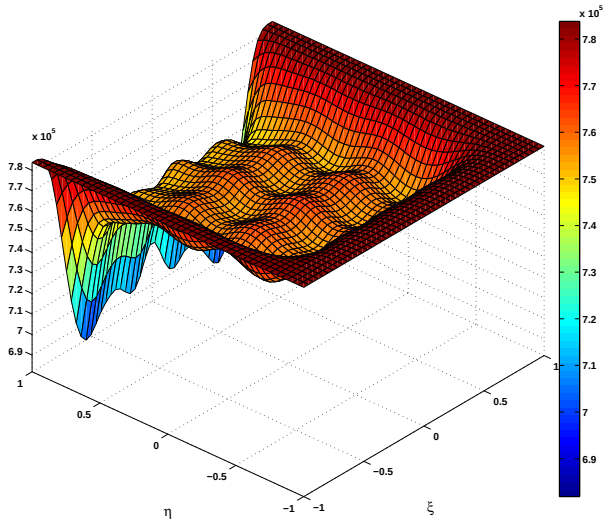

Figure 6.42: Cost function J_{ke} with respect to 8 actuator/sensor placement, $N = M = 4$, $RM = 6$, $g = 0.68$.

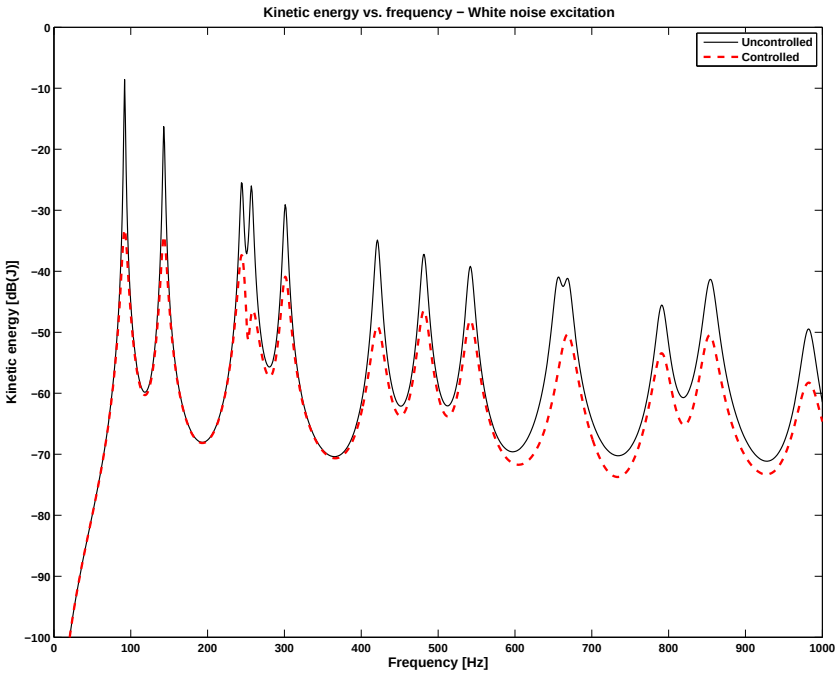

Figure 6.43: Spectrum of kinetic energy assuming white noise excitation, before and after control, for the optimum solution of Fig.6.41a. The average control effort for the controller was limited to $300\,\mathrm{N}^2$. $\mathbf{G}_{opt} = \mathrm{diag}\{0.606 \quad 0.071 \quad 0.063 \quad 0.714 \quad 0.609 \quad 0.707 \quad 0.659 \quad 0.682\}$.

6.5 Results with the addition of complicating effects

Here comes the most interesting results of the study. At the simple plate with general boundary conditions, other external complicating effect were added, to aggravate the dynamics of the structure, i.e., the mass and stiffness matrix of the plate, as described by Dozio [3]. In order to not increase too much the CPU time of computing, all simulations were made with $N = M = 4$ (which provide an excelent approximation of the first frequencies), with the placement of 8 controllers. The most characteristic results are shown, as a starting point for the most varied applications.

6.5.1 Elastic point supports

Ideal support conditions, i.e., exactly zero normal displacement of the plate, imply infinitely rigid supports, which rarely occur in practice. So the elasticity of any intermediate support is introduced as described in [3]. The plate is a simply supported plate (SSSS), which characteristics are listed in Table 5.1. The control effort weighting coefficient is set to $R = 1/800$, and an optimization of the kinetic energy is performed. In Fig.6.44 the 3D representation of the performance index, clearly shows a maximum peak at the position of the point support. Figures 6.45 and 6.46 presents one optimal solution with the realtive spectrum of the kinetic energy.

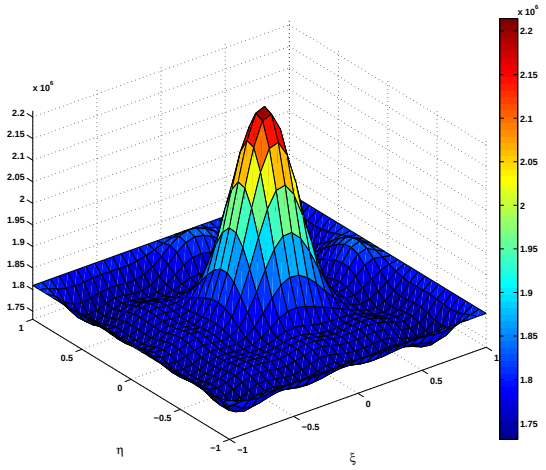

Figure 6.44: Cost function J_{ke} with respect to 8 actuator/sensor placement, $N = M = 4$, $RM = 6$, $g = 1.45$. Point support at position $(0.1, 0.1)$, with dimensionless translational stiffness $k^T a^3/D_{11} = 1 \times 10^8$.

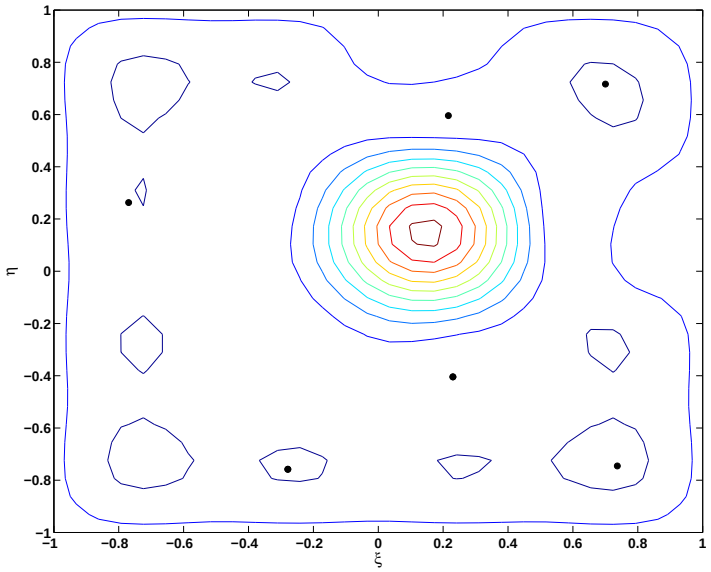

Figure 6.45: $J_{ke} = 1.557 \times 10^6$.

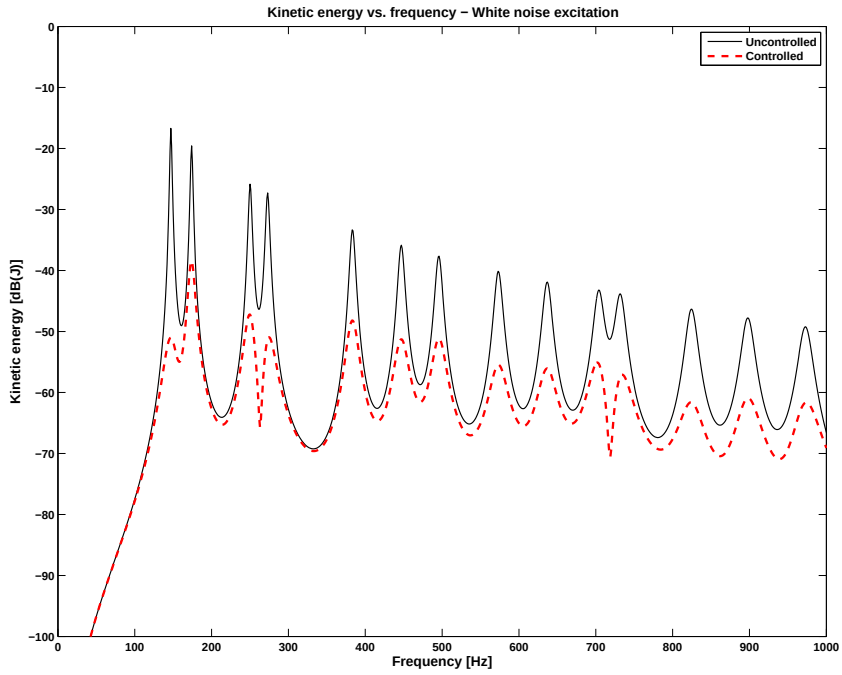

Figure 6.46: Spectrum of kinetic energy assuming white noise excitation, before and after control, for the optimum solution of Fig.6.45. The average control effort for the controller was limited to 800 N^2. $\mathbf{G}_{opt} = \mathrm{diag}\{1.413 \quad 1.179 \quad 1.313 \quad 1.413 \quad 1.242 \quad 1.313 \quad 1.142 \quad 1.459\}$.

6.5.2 Elastic line supports

At this time the translation spring is imposed on the entire line crossing the plate. The simply supported plate (SSSS) with the same dimensions, at this time is modeled with different material properties to prove the capabilities of the method. A T-graphite/epoxy is considered, which properties are listed in Table A.3. The control effort weighting coefficient is set to $R = 1/1200$, and an optimization of the kinetic energy is performed. In Fig.6.47 the 3D representation of the performance index clearly shows a maximum peak at the entire line support. Figures 6.48 and 6.49 presents one optimal solution with the realtive spectrum of the kinetic energy.

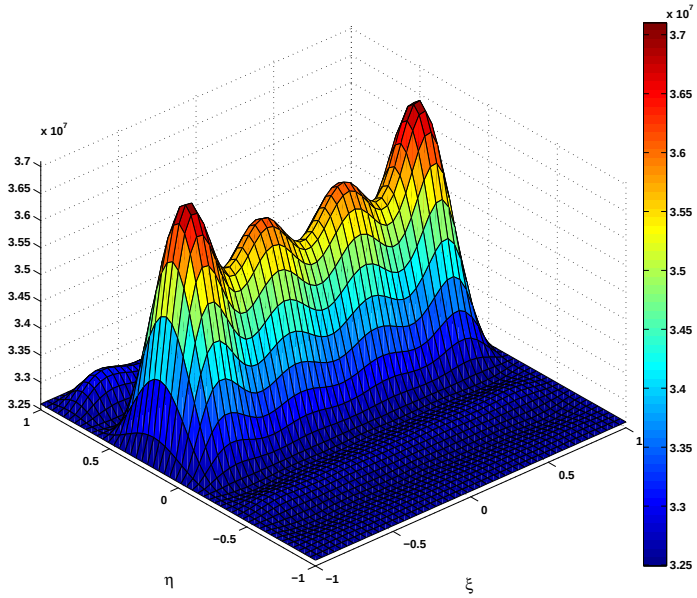

Figure 6.47: Cost function J_{ke} with respect to 8 actuator/sensor placement, $N = M = 4$, $RM = 6$, $g = 1.24$. Line support at position $\eta = 0.2$, with dimensionless translational stiffness $k^T a^3/D_{11} = 1 \times 10^9$.

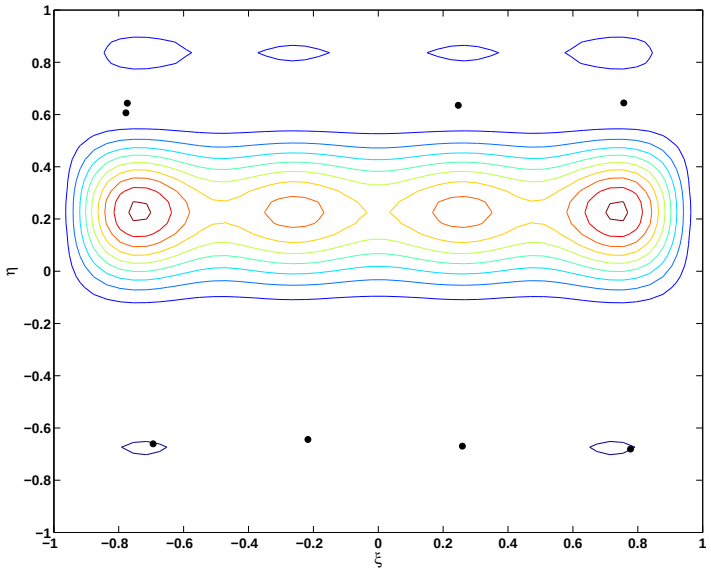

Figure 6.48: $J_{ke} = 3.230 \times 10^7$.

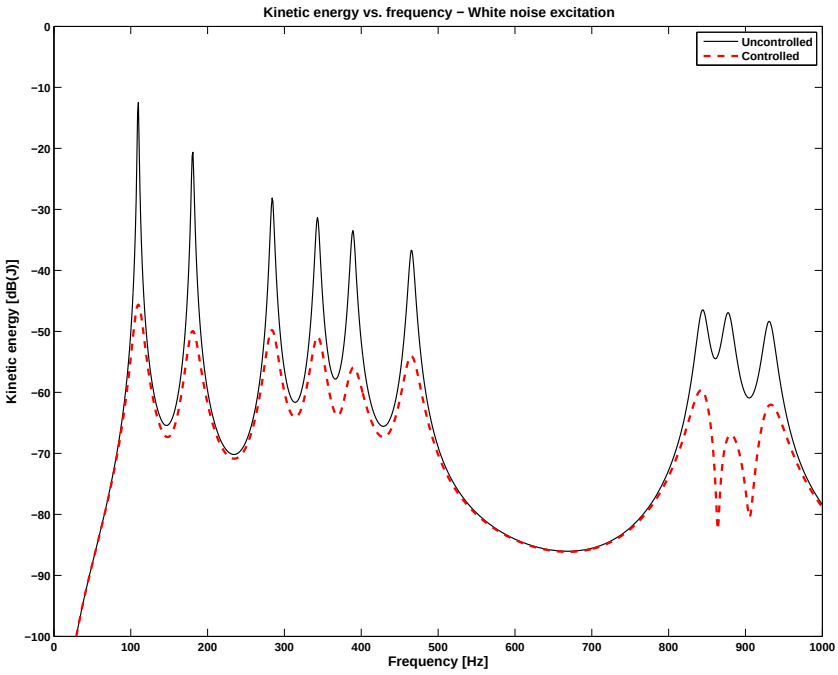

Figure 6.49: Spectrum of kinetic energy assuming white noise excitation, before and after control, for the optimum solution of Fig.6.48. The average control effort for the controller was limited to 1200 N^2. $\mathbf{G}_{opt}$ = diag{0.878 1.010 0.147 0.822 0.476 1.018 0.806 1.248}.

6.5.3 In-plane loaded plate

Keeping the same tipe of material (T- graphite/epoxy) this time a constant in-plane load per unit width is considered. The routine involves the insertion of in-plane loads N_x and N_y acting in the x-and-y directions, respectively, together with constant in-plane shear force per unit width N_{xy}. For this simulation only N_x is considered, in order to perceive its effect on the performance index. The control effort weighting coefficient is set to $R = 1/10$, and an optimization of radiated soun power is performed. In Fig.6.50 the 3D representation of the performance index shows a particolar shape of the local minima that exhibit an elongation in the direction opposite to the N_x direction. Figures 6.51 and 6.52 presents one optimal solution with the realtive spectrum of the radiated sound power. It can also be noticed a lower acoustic performance index with respect to the previous similar cases, because of the larger stiffness of the structure due to the preload to which it is subjected.

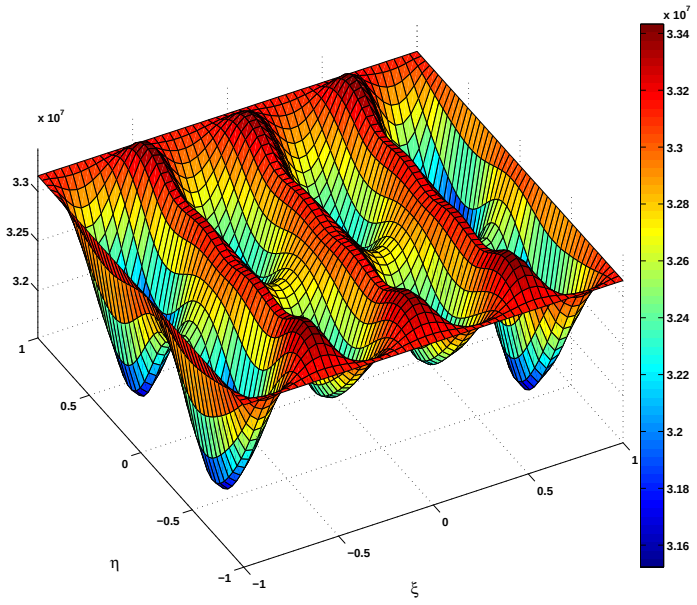

Figure 6.50: Cost function J_{ac} with respect to 8 actuator/sensor placement, $N = M = 4$, $RM = 6$, $g = 0.55$. In-plane load per unit width $N_x = 100$.

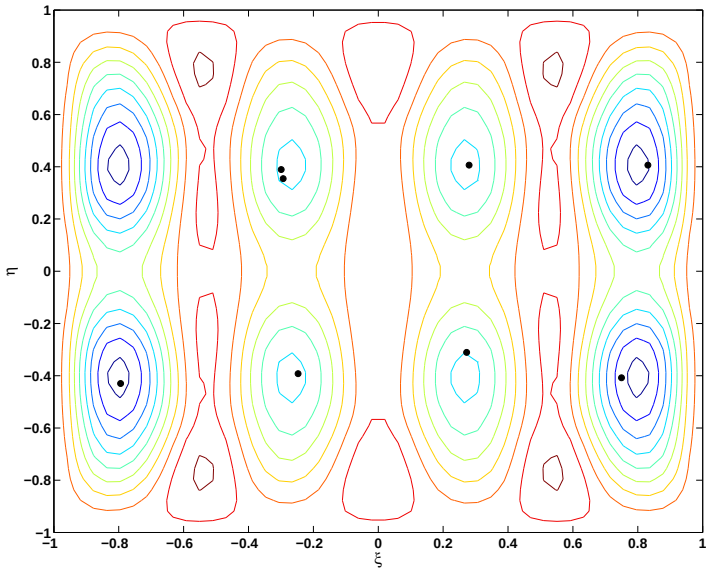

Figure 6.51: $J_{ac} = 2.661 \times 10^7$.

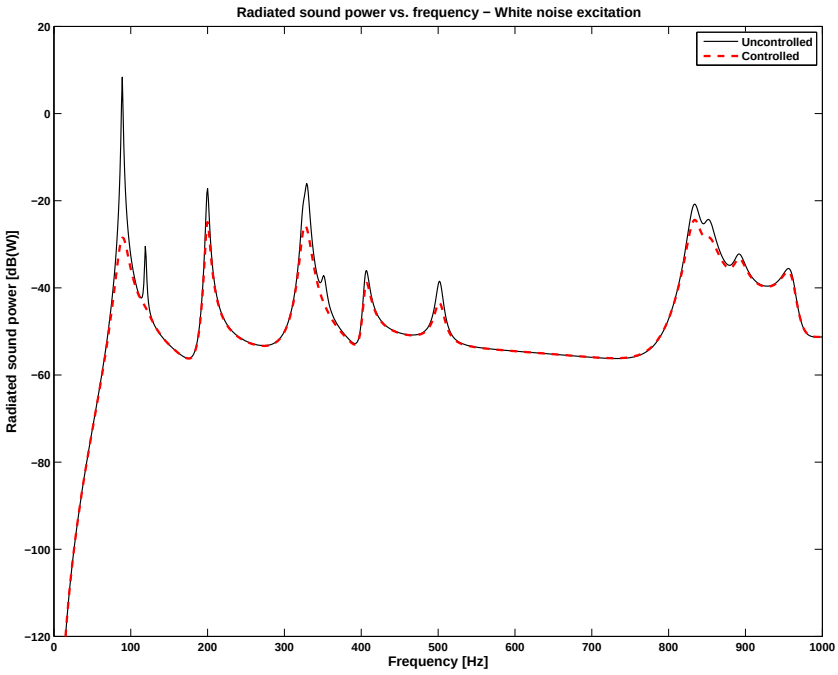

Figure 6.52: Spectrum of radiated sound power assuming white noise excitation, before and after control, for the optimum solution of Fig.6.51. The average control effort for the controller was limited to $10\,\mathrm{N}^2$. $\mathbf{G}_{opt} = \mathrm{diag}\{0.541 \quad 0.533 \quad 0.374 \quad 0.693 \quad 0.478 \quad 0.598 \quad 0.704 \quad 0.557\}$.

6.5.4 Rigid concentrated masses

Often plates may be loaded with a variety of devices attached to them. Such loading conditions represent a further complicating factor for the plate analysis in addition to dealing with general boundary conditions and intermediate elastic supports. Tipically, they have a strong effect on the natural frequencies and mode shapes of the loaded plate and therefore their contribution cannot be disregarded without adversely affect the accuracy of the solution. The approximation of this behavoiur is made considering a concentrated mass on a fixed location of the plate. The control effort weighting coefficient is set to $R = 1/50$, and an optimization of radiated sound power is performed. In Fig.6.53 the 3D representation of the performance index shows a sort of "forbidden region", corresponding to the location of the attached mass, where the controllers cannot be effective . Figures 6.54 and 6.55 presents one optimal solution with the realtive spectrum of the radiated sound power.

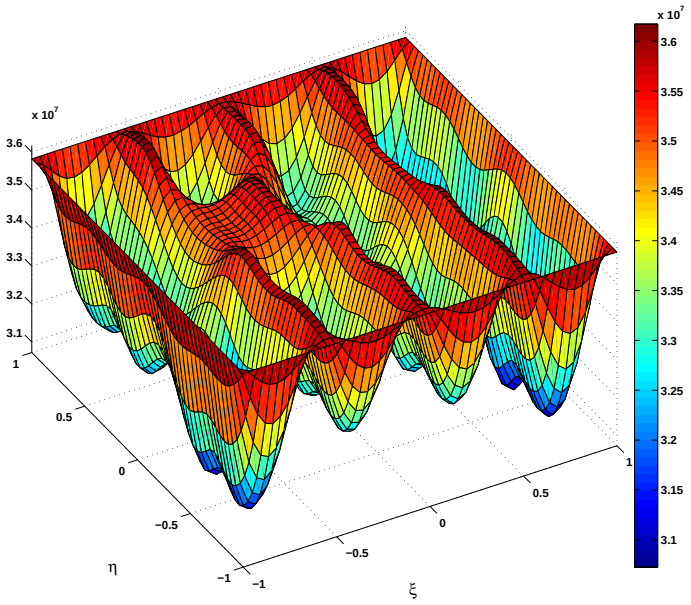

Figure 6.53: Cost function J_{ac} with respect to 8 actuator/sensor placement, $N = M = 4$, $RM = 6$, $g = 2.37$. Rigid concentrated mass $m = 30\%\, m_{plate}$ at position (-0.2, 0.3).

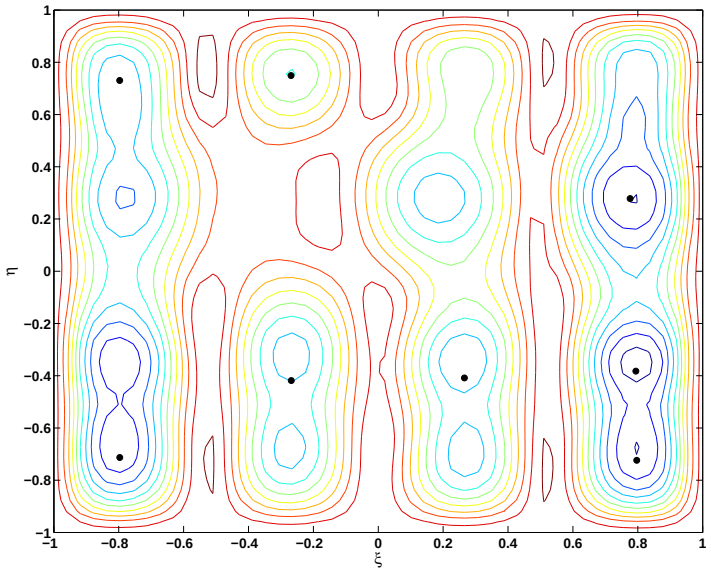

Figure 6.54: $J_{ac} = 1.806 \times 10^7$.

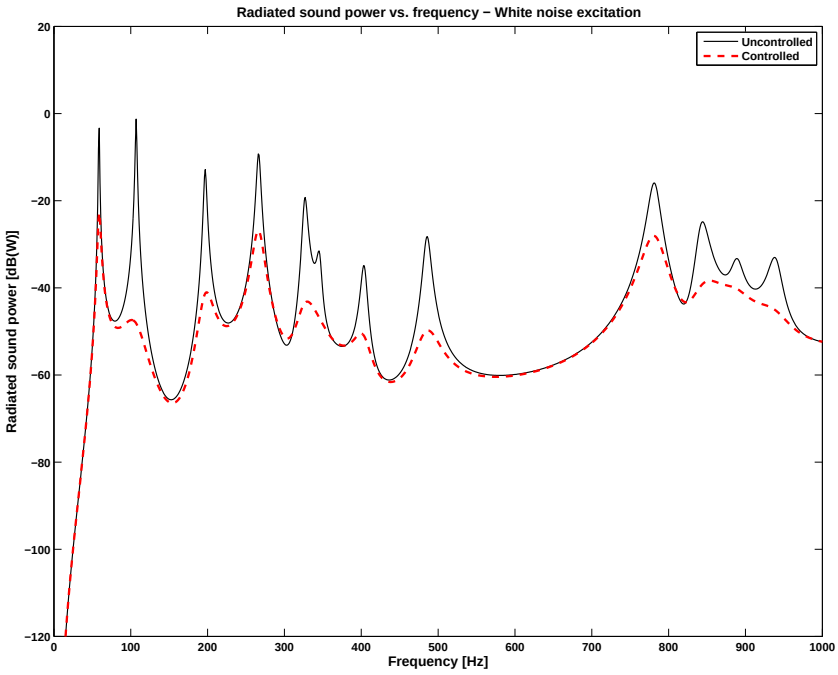

Figure 6.55: Spectrum of radiated sound power assuming white noise excitation, before and after control, for the optimum solution of Fig.6.54. The average control effort for the controller was limited to $50\,\mathrm{N}^2$. $\mathbf{G}_{opt} = \mathrm{diag}\{2.033 \quad 1.715 \quad 1.492 \quad 1.632 \quad 1.486 \quad 1.742 \quad 1.869 \quad 2.375\}$.

6.5.5 Sensors and actuators with mass

In light of the previous result, a simulation where the attached masses were constituted by the controllers, which positions have to be optimized, is performed. This leads to an optimization with changing dynamic, since the mass matrix changes at each interation. The algorithm converges even in this case, making the results even more realistic. A (CCSS) T-graphite/epoxy plate is considered with in-plane load N_y applied. The control effort weighting coefficient is set to $R = 1/1000$, and an optimization of kinetic energy is performed. In Fig.6.56 the 3D representation of the performance index is plotted. Figures 6.57 and 6.58 presents one optimal solution with the realtive spectrum of the kinetic energy.

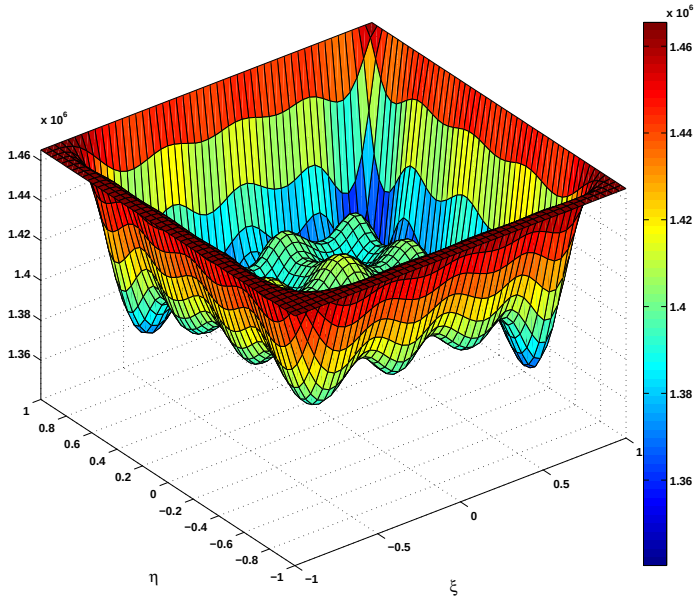

Figure 6.56: Cost function J_{ke} with respect to 8 actuator/sensor placement, $N = M = 4$, $RM = 6$, $g = 1.29$. Sensor/actuator mass $m = 3\%\, m_{plate}$. In-plane load per unit width $N_y = 100$.

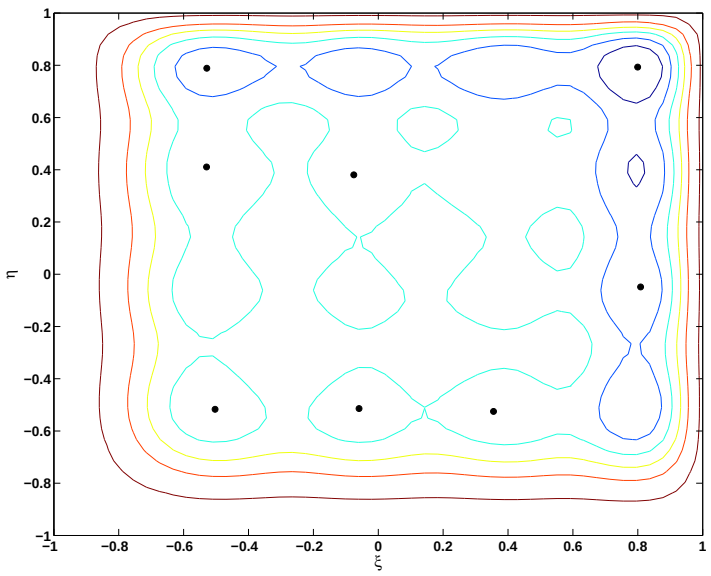

Figure 6.57: $J_{ke} = 9.273 \times 10^5$.

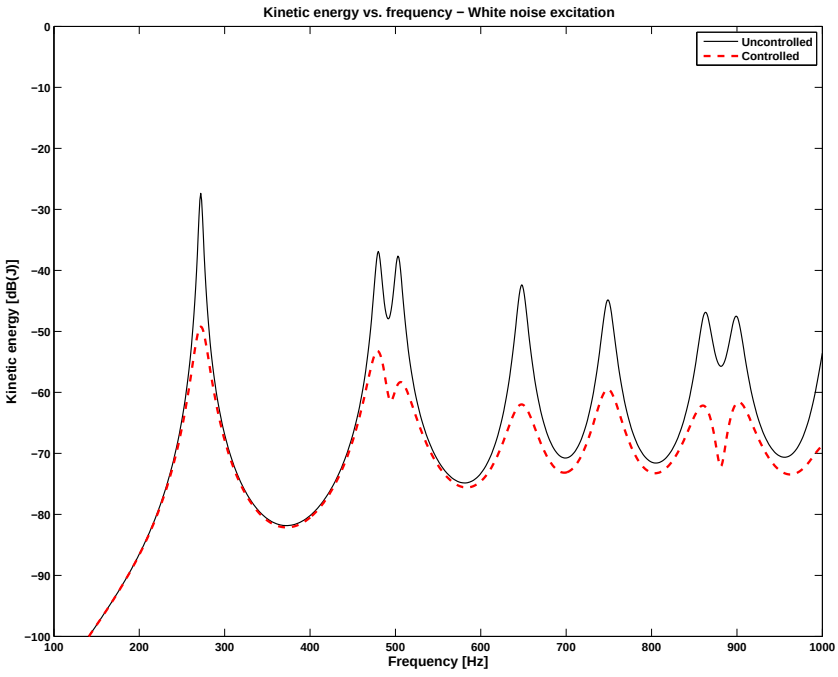

Figure 6.58: Spectrum of radiated sound power assuming white noise excitation, before and after control, for the optimum solution of Fig.6.57. The average control effort for the controller was limited to $1000\,\mathrm{N}^2$. $\mathbf{G}_{opt} = \mathrm{diag}\{1.347 \quad 1.271 \quad 1.241 \quad 1.193 \quad 1.216 \quad 1.379 \quad 1.433 \quad 1.298\}$.

Chapter 7

Conclusions

A NEW emproved method is presented for optimal design of placement and gains of actuators and sensors in output feedback control system, for kinetic energy and acoustic optimization, on various plate problems with an arbitrarily selected subset of complicating factors including in-plane stresses, elastic boundaries, concentrated attachments and internal supports.
A structural modelization (reffering to Dozio [3]) and an acoustic modelization (referring to Gibbs et al. [6] and Fahy and Gardonio [5]) of a plate were performed summarizing the entire problem in a state space representation. The method enhances the nonlinear programming approach with the use of analytical expressions for the gradients of the performance functions. This method is efficient and can handle a large number of optimization variables. It has a good convergence with an excellent approximation for the first natural frequencies.
Increasing the order of the series expansion for the modelization of the plate, the time-computing for the optimization procedure grows exponentially, due to the resolution of Lyapunov equations for bigger and bigger matrices. So only few terms were considered, till $N = M = 10, 12$, which, however, lead to a good approximation for most of the real problems. Moreover, the two performance indeces considered for the optimization are strongly dependent from the weighting control effort coefficient, so it should be accurately selected in order to generate reliable results.
Several numerical studies were performed finding that multiple local minima for the performance functions are possible for the optimal placement problem. They are located all over the plate and in some way they are connected to the minimization of a certain range of frequencies. Local minima on the center of the plate, well control the low frequency range, instead those closest to the edges well control the high frequency range. This makes sense because

low-frequency oscillations involves the first vibration modes and manifest large displacements in the central areas of the plate, while high-frequency oscillation modes also involve higher modes, with displacement also in the extreme areas, in the edges proximity.
In conclusion, the present analysis has shown the versatility and reliability of the approach, that can be considered a valuable tool for projecting control systems for thin rectangular plates for a wide class of problems with complicating effect.

7.1 Future developments

The work presents a large variety of numerical or phisical aspects that can be improved, or adapted to different types of applications and challenging situations, starting from the complicating effects for the structure, to the definition of new performance functions to be minimize.
Here follows, as an example, a small list of topics that can be taken as a direction path for future research work.

- Improvement of the numerical optimization thecnique using Hessian based methods, instead of a Gradient based one.
- Consider not-colocated sensors and actuators, with their own internal dynamics.
- Consider centralized control or other tipe of control strategies.
- Define new tipes of perfomance indeces, also based on the frequency domain.
- Built a structure model with the inclusion of varying in-plane loads, cutouts, non-uniform thickness.
- Include a new tipe of plate geometry in the optimization procedure.
- Extend the method to the resarch of optimal location for sensors and actuators on three-dimensional structures.

Appendix A

Input parameters

THE optimization process needs the inclusion of some input variables related to the type of optimization performed, the characteristics of the plate used, with the corresponding boundary conditions and complicating effects, and the acoustic model adopted. In the following, these variables are described.

According to Eq.6.3 and the state vector adopted in Eq.3.43, the weighting matrix $\mathbf{Q}$ exploited in the kinetic energy optimization is:

$$\mathbf{Q} = \begin{bmatrix} 0 & 0 & 0 \\ 0 & \mathbf{I} & 0 \\ 0 & 0 & 0 \end{bmatrix} \tag{A.1}$$

While, according to Eq.3.42, the weighting matrix $\mathbf{Q}$ exploited in the acoustic optimization is:

$$\mathbf{Q} = \begin{bmatrix} 0 \\ \mathbf{D}_{ac} \\ \mathbf{C}_{ac} \end{bmatrix} \begin{bmatrix} 0 & \mathbf{D}_{ac} & \mathbf{C}_{ac} \end{bmatrix} \tag{A.2}$$

In the following, the other input variables are tabulated:

Table A.1: Variables of the structural model.

Plate variables	
a, b	x and y dimensions of the plate
N_{sa}	number of sensor/actuators used in the simulation
$M = N$	terms of the series expansion in x and y direction
m_{sa}	mass of sensor/actuators with resepct to the plate mass
ζ	modal damping coefficient
R	control effort penalty
Complicating effects	
bcs	boundary conditions
mat	material of the plate (listed in Tab.A.3)
$\Gamma_{pre} = \begin{bmatrix} N_x & N_y & N_{xy} \end{bmatrix}$	in-plate loads per unit width
$\Gamma_{eb} = \begin{bmatrix} \text{Trasl. coeffs.} \\ \text{Rotat. coeffs.} \end{bmatrix}$	dimensionless values of the transverse spring and rotation spring for elastic boundary condition
$\Gamma_{lsx} = \begin{bmatrix} \xi_i \\ \text{Elastic coeffs.} \end{bmatrix}$	ξ coordinates and elastic coefficients of elastic intermediate lines supports
$\Gamma_{lsy} = \begin{bmatrix} \eta_i \\ \text{Elastic coeffs.} \end{bmatrix}$	η coordinates and elastic coefficients of elastic intermediate lines supports
$\Gamma_{ps} = \begin{bmatrix} \xi_i \\ \eta_i \\ \text{Elastic coeffs.} \end{bmatrix}$	ξ and η coordinates and elastic coefficients of elastic intermediate point supports
$\Gamma_{pm} = \begin{bmatrix} \xi_i \\ \eta_i \\ m_i \end{bmatrix}$	ξ and η coordinates and masses of rigid concentrated masses

Table A.2: Variables of the sound radiation model.

RME variables	
E_x	elementary radiators on the x axis
E_y	elementary radiators on the y axis
m	most significan radiation modes
ord	order of fitting transfer functions
f_{max}	maximum frequency of interest
Phisical variables	
ρ	air density [kg/m^3]
c	speed of sound [m/s]

Table A.3: Material properties embedded in the routine.

	Material	D_{22}	D_{12}	D_{66}	ν	
M0	Isotropic	D_{11}	νD_{11}	$(1-\nu)D_{11}/2$	0.3	
M1	Orthotropic-1	$D_{11}/2$	νD_{11}	D_{22}	0.3	
M2	Orthotropic-2	$2D_{11}$	νD_{11}	$0.35D_{11}$	0.3	
		E_1(GPa)	E_2(GPa)	G_{12}(GPa)	ν_{12}	ρ(kg/m^3)
M3	T-graphite/epoxy	185	10.5	7.3	0.28	1600
M4	B-boron/epoxy	208	18.9	5.7	0.23	2000
M5	K-aryl/epoxy	76	5.6	2.3	0.34	1460

More material properties can be added modyfing the MATLAB script.

Bibliography

[1] Makola M. Abdullah. "Optimal location and gains of feedback controllers at discrete locations". *AIAA Journal*, 36(11):2109–2116, November 1998.

[2] O. Beslin and J. Nicolas. "A hierarchical functions set for predictin very high order plate bending modes with any boundary conditions.". *Journal of Sound and Vibration*, 202, 1997.

[3] Lorenzo Dozio. "On the use of the Trigonometric Ritz method for general vibration analysis of rectangular Kirchoff plates". *Thin-Walled Structures*, 49:129–144, 2011.

[4] Wouter P. Engels, Oliver N. Baumann, and Stephen J. Elliot. "Centralized and decentralized control of structural vibration and sound radiation.". *2000 Acoustic Society of America*, 119(3):1487–1495, March 2006.

[5] F.J. Fahy and P. Gardonio. *"Sound and Structural Vibration (2nd edn).".* Academic Press - Elsevier, 2007.

[6] Gary P. Gibbs, Robert L. Clark, David E. Cox, and Jeffrey S. Vipperman. "Radiation modal expansion: Application to active structural acoustic control.". *Journal of Acoustical Society of America*, 107(1):332–339, 2000.

[7] Arthur W. Leissa. "The free vibration of rectangular plates". *Journal of Sound and Vibration*, 31, 1973.

[8] P. Venkataraman. *"Applied Optimization with MATLAB Programming".* Wiley, 2001.

[9] K. Xu, P. Warnitchai, and T. Igusa. "Optimal placement and gains of sensors and actuators for feedback control". *Journal of Guidance, Control, and Dynamics*, 17(5):929–934, 1993.